

DISSERTATION

DEVELOPMENT OF PAPER-BASED ANALYTICAL
DEVICES FOR PARTICULATE METALS IN WELDING FUME

Submitted by

David M. Cate

Graduate Degree Program in Bioengineering

In partial fulfillment of the requirements

For the Degree of Doctor of Philosophy

Colorado State University

Fort Collins, Colorado

Fall 2015

Doctoral Committee:

Advisor: Charles S. Henry
Co-Advisor: John Volckens

David Dandy
Jennifer Peel
Kevin Lear

Copyright by David Michael Cate 2015
All Rights Reserved

ABSTRACT

DEVELOPMENT OF PAPER-BASED ANALYTICAL DEVICES FOR PARTICULATE METALS IN WELDING FUME

Exposure to metal-containing particulate matter places a tremendous burden on human health. Studies show that exposures lead to cardiovascular disease, asthma, flu-like illnesses, other respiratory disorders, and to increased morbidity. Individuals who work in occupations such as metalworking, construction, transportation, and mining are especially susceptible to unsafe exposures because of their proximity to the source of particle generation. Despite the risk to worker health, relatively few are routinely monitored for their exposure due to the time-intensive and cost-prohibitive analytical methods currently employed. The current paradigm for chemical speciation of workplace pollution is outdated and inefficient.

Paper-based microfluidic devices, a new type of sensor technology, are poised to overcome issues associated with chemical analysis of particulate matter, specifically the cost and timeliness of exposure assessment. Paper sensors are designed to manipulate microliter liquid volumes and because flow is passively driven by capillary action, analysis costs are very low. The objective of this work was to develop new technology for rapidly measuring Ni, Cu, Fe, and Cr in welding fume using easy-to-use paper devices. This dissertation covers the development of two techniques for quantifying metal concentration: spot integration and distance-based detection. Metal concentrations as low as 0.02 ppm are reported. A method for controlling reagent deposition as well as a new interface for multiplexed detection of metals, is discussed.

ACKNOWLEDGEMENTS

The research described in this dissertation was funded from several sources. The author was funded from 2011-2014 from the National Institute for Occupational Safety and Health (OH010050) and the National Institute of Environmental Health Sciences (ES019264). Work from 2014-2015 was supported by grants from the State of Colorado, Colorado State University, and the National Science Foundation (1415655). This work has not been formally reviewed by any government agency; the views expressed in this dissertation are solely those of the author.

There are many individuals whose efforts toward the completion of this dissertation should be acknowledged. Without their support and assistance, the work described herein would not be possible. Brief descriptions of group and individual efforts are described.

Charles Henry Lab: The majority of the chemistry, fabrication, and design work was performed in the Henry lab. Several group members contributed to my work. Specifically, Pavisara Nanthalasurasak and Pornpak Riwkulkajorn assisted with colorimetric assay development and helped establish a protocol for microwave-assisted acid digestion of welding fume samples. I want to especially thank Dr. Scott D. Noblitt for holding the entire group to a high standard of research integrity. He provided valuable insight into my work, including the design of LabView VI's for generating colorimetric gradients and assisting with data analysis for work presented in Chapter 4. During her brief time with the lab, Wijitar Dungchai helped expand our work with paper-based sensors.

John Volckens Lab: Dr. Christian L'Orange provided technical support and donned a welding overcoat several times to help me acquire welding fume samples. Dr. Nicholas Good very generously donated his time to assist me in setting up the aerosol collection chamber on several occasions. I would also like to thank Casey Quinn, Dan Miller-Lionberg, and Dr. Kristen Koehler for their generous support and assistance.

My advisors, Charles S. Henry and John Volckens, were tremendous throughout this process. Together, they guided my research and challenged me when necessary. They established a great rapport with me from the beginning and I have enjoyed my time under their tutelage. A former advisor once told me that picking a good project in graduate school is important, but not nearly as significant as choosing the correct advisor(s). I wholeheartedly support this assertion. Chuck and John have helped me succeed by generously sharing with me some of their professional and personal experiences. I am forever grateful and blessed to have worked with them.

Finally, I want to thank my parents, Lowell and Sharon Cate, for their love and support throughout this process. Words cannot express my gratitude towards them. Thank you Andrew, Leah, Deborah, and Rebecca (and Eden!) for your support and encouragement. Lastly, I want to acknowledge Dr. Emi Y. Tokuda for her support over the last several years, and I wish her success and happiness in the years to come.

Some of the method development and data analysis was performed by other individuals whose contributions are listed, organized by chapter.

Chapter 2: Pavisara Nanthesurasak and Pornpak Riwkulkajorn helped test calibration curves for Fe, Ni, Cu, and Cr with the four-arm paper sensor. They also assisted in determining the correct pH for the acid digestion procedure. Dr. Christian L'Orange generated MIG welding fumes for analysis.

CHAPTER 3

The results presented in this chapter were developed with Dr. Wijitar Dungchai, a visiting scholar in the Henry laboratory. I developed the methods for measuring nickel and assisted Wijitar with method development for measuring glucose and reduced glutathione.

CHAPTER 4

For this work, Dr. Scott Noblitt advised in a number of areas, including weighted regression analysis of the data and developing the LabView gradient generation virtual interface.

TABLE OF CONTENTS

ABSTRACT	ii
ACKNOWLEDGEMENTS	iii
LIST OF SYMBOLS	ix
CHAPTERS	
1. INTRODUCTION	1
Atmospheric Aerosols.....	1
Occupational Exposure to Metals in Particulate Matter	4
Techniques for Quantifying Metal Exposures in the Workplace.....	5
Paper-Based Microfluidic Devices	8
Material Choice and Fabrication Methods.....	11
Reagent Deposition by Inkjet Printing.....	15
Detectors and Readout	18
Determination of Transition Metals with μ PADs.....	23
References.....	27
2. RAPID DETECTION OF TRANSITION METALS IN WELDING FUMES USING PAPER-BASED ANALYTICAL DEVICES	35
Chapter Overview	35
Introduction.....	36
Methods.....	39
Chemicals and Materials	39
Welding Fumes Sampling	39
μ PAD Fabrication and Colorimetric Assay	40
Filter Extraction and μ PAD Analysis	41
Image Processing	43
Data Analysis	44
Results.....	44
Metal Determination Using μ PADs.....	44
Method Validation	48
Discussion.....	50
Conclusions.....	52
Closing Comments.....	53
References.....	55
3. SIMPLE, DISTANCE-BASED MEASUREMENT FOR PAPER-ANALYTICAL DEVICES.....	58
Chapter Overview	58
Introduction.....	59

Experimental Methods	62
Materials and Equipment	62
Device Operation	63
Glutathione Detection	65
Glucose Detection	65
Analysis of Glutathione and Glucose in Human Serum	66
Nickel Detection	66
Analysis of Ni in Combustion Incineration Ash.....	66
Results and Discussion	67
Glucose Quantification	67
Quantification of Nickel in a Combustion Ash Sample.....	69
GSH Quantification Assay.....	71
Conclusions.....	75
References.....	77
 4. MULTIPLEXED PAPER ANALYTICAL DEVICE FOR QUANTIFICATION OF METALS USING DISTANCE-BASED DETECTION.....	80
Chapter Overview	80
Introduction.....	81
Experimental Methods	85
Materials and Equipment	85
Device Fabrication and Operation	85
Inkjet Cartridge Modification and Reagent Printing	88
Ink Formulation and Gradient Creation.....	90
Nickel Detection	92
Copper Detection	93
Iron Detection	93
Welding Fume Standard Reference Material.....	94
Data Analysis	94
Results and Discussion	95
Detection of Fe, Ni, and Cu in Single Channels	95
Extending Dynamic Range	96
Varying Channel Width	96
Distance-Based Detection of Ni, Cu, and Fe in Single Channels	98
Simultaneous Distance-Based Detection of Ni, Cu, and Fe	102
Multi-Channel Device Geometry.....	102
Analyte Measurements.....	104
Interferences.....	108
Welding Fume Reference Material	110
Conclusions.....	111
References.....	112
 5. EMPIRICAL OBSERVATIONS ON FLOW RATE AND ANALYTE DEPOSITION FOR DISTANCE-BASED DETECTION.....	114
Chapter Overview	114
Capillary-Driven Flow in Porous Media.....	114

Influence of Variables	118
Gravity	118
Wax Boundaries.....	119
Lamination	120
Reaction Rate Constants	123
Closing Comments.....	125
References.....	127

6. CONCLUSIONS AND CONSIDERATIONS FOR THE FUTURE OF MICROFLUIDIC PAPER-BASED ANALYTICAL DEVICE TECHNOLOGY	129
Chapter Overview	129
Improving μ PAD Detection of Metals.....	129
Chemical Modification of the Substrate	129
Physical Modification of the Substrate	131
Moving Away from the Benchtop	132
Potential Pitfalls Inhibiting Widespread Use	133
Considerations for the Future.....	134
References.....	136

APPENDICES

A1. RECORDING COLORIMETRIC INTENSITY FOR QUANTIFYING METALS WITH μPADS	138
A2. PRINTING COLORIMETRIC REAGENTS FOR DISTANCE-BASED DETECTION OF MULTIPLE METALS	141
Creating Reagent Gradients	141
Statistical Analysis of Distance-Based Detection.....	144

LIST OF SYMBOLS

d_p	Particle Diameter
d_{ae}	Aerodynamic Particle Diameter
PM	Particulate Matter
ICP-OES	Inductively Coupled Plasma – Optical Emission Spectrometry
AAS	Atomic Absorption Spectrometry
FAAS	Flame Atomic Absorption Spectroscopy
ETAAS	Electrothermal Atomic Absorption Spectrometry
AFS	Atomic Fluorescence Spectrometry
AKD	Alkyl Ketene Dimer
GFAAS	Graphite Furnace Atomic Absorption Spectrometry
XRF	X-ray Fluorescence Spectrometry
ICP-MS	Inductively Coupled Plasma – Mass Spectrometry
ECL	Electrochemiluminescence
μ PAD	Microfluidic Paper-Based Analytical Device
NIOSH	National Institute for Occupational Safety and Health
OSHA	Occupational Safety and Health Administration
LFA	Lateral-Flow Assay
PAH	Polycyclic Aromatic Hydrocarbon
NP	Nanoparticle
TIG	Tungsten Inert Gas
SMAW	Shield Metal Arc Welding

MIG	Metal Inert Gas
MCE	Mixed Cellulose Ester
POC	Point-of-Care
SS	Stainless Steel
TWA	Time Weighted Average
PEL	Permissible Exposure Limit
L, l_m	Wicking distance of the fluid front
D	Average pore radius (dry)
C	Analyte concentration
dmgH ₂	Dimethylglyoxime
Bphen	Bathophenanthroline
PDDA	Polydiallyldimethylammonium chloride
1,5-DPC	1,5-Diphenylcarbazide
1,10-Phen	1,10-Phenanthroline
GSH	Glutathione
DPCO	Diphenylcarbazone
SDS	Sodium dodecyl sulfate
W _c	Channel width (before melting)
W _p	Printed wax barrier width
DOD	Drop-on-Demand
Z	Inverse of Oh
Oh	Ohnesorge number
d	Printhead diameter

x_f	Maximum recorded distance
t_f	Time at distance x_f
$I(D)$	Non-dimensionalized distance
μ	Dynamic viscosity
θ	Contact angle of liquid-capillary
θ_b	Contact angle of liquid-boundary
γ, σ	Liquid-air surface Tension
ρ	Liquid Density
ρ_c	Cellulose Density
g	Acceleration due to gravity
ϕ	Porosity
m_0	Paper mass
r_{eff}	Effective pore radius
p_c	Capillary pressure
p_{atm}	Atmospheric pressure
β	Constant of proportionality
b	Paper thickness
v	Fluid velocity
k	Substrate permeability
k (Chapter 5)	Equilibrium constant
SS_E	Sum of squared error
\bar{x}	Weighted x-centroid

S _{xx}	Weighted sum of squares in x direction
CI	Confidence Interval
PI	Prediction Interval
$v_{unbonded}$	Linear flow rate in unbonded channel
v_{bonded}	Linear flow rate in bonded channel

CHAPTER 1: INTRODUCTION

Stricter regulations on waste disposal methods and cleaner manufacturing processes have reduced the incidence of both acute and chronic discharges of metals to waterways and the release of metals in air. Despite these changes, the current paradigms for environmental monitoring have largely remained the same for the last several decades. Methods for analyzing metals in environmental media (i.e., in water and air) such as inductively coupled plasma optical emission spectrometry (ICP-OES) and atomic absorption spectrometry (AAS) boast sub part-per-billion sensitivity, but are cost and labor intensive. For example, chemical speciation of five different metals with ICP-OES can exceed \$150 for just *one sample*. Moreover, most conventional instruments lack the portability required for effective hazard communication and remediation at the point-of-need. The work presented in this dissertation describes the development of two paper-based microfluidic sensors for quantifying metals using two different techniques for analyzing colorimetric reaction products: spot integration and distance-based detection. Both methods are ultra-low cost (< \$0.20 per sample), simple, portable, and disposable. Device application was demonstrated for quantifying the metal content in welding fumes collected onto air sampling filters. Spot integration is performed with a desktop scanner and open-source computer software while distance-based detection requires no external instrumentation for analysis of collected samples.

Atmospheric Aerosols

Microscopic particles floating in air, termed aerosols, come from many sources and are generated in several ways: soil, mineral and road dust, incomplete combustion of fossil fuels, salt from ocean spray, ice, photochemical conversion processes, and cloud formation.⁴³ Throughout the

dissertation, the terms aerosol and airborne PM are used interchangeably. The physical and chemical characteristics of aerosols are as diverse as their sources of generation; suspended particles have diameters (d_p) that vary over six orders of magnitude (10^{-9} - 10^{-4} m), from small molecules and viruses at the smallest, to bacteria and pollen at the largest.⁴⁸ Although generally comprised of a mixture of water, salts, metal oxides, silicates, and carbonaceous material, the characteristics of aerosols are both a function of the source (natural/anthropogenic), and other physical and chemical reactions (e.g. oxidation, condensation, nucleation) that occur once in the atmosphere. Globally, airborne PM is generated from natural sources (e.g. sea salt, dust), though anthropogenically-derived PM typically dominates in urban and industrialized zones and can be further classified as indoor or outdoor.⁴⁹ Both indoor and outdoor PM are generated from a number of sources: domestic or industrial cooking (i.e. combustion), building materials, air conditioning, consumer products, and heating, to name a few. Although the relative ratios of indoor/outdoor PM constituents vary, the predominant chemical components are similar. Examples include polycyclic aromatic hydrocarbons, organic dusts, tobacco, metals, and sulfates.^{55, 56} Despite epidemiological evidence associating both acute and chronic exposure to ambient PM with adverse health outcomes in humans (especially for children and the elderly), fundamental uncertainty still persists regarding the physical and chemical properties of particles that govern their effect on health. Complex associations between exposure and aerosol composition, coupled with expensive analytical methods limit the size and scope of epidemiological (and toxicological) studies, making the development (and implementation) of exposure regulations challenging.⁵⁸

Aerosols present a unique health risk because their size generally dictates whether they are inhalable (50% cutoff at $d_{ae} = 100 \mu\text{m}$), and if so, where they ultimately deposit in the body.

Assuming a steady inhalation rate of 1 L s⁻¹, approximately 60-90% of particles with aerodynamic diameters (d_{ae}) between 2.5 and 10 μm (termed coarse PM) deposit via impaction between the trachea and terminal bronchus in humans.⁶¹ Stopping distances are comparatively large for coarse particles, especially for those near airway walls, where air streamlines suddenly change directions (i.e. at lung bifurcations). For example, a $d_{ae}=10 \mu\text{m}$ particle in the trachea has a stopping distance of ~120 mm, much greater than the average diameter of the trachea (~18 mm); it's no surprise then, that most particles as large as 10 μm deposit in the upper lung and head airways. Fine particles ($d_{ae} < 2.5 \mu\text{m}$) tend to deposit both in head airway spaces, as well as deeper in the lung (i.e. alveoli). The Brownian motion of fine and ultrafine particles ($d_{ae} < 0.1 \mu\text{m}$) leads to an increased likelihood they will deposit in small airways by diffusion, where tube diameters are short and air residence times are long (~0.5 s). Approximately 10% of ultrafine particles deposit in upper airways as well.⁶³ The danger for particles that reach alveolar space is the potential for access to the bloodstream via the blood-air exchange barrier, where they can be transported to virtually every organ, including the brain.⁶⁴ Particle shape too, can dictate particle toxicity; tube-like structures such as asbestos fibers are an excellent example of shape-induced toxicity.⁶⁷

The impact of aerosol chemistry on particle toxicity is not well understood.⁶⁹ Chemical components of PM are highly diverse, ranging from neutral and highly soluble substances (NaCl, (NH₄)₂SO₄) to sooty, carbonaceous, insoluble species. Toxicological evidence has shown that bioavailable metals, for example, influence PM toxicity. The mechanism proposed is that metals are redox-active and can catalyze reactions that lead to the production of free radicals, inducing cellular damage.⁶⁹ For example, oil fly ash containing a substantial proportion of transition metals (Fe, Cu, Ni, V, Zn) augmented pulmonary hypertension and mortality rates when lavage fluids

were analyzed in murine models.⁷⁰ Lead air quality standards, for example, have been among the most stringent of any bioaccessible metal due to its adverse impact on human health (action level is $10 \mu\text{g dL}^{-1}$).⁷¹ In most air pollution/ source apportionment studies, total elemental concentrations are determined; however, the ability to identify specific elemental fractions could provide information about PM emission sources or their potential bioavailability (if chemical oxidation states were determined).⁷² It is also important to consider (and monitor) the site of particle origin because chemical speciation of airborne metal-containing PM is known to vary. For example, one particular study of urban and industrial sites in Greece found that although particle mass concentrations were similar for both, total metal concentrations (and metal type) were significantly different.⁷¹ This case study highlighted the necessity for site-to-site chemical monitoring, and that emission sources of metal-containing PM are unique to the type, location, and duration of the specific technique.

Occupational Exposure to Metals in Particulate Matter

Mass concentrations of workplace aerosols are typically higher than in ambient air (whether indoors or outdoors).⁷³ Many of the processes that generate metal-containing PM are industrial combustion and vapor condensation processes; much of this fraction of PM can be categorized as fine particulate matter. Because the size distribution of fine PM is $< 2.5 \mu\text{m}$, it remains airborne for long periods of time and can penetrate indoor air environments. Occupations such as metalworking, construction, transportation, and mining are at elevated risk because chronic inhalation of toxic metal particulates can lead to a number of cardiovascular and respiratory diseases, and even early death. The resulting healthcare costs associated with occupational respiratory diseases alone exceed \$10B each year in the United States and result in approximately

425,000 premature deaths annually world-wide.⁷⁴ Metals present in PM (e.g. Cu, Cr, Ni) are identified as contributing factors to daily morbidity and mortality. Studies indicate that bioavailable metal particulates mediate cardiopulmonary injury in healthy individuals and induce chronic inflammation via cellular oxidative stress.^{70, 75} Of particular concern is exposure to welding fumes, known to contain hazardous levels of particulate metals such as Cr(VI), Ni, Cu, Mn, and Pb.⁷⁶ The aerosol generated from welding contains both gases and fumes consisting of metal oxide PM (among others); the specific contents of which are dependent on the welding technique, filler wire and flux composition, and the material on which the welding is performed.⁷⁷⁻⁸⁰ Worldwide, the most common substrate for welding is stainless steel because of its anti-corrosion, anti-rust, and anti-staining properties.⁸¹ Epidemiological studies have linked occupational welding exposure to respiratory diseases, lung and bladder cancer, asthma, chronic bronchitis, and DNA damage in lymphocytes.⁸²⁻⁸⁶ For example, a study performed in 2007 revealed that worker exposure to Mn within the range 0.01-2.67 mg m⁻³ could induce subclinical effects on the nervous system such as increased emotional irritability, dysmnesia, sleepiness, loss of concentration, and limb paresthesia.^{87, 88} Bridge welders working in confined spaces with mean exposures to Mn between 0.11-0.46 mg m⁻³ showed a high rate (~80%) of sleep disturbance.⁸⁹ Welders also have a high incidence rate of cardiovascular mortality, specifically ischemic heart disease.⁹⁰⁻⁹³ Even with local ventilation and respirator protection, welders can still be exposed to potentially harmful levels of metal-containing PM, especially if one considers chronic exposure over the course of a working lifetime (~30-40 years).⁹⁴

Techniques for Quantifying Metal Exposures in the Workplace

In workplace settings the chemical composition of PM is usually characteristic of the processes generating the aerosol, a metaphorical “chemical fingerprint” of chemical concentrations. The current paradigm for regulatory workplace monitoring by organizations like the U.S. Occupational Safety and Health Administration is an air sample taken near the breathing zone of an individual over the course of an eight-hour shift. Exposure assessment at the individual level is designed to accomplish the following: 1) to maintain regulatory compliance and monitor continued performance, 2) to determine if a health risk exists by comparison with established legal limits, 3) to ascertain the reason for the health risk, 4) to implement safe practices if necessary, 5) to check control systems for quality assurance (e.g. personal protective equipment, HVAC, ventilation), and 6) to gather exposure data for epidemiological studies.⁹⁵ Exposure monitoring at the individual level is critical for risk assessment because measuring PM from group data (i.e. an area-wide measurement), in many cases, improperly depicts personal exposures (and risks).⁹⁶ Personal exposure rates are often distributed log-normally with respect to mass concentration and are known to vary in duration and location, even within similar job titles and economic sectors. Sampling equipment (e.g. filters, pumps, impaction cassettes) placed on the individual is designed to estimate health-relevant exposure during a work shift. For risk evaluation, exposure assessment should be aimed at measuring biologically relevant exposures, however the overall cost of analysis – especially if one considers repeated measures – often precludes routine monitoring. Chemical speciation (and concentration analysis) is performed offsite at a central facility; however, the time from sample collection to reporting (i.e. hazard communication) is typically several weeks.

Techniques for quantifying toxic metals and metalloids in bulk date back to the 1950's, when flame atomic absorption spectroscopy (FAAS) was modernized.⁹⁶ Elemental composition in FAAS is determined by analyzing the absorption of optical radiation by free metal atoms in gases. Electrons are promoted to higher orbitals when excited using a lamp source. Free atoms are produced in FAAS when a nebulized spray of metal analytes is passed through a high-temperature (2300-2700 °C) air/acetylene or nitrous-oxide/acetylene flame; the light source is incident with metal atoms passing through the flame. Every metal atom absorbing light emits radiation at a unique wavelength characteristic of that element; the radiation flux measured in the presence and absence of the sample is then used to determine analyte concentration. Today, the most widely used techniques for trace metal determination are electrothermal atomic absorption spectrometry (ETAAS), atomic fluorescence spectrometry (AFS), graphite furnace atomic absorption spectrometry (GFAAS), X-ray fluorescence spectrometry (XRF), and inductively couple plasma – mass spectrometry (ICP-MS). Sample matrix, pre-treatment steps, and analyte concentration in the sample are all considerations that can determine which technique to choose; typical detection ranges are shown in Figure 1-1. For analysis of metal-containing PM in the workplace, ICP-OES is perhaps the most commonly used method (OSHA standard ID-125G). ICP-OES is sensitive and capable of high-throughput, multiplexed detection of several transition metals. However the cost of ICP analysis (\$100-\$200 per sample) often precludes routine monitoring of personal exposures.⁹⁷ According to the Department of Labor, in 2012 there were approximately 350,000 welders, cutters, solderers, and brazers in the U.S.⁹⁸ The analytical costs (not including personnel time and equipment) to assess each welder's exposure once to only a single metal species would exceed \$33,000,000 per year. In the developed world, such costs tend to preclude routine exposure assessment; in the developing world, these costs render exposure assessments practically

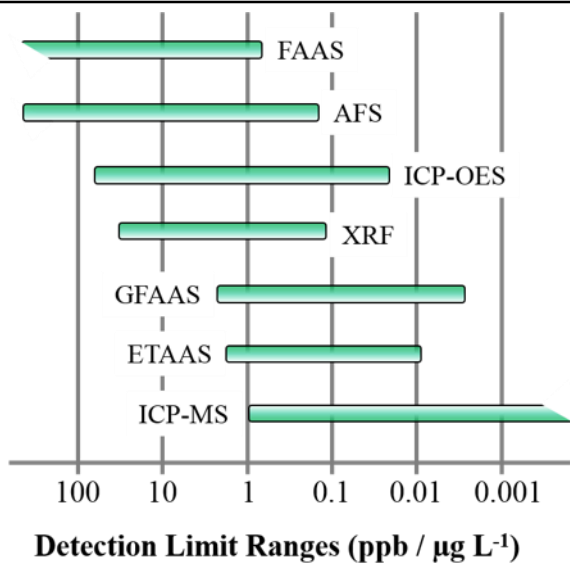


Figure 1-1 | Detection limits for analytical methods commonly used for determination of trace metals.

impossible. Consequently, there is a need for rapid, sensitive, and cost-friendly alternatives for monitoring workers' exposure to PM metals that would enable broader screening of occupational exposures.⁹⁹

Paper-Based Microfluidic Devices

Paper has been used as a substrate material in analytical testing for millenia. As early as 23 to 79 A.D., paper saturated with extract from gallnuts was used for detecting the presence of ferrous sulfate in verdigris, the bluish patina that forms on copper, brass, and bronze surfaces from oxidation.¹⁰⁰ Some of the earliest scientific reports date back to litmus paper in the early 1800s.¹⁰¹ As a substrate material, paper (and related porous hydrophilic materials) has many unique advantages over traditional substrates (i.e. glass, silicon, and polymers); paper provides power-free fluid transport via capillary action, has high surface-to-volume ratio for chemical interaction and detection, is lightweight ($\sim 10 \text{ mg cm}^{-2}$), and also has the capacity for storing reagents in active form within the fiber network.¹⁰²⁻¹⁰⁵ Properties of paper are compared to more traditional

Table 1-1 | Properties of cellulosic (paper) substrates compared to glass, silicon, and PDMS. Adapted from ref. 15 with permission from Springer.

Property	Material				Impact
	Glass	Silicon	PDMS	Paper	
Flexibility	None	None	Some	High	Multi-layer construction; less likely to become damaged during transport, handling, and repeated use
Permeability	Solid	Solid	Gas	Gas/liquid	Permeable materials are amenable for cell culture, multi-layer construction, gas sensing applications
Surface-to-volume ratio	Low	Low	Low	High	Paper provides more surface area for chemical reactions per unit area/volume
Fluid control (primarily)	Active	Active	Active	Passive	Active pumping requires external instrumentation. Imbibition in paper is controlled by capillary action.
Biocompatibility	Yes	Yes	Yes	Yes	Amenable for biological applications
Optical transparency	Yes	No	Moderate	No	Not compatible with many optical microscopy techniques
Biodegradability	No	No	Limited	Yes	Recyclable; can incinerate
Ease of fabrication	Moderate	Difficult	Moderate	Easy	Commercially available resources can be used for fabrication
Fabrication throughput	High	High	Low	High	Lower cost of fabrication per device
Functionalization	Difficult	Moderate	Moderate	Simple	Ability to change surface properties for unique chemical applications
Chemical homogeneity	Yes	Yes	Yes	No	Changing surface chemistry can decrease assay precision
Material cost	Moderate	High	Moderate	Low	Very low cost per device factor

substrates in Table 1-1.¹⁰⁵ These benefits culminate in a broad range of applications suitable for analysis with paper devices, such as blood glucose monitoring,¹⁰⁶ foodborne pathogen testing,¹⁰⁷ and screening for toxic metals in air or water.^{108, 109} Besides acid/base chemistry, paper has long played an important role in the development of early chromatographic and electrophoretic

separations.^{110, 111} To control fluid flow during analyte separation experiments, hydrophobic materials like paraffin were embedded into porous substrates, a practice which dates back to 1902.¹¹² One of the earliest reports on the development of a paper-based semi-quantitative “spot (or ring) colorimetry” test was in 1937 for estimating nickel and copper concentrations in water.¹¹³⁻

¹¹⁵ Analyte losses from reagent spreading was prevented by the inclusion of a wax barrier to confine reagents within a uniform area. Hydrophobic paraffin rings embedded in paper were made by applying a heated metal plate (10×5×1.3 cm) containing an array of predrilled holes (of appropriate diameter) to the surface of a paraffin slab, transferring molten paraffin to the plate. Paraffin coated the plate on all non-drilled surfaces. After transferring paraffin from the plate to paper, an array of analyte sensing zones were created and ready for reagent storage. Barrier width was determined by filter pore size, contact time, pressure, and temperature of the metal tool, variables which are relatively easy to control. Paraffin’s chemical inertness and compatibility with cellulosic materials make it an excellent material for preventing cross contamination between reagent zones.¹¹⁵⁻¹¹⁸ Barrier materials comprised of rosin, waxes, cellulose esters, ethyl cellulose, fluoropolymers, silicones, and polystyrene have also been proposed.^{15, 40, 119-121} As Figure 1-2 demonstrates, the physical footprint of early devices was significantly larger than paper sensors today, despite the fact that early μPADs were typically one or two-dimensional and functionally less complex.¹²² Improvements to some of the earliest paper-based devices eventually led to some important contributions in medicine, specifically for point-of-need “early diagnosis” detection. Seminal work to develop the first paper device for semi-quantitative detection of glucose in urine (1956)¹²³ led to modern immunochromatographic test strips (called lateral-flow immunoassays or “dipstick” tests) such as the home pregnancy test or glucose monitoring for diabetics.¹²⁴⁻¹²⁶ A typical lateral-flow assay strip (or LFA) consists of a sample pad, a reagent pad, and a test

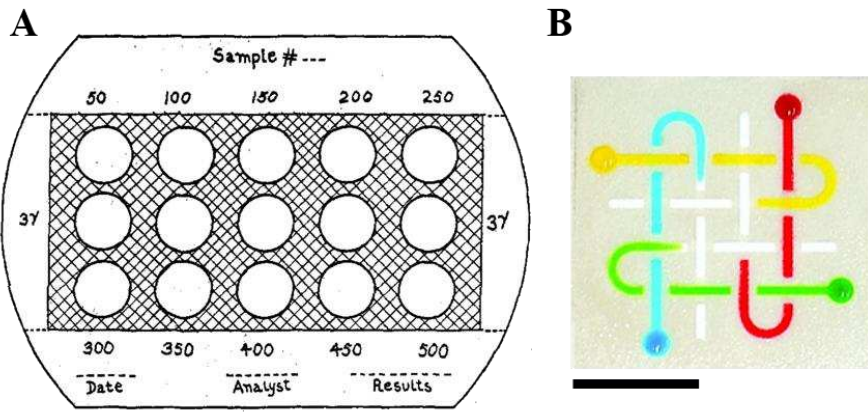


Figure 1-2 | A comparison of a μPADs from the early (A) 20th and (B) 21st centuries. Hash marks in the device on the left represent hydrophobic paraffin; open circles represent open hydrophilic pores. Reprinted with permission from ref 114. Copyright 2015 American Chemical Society. The sensor on the right contains multiple layers embedded with a hydrophobic photoresist; layers are stacked to create a 3D μPAD. Black scale bars each represent 1 cm. Reprinted with permission from ref 122. Copyright 2015 National Academy of Sciences.

“capture” line for sample quantification. Analyte is added to the sample pad and flows along a hydrophilic cellulosic membrane, binding to antigen-specific antibodies at the reagent pad, before ultimately binding to capture agents (e.g. gold nanoparticles, latex microspheres) that are pre-patterned on the test line. Analysis is rapid, straightforward, and amenable for measuring a range of disease biomarkers.¹²⁷⁻¹²⁹ Although reliable, LFAs are generally limited in their analysis to a discreet (i.e. quantized) “yes/no” output. In many circumstances, however, knowing (with reasonable uncertainty) how much analyte is present is important, for example, when measuring the concentration of polycyclic aromatic hydrocarbons in the atmosphere.¹³⁰

Material Choice and Fabrication Methods

In the last several years there has been a shift in the paper sensing community from rudimentary design and fabrication concepts to more advanced techniques. In 2007, Martinez et al. reported the first microfluidic paper-based analytical device (μPAD) for multiplexed chemical analysis. The

breakthrough in their work stemmed from the creation of a multi-branch tree-shaped μ PAD where three different reagents were spotted for glucose and protein assays; previous demonstrations included only single-analyte detection (per sample).¹³¹ Although some debate persists as to the reason for paper's increasing popularity as an analytical substrate; the answer might arise from the development of new microfabrication technologies, enabling fabrication of new types of devices.¹³² There are a variety of substrate materials available to the user, such as cellulose paper, nitrocellulose, glass fiber, and various polyester filters; however, choice is primarily based on application and method of fabrication. The majority of the paper community uses cellulosic filter paper/membranes, specifically Whatman 1 (~11 μ m pore diameter), 4 (~22 μ m pore diameter), and nitrocellulose (~0.5 μ m pore diameter). Whatman filter paper is popular because it is affordable (~0.001 cents cm^{-2}), nearly chemically homogeneous with zero additives ($\geq 98\%$ α -cellulose), has a relatively smooth surface (micrometer root mean squared roughness),¹³³ is compatible with most solvents, scatters light abundantly (high contrast between paper background and colorimetric assays), has good mechanical stiffness, and wicks fluid in a defined manner.^{28, 105, 134-140} Filter paper is also an excellent substrate for storing dry reagents during shipping/transport because it is less labile in changing environmental conditions. Moreover, biomolecules exhibit a high degree of non-specific adsorption towards membranes/filters composed of nitrocellulose, which has consequently propelled the use of these membranes for immobilization of enzymes,^{141, 142} proteins,¹⁴³ DNA,¹⁴⁴ and RNA^{144, 145} in biomedical applications. Interestingly, standard photocopy paper – although inexpensive and abundant – has not been well-utilized in the literature, possibly because liquid penetration (i.e. flow velocity) is extremely slow due to small (~100 nm¹⁴⁶) pore sizes. Flow velocities in Whatman 1 (~2 mm min^{-1}) and 4 (~3 mm min^{-1}) filter paper are moderate to fast, respectively, compared to photocopy paper. Moreover,

copy paper typically contains ~10% alkyl ketene dimer, rendering the surface partially hydrophobic, which is disadvantageous for many applications requiring moderate to rapid fluid wicking.¹⁴⁷

There are many fabrication techniques reported in the literature for patterning defined boundaries in paper substrates; the most popular are given in Table 1-2. To date, the most widely used techniques for creating hydrophobic barriers are those involving wax patterning.¹⁰³ Whether by printing, dipping, or screen-printing, wax-based fabrication methods are amenable for laboratory-scale μPAD processing. Unlike photolithography – which is a cross-over technique for fabricating PDMS microfluidic devices – wax patterning is rapid (results in under 5 min), inexpensive (10x cheaper per 100 cm² than SU-8 patterning)¹⁰⁴, requires minimal technical expertise, and can be performed outside of a controlled laboratory environment. For these reasons, wax patterning is typically better suited for point-of-need applications than other approaches.¹⁴⁸ Regardless of the specific technique, all wax-based approaches rely on the spread of molten wax to create 3D hydrophobic barriers; wax is typically heated above 120 °C for ~60 s to fully penetrate the paper substrate (~50-200 μm thick). A disadvantage of this method is that wax spreads laterally (and vertically), decreasing channel resolution in the process. Fortunately, wax spreading is predictable. As is the case for modeling fluid movement in capillary fibers, Washburn's equation can be used to describe the spreading (L) of molten wax in paper:

$$dL/dt = \sqrt{\frac{\gamma D \cos\theta}{4\eta}} \quad (1.1)$$

where the change in penetration distance with time (dL/dt) of the fluid front is a function of fluid surface tension (γ), average pore radius (D), fiber contact angle (θ), and viscosity (η).¹⁴⁹ In many instances, the contact angle between the eluent (H₂O) and substrate (cellulose) is approximately

Table 1-2 | μPAD fabrication techniques, arranged by method.

Fabrication Technique	Channel Resolution (μm)	Cost	Advantages	Limitations
Wax patterning ¹⁻⁷	~ 500	Low	High throughput, solid ink printers are commercially available	Low patterning resolution, paper requires heating (150 °C), incompatible with organic solvents
Inkjet printing ⁸⁻¹⁴	~ 300	Low	Versatile, one-step reagent and hydrophobic barrier printing	Cost can be high depending on reagents
Flexographic printing ¹⁵	~ 500	Moderate	High throughput (300 m min ⁻¹)	Complex, requires specialized equipment, multi-step, limited to single reagent printing
Screen printing ^{17, 18}	~ 600-700	Low	High throughput, versatile	Inter-device reproducibility is low, low resolution
Laser printing/cutting ²²⁻²⁶	~ 500	High	No backing material needed, Cuts through multiple materials	Very expensive
Photolithography ^{17, 27-32}	~ 100-200	High	High resolution (narrow) channels, chemical resistivity	Expensive, requires organic solvents, paper can change mechanical properties
Paper cutting/shaping ³³⁻³⁷	~ 100	Low	High throughput, No chemicals are required for printing	Low mechanical stability, rely on solid supports, expensive
Drawing ^{2, 28, 31}	Very low	Very low	Simple, compatible with a variety of substrate materials	Low resolution, low precision
Dip-coating ^{38, 39}	Very low	Low	Rapid, simple, homogeneous reagent deposition	Consumes a lot of reagent, low precision
Vapor deposition ⁴⁰⁻⁴²	~ 800	Medium	One-step process, solventless, substrate independent	Requires expensive deposition masks, vacuum, time-intensive, low precision
Stamping ⁴⁴⁻⁴⁶	~ 600	Low	Rapid, low cost, special training not required	Lower resolution than other methods, requires thick (> 1mm thick hydrophobic barriers)

zero and can be ignored in equation 1.1; when valid, this assumption describes a substrate as being “fully wetted”.¹⁵⁰⁻¹⁵² It should also be noted that melting time and the amount of applied heat also impact wax viscosity, meaning that final barrier width is also a function of the initial amount of wax present and the temperature at which it’s melted. When patterning wax to delineate the borders of a hydrophilic channel in a porous material, the inner channel width (W_c) can be defined as the following:

$$W_c = W_p - 2L \quad (1.2)$$

where W_p is the printed hydrophobic barrier width and L is any additional distance molten wax spreads laterally through the substrate (perpendicular to substrate thickness).²⁸ A couple solutions have been proposed in the literature to increase patterning resolution, for example, nitrocellulose contains smaller, more uniform, pore sizes for more precise control over the melting process; channels as narrow as 300 μm have been fabricated with nitrocellulose.¹ Wax spreading can also be minimized by applying vacuum to the substrate.⁹ No matter what technique a researcher or manufacturer chooses, consideration should be given to factors like fabrication complexity, equipment availability, material costs, solvent/reagent compatibility, and the intended application of the analytical test. Some methods however, are far more versatile than others. Recent advancements in printing technology have increased the utility of inkjet printing for μPADs , beyond the fabrication methods listed in Table 1-2, to now include reagent patterning with high spatial resolution.

Reagent Deposition by Inkjet Printing

Inkjet printing has emerged as a powerful tool for patterning and depositing assay reagents on paper substrates. Picoliter-sized droplets create well-defined patterns (μm to cm) on the substrate,

and repeated printing cycles of one or more reagents can create layered patterns on paper. Furthermore, any commercial desktop printer is capable of printing multiple reagents simultaneously from four (magenta/yellow/cyan/black) or more color cartridges. Intense commercial interest has essentially led to two main modes of printing: continuous and drop-on-demand (DOD). There are advantages and limitations to each printing mode (including sub-modes) depending on end-user application. In continuous inkjet printing, droplet creation/ejection from a nozzle is constant and controlled by a high-pressure pump vibrating a piezoelectric crystal, commonly made from lead zirconium titanate. Signals from the printer selectively charge a fraction of the droplets, which deflect away from the printer nozzle and recirculate through the printer (no waste generated). Uncharged droplets get ejected onto the substrate (to form an image).¹⁵³ Continuous printing is efficient, particularly at high speeds, which is conducive for industrial applications requiring large volume printing. For laboratory-scale research and design, however, continuous printing systems are not cost effective. In contrast to continuous inkjet printing, DOD-mode printers eject reagent droplets only when necessary, are more cost feasible, print at higher patterning resolutions, consume less reagent (~ 20 µm droplet diameter), and do not require droplets to be charged for printing.¹⁵⁴ Only two modes of DOD printing have been used for µPAD research to date, thermal and piezoelectric, although thermal printing is seldom used because temperatures inside the ink cavity of a thermal-jet printer can reach 300 °C.¹⁵⁵ Biomolecules (e.g. proteins), which are commonly patterned on paper, can denature at much lower temperatures (40-80 °C).^{156, 157} To accommodate the printing of proteins, piezoelectric printers are used in which droplets are ejected by a voltage-induced pressure wave inside the ink cavity. Little heat is generated in the process, which protects heat-sensitive reagents. To date, most applications involving reagent printed materials – where the printed feature of the µPAD is not a hydrophobic

barrier – are biomedical,^{154, 158-161} very few demonstrations have been made of inkjet patterning for detecting analytes from environmental sources. Reported assay targets include: metals,¹⁶² volatile organic compounds,^{163, 164} phenolic compounds,¹⁶⁵ volatile food products,¹⁶⁶ and explosives.¹⁶⁷ Although important because they show the broad spectrum of reagents that can be deposited via inkjet printing, most of these works fail to showcase a unique advantage that automated inkjet patterning has compared with other patterning methods: simultaneous printing of multiple reagents. The presence of multiple ink cartridges would theoretically allow a user to configure the printer using the color dimension/intensity feature to achieve various outcomes: to deposit multiple reagents, to with varying reagent concentration (i.e., color transparency), to print a mixture/ratio of reagents from different cartridges, or to print a reagent gradient onto the substrate.¹⁵⁴ As recently demonstrated, only one example of multiple reagent mixing by printing has been shown.¹⁶⁸ In their work, Zhang et al. used inkjet printing to optimize the ratio of two enzyme combinations (glucose oxidase/horseradish peroxidase and diaphrose/alcohol dehydrogenase) to achieve the most effective bienzymatic colorimetric reactions. Printing reduced both optimization time and workload compared to standard procedures.

In work for my dissertation, I show for the first time that gradients of colorimetric reagents can be printed on paper substrates for improving measurement performance simply by adjusting color patterns in graphical software. Creating a gradient of patterned reagents with micrometer resolution using other application methods has proved very challenging to date. As shown in Figure 1-3, a colorimetric indicator can be deposited on filter paper where the change in indicator concentration per unit length (dC/dx) varies according to a user-defined continuous or piece-wise function. Small incremental changes in reagent concentration produce more (quantitative) data

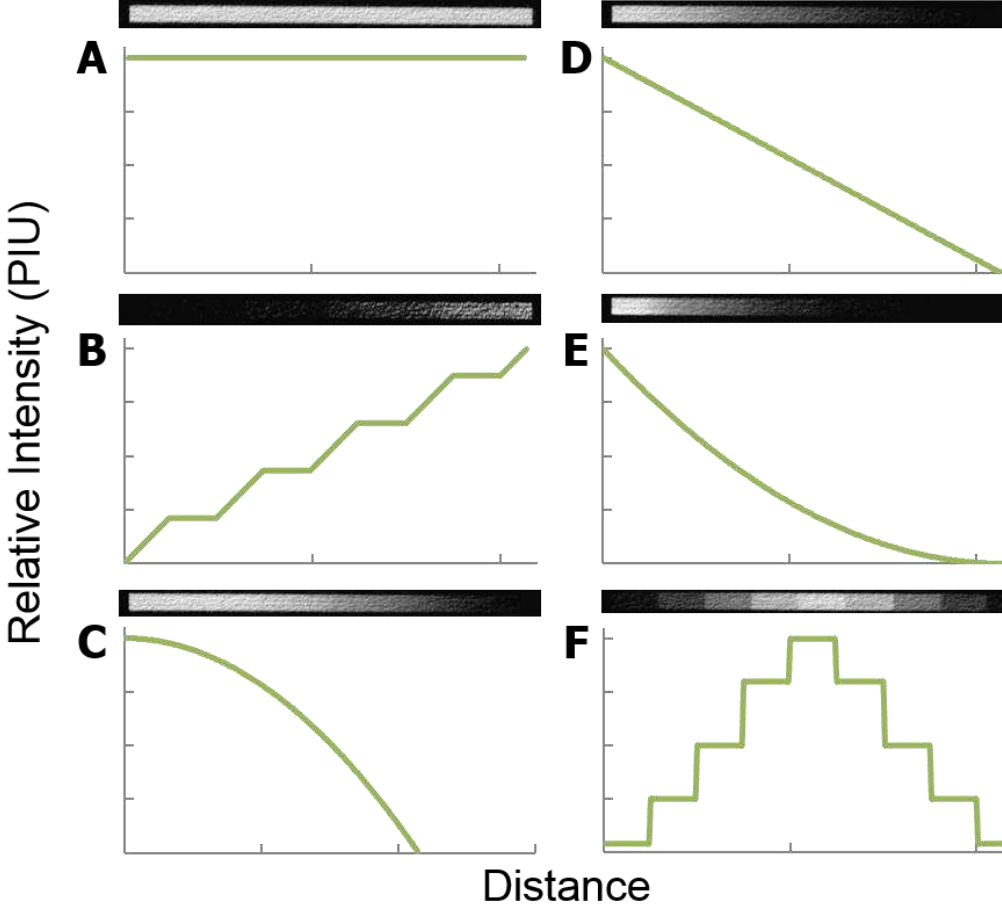


Figure 1-3 | Continuous and step-wise functions demonstrate the capacity of inkjet printing for precisely depositing reagents on a paper substrate. Plots depict printed ink intensity along a length of Whatman 1 filter paper; images show actual printouts in monochrome above each graph.

from an assay compared with a technique like “zone printing”, where reagents are spotted on the substrate as zones of homogeneous concentration. In this manner, the gradient elicits more information for the user than the zone approach, which essentially compresses information into “bins” of data. For biomedical applications, gradient printing also more closely mimics *in vivo* biology, where chemotaxis is often controlled via gradients of signaling molecules.

Detectors and Readout

For paper sensors to have an impact on the future of point-of-need medical or environmental diagnostics, data collection (i.e. assay readout), must be simple, inexpensive, and rapid. Early LFAs were popular because they provided a quick “yes/no” answer; however, lack of quantitative information has limited the reach of LFA technology. Although colorimetry – the most common analytical method of contemporary μPADs – is relatively simple, perception of color (i.e. hue) is subjective, which can lead to inaccuracies (false positives/ negatives) during analysis. Consequently, market demand has increased for measurement strategies that are not only inexpensive and portable, but also exhibit high detection sensitivity, throughput, automation, and inter-device reproducibility. Devices for detection and analysis that have been reported in the literature or in commercial space broadly fit into three categories: digital cameras/smartphones, handheld readers, and non-instrumented systems. A visual representation of some available technologies that fit into these categories is presented in Figure 1-4.

Bulky, benchtop instrumentation is typically too expensive for application in point-of-need settings. For instance, some μPAD technologies still use benchtop potentiostats, which can cost in excess of \$10,000, with commercially available handheld units costing >\$1000. If μPAD technology is to have an impact in the medical or environmental community, the cost-structure system for detectors must be much lower. To this end, several groups have designed custom handheld devices that are inexpensive and user-friendly for a variety of applications. Zhao et al.¹⁶⁹ built a custom low-cost eight-channel potentiostat for amperometric detection of glucose, lactate, and uric acid. The authors included a custom holder for a paper sensor with eight individual electrochemical wells. Though their design was based on previous work,¹⁷⁰ this system was the

first of its kind to incorporate the detection of multiple electrochemical assays simultaneously and from the same analyte sample. The current sensitivity ranged from 10's of nA to over 1 mA and the total unit cost was ~\$90. More recently, the number of channels in a handheld potentiostat was increased to 48.¹⁷¹ Other off-the-shelf handheld devices have also been reported for measuring water contamination electrochemically,¹⁷² or explosives via fluorometry.¹⁷³

The potential of telemedicine using μPADs was first demonstrated in 2008 for the determination of clinically relevant concentrations of glucose and protein in artificial urine.^{106, 174} Due to their market penetration and worldwide ubiquity, smartphones have created new opportunities for analysis in resource-limited settings either through on-site processing or remote data transfer to a centralized facility. Moreover, increased device data storage capacity enables information to be collected on-site and stored for transport to a central location without requiring sample relocation. Because modern smartphones possess both a light source (LED flash) and a digital camera for detection, they are also amenable for tasks typically performed with more expensive spectrophotometers, fluorometers, or silicon photodetectors.¹⁷⁵ Camera phones have recently been demonstrated for detection of phage and bacterial pathogens,¹⁷⁶⁻¹⁸⁰ pharmaceuticals,^{181, 182} biomarkers,¹⁸³⁻¹⁸⁷ explosives,¹⁸⁸ and toxic metals.^{108, 189} Although smartphones are superior to flatbed scanners with regards to portability, they suffer from changing ambient light conditions, rendering image intensities inconsistent. Recently, several groups addressed this problem by developing intensity-correction software for smartphones or by creating devices to physically block ambient light during image acquisition. In these examples, the phone's flash provides a (near) constant source of illumination by which to quantify assay results. For example, instead of using typical RGB intensity for quantification, Shen et al.¹⁹⁰ used chromaticity values to construct

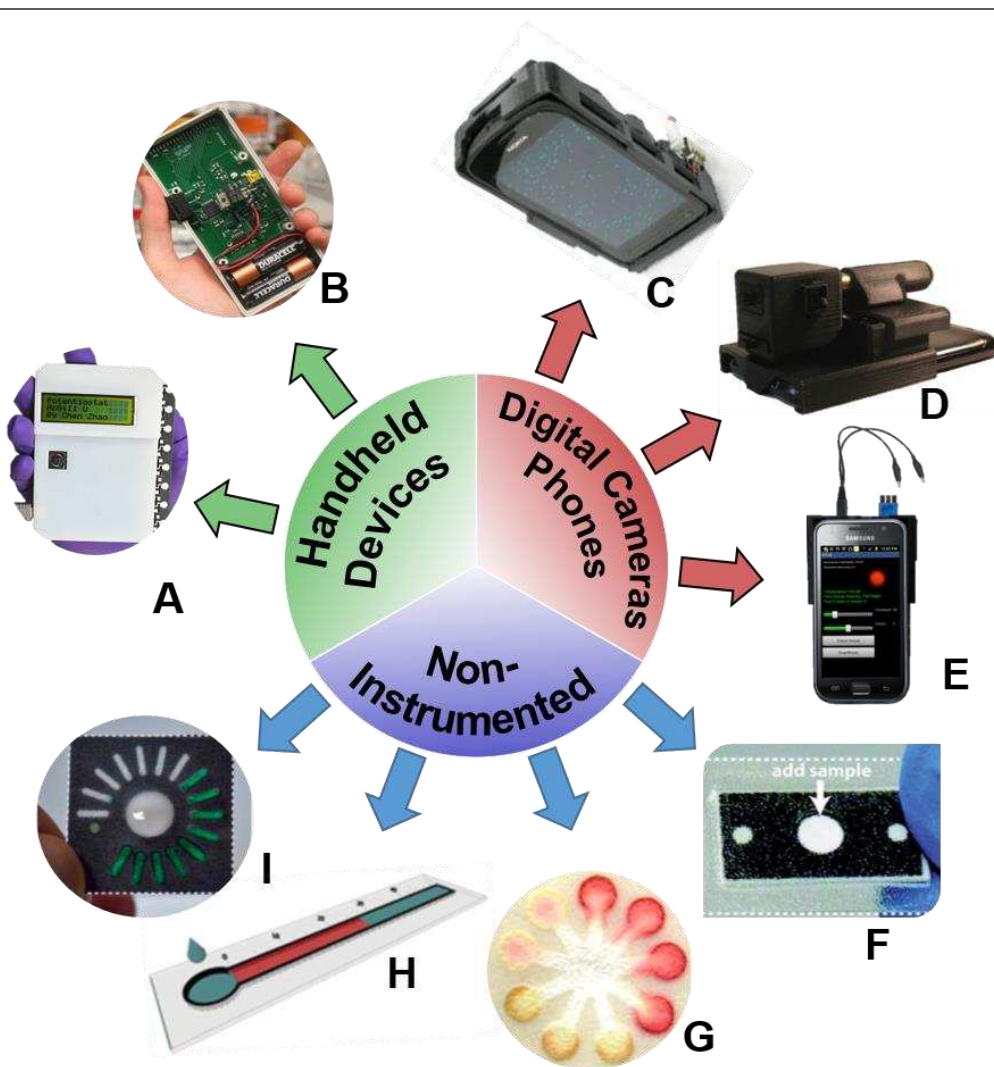


Figure 1-4 | Examples of devices and techniques for semi-quantitative to quantitative assay readout. Portable, handheld devices (A) Electrochemical biosensor array. Reproduced with permission from ref 144. Copyright 2013 IOP Publishing. (B) Handheld potentiostat. Reproduced with permission from ref 170. Copyright 2011 PLOS One. (C) Optical imaging of nanoscale objects with a cellphone. Reproduced with permission from ref 179. Copyright 2014 American Chemical Society. (D) An adapter on a smartphone measures fluorescence of albumin in urine. Reproduced with permission from ref 184. Copyright 2013 Royal Society of Chemistry. (E) Smartphone used to measure electrochemiluminescence. Reproduced with permission from ref 188. Copyright (2013), with permission from Elsevier. (F) Paper device using ‘time’ as a readout. Reproduced from ref 68 with permission from Royal Society of Chemistry. (G) Multiple colorimetric indicators for glucose. Reproduced with permission from ref 174 with permission from Elsevier. (H) Distance-based detection of nickel. Reproduced with permission from ref 66. Copyright 2013 with permission from the Royal Society of Chemistry. (I) Bar-code device. Reproduced with permission from ref 195. Copyright 2012 Wiley-VCH Verlag GmbH & Co. KGaA Weinheim.

a reference chart with known color spaces to compensate for measurement errors due to ambient light. To overcome their ambient light problem, Thom and coworkers¹⁹¹ modified a commercially available iPhone 4S case with a polyethylene tube designed to eliminate most incident light and ensure the most appropriate focal length for every acquired image. In a similar fashion, the Erickson laboratory^{181, 184} has used a modified attachment to a smartphone that included an internal reference to minimize lighting effects for quantifying biomarkers in sweat, saliva, and blood.

Although much work has been done to reduce the cost and increase the portability of external readers, another goal (particularly for point-of-need applications) is the development of accurate and easy-to-use devices that do not require external instrumentation. One approach for non-instrumented analysis is use of a visual color intensity comparator integrated with the device. Calibration standards can be external (e.g. reference card), or on-device.^{192, 193} Weaver et al.¹⁸² developed an inexpensive “color tab” test for rapid screening of potentially low-quality pharmaceutical drugs. Discreet patches of a colorimetric reagent reacted with a pharmaceutical wiped across the device; the intensity of the subsequent reaction (if any) was indicative of a counterfeit analyte. Another strategy called “barcode” reading has been developed that breaks the continuous flow path into discrete segments; the number of segments that change color are then counted to provide an indication of analyte concentration. In this case, the number of segments tallied is proportional to analyte concentration. This semi-quantitative approach has gained popularity due to its simplicity and applicability to a wide variety of chemistries. Since the first reported method for a paper-based digital readout,¹⁹⁴ groups have expanded this technique for other analytes.^{45, 195} Quantifying analyte concentration using “time” is another alternative detection method where the time taken for signal to develop is the performance metric. Lewis et al.¹⁹⁵

developed a system for quantifying active enzyme concentrations with high sensitivity using this timed readout approach. A control region was implemented to account for temperature, pressure, relative humidity, and sample viscosity effects. For example, if the recorded ambient temperature during the assay were <15°C, one additional minute was added to the vertical axis of the calibration curve to elicit the correct analyte measurement.

For my dissertation, I propose an alternate measurement strategy called distance-based detection for quantitative assessment of transition metals. Originally developed in 1985 by Zuk et al.¹⁹⁶ for measuring drugs in biological fluids, distance-based detection is a quantitative measurement technique relies on reading the length of a colored reaction product along a paper channel with the unaided eye. Each μPAD contains a sample reservoir and channel patterned with a colorimetric indicator specific for an analyte of interest. As analyte flows down the channel, insoluble complexes formed between metal and indicator precipitate, generating a colored band with a length proportional to analyte mass. Visual quantification is aided by a ruler printed beside each device, similar to reading temperature on a thermometer. The advantage this detection strategy has over instrumented methods is that it is highly amenable for mass distribution at the point of need. Large sample-size testing is more feasible with distance-based quantification methods compared with devices requiring instrumentation for analysis.

Determination of Transition Metals with μPADs

Paper-based approaches for environmental monitoring are attractive because accurate, low-cost monitoring is pivotal for environmental applications where routine testing is performed, such as for the analysis of river/soil contamination, occupational exposures, or air pollution. As shown in

Table 1-3 | Analytical methods for quantifying metals with μPADs.

Measurement Technique	Method Simplicity	Metal Species	LOD	Multiplexed Detection	Sample Matrix
Colorimetric	Easy-Moderate	Fe ²⁺ , Ni ²⁺ , Cu ²⁺	1-1.5 μg	Yes	medical incineration ash ¹⁶
		Fe ²⁺ , Ni ²⁺ , Cu ²⁺ , Cr	0.12-0.75 μg	Yes	road dust, welding fumes ¹⁹⁻²¹
		Cu ²⁺	0.06 ppm	No	tap water, mine tailings ⁴⁷
	Moderate	Hg ²⁺ , Cd ²⁺ , Pb ²⁺ , Ag ⁺ , Ni ²⁺ , Cu ²⁺ , Zn ²⁺ , Co ²⁺	10 ppm	Yes	sewage water ⁵⁰
		Hg ²⁺	0.01 ppm	No	pond and river water ^{51, 52}
	Moderate	As ³⁺	1×10 ⁻³ ppm	No	tap water ⁵³
		Pb ²⁺ , Cd ²⁺	0.25 ng	Yes	road dust ^{20, 54}
		Au ³⁺	1 ppm	No	gold-refining waste ⁵⁷
	Difficult	Pb ²⁺ , Zn ²⁺	1×10 ⁻³ ppm	Yes	aqueous solution ⁵⁹
		Pb ²⁺ , Cd ²⁺ , Cl ⁻	~1×10 ⁻³ ppm	No	juice, rainfall, soil ⁶⁰
ECL	Difficult	Pb ²⁺ , Hg ²⁺	2.1×10 ⁻⁷ ppm	Yes	lake water ⁶²
Distance (this work)	Easy	Fe ²⁺ , Ni ²⁺ , Cu ²⁺	1-5 μg	Yes	medical incineration ash, welding fumes ^{65, 66}
Time	Easy	Hg ²⁺ , Pb ²⁺	1×10 ⁻³ ppm	Yes	tap water ⁶⁸

Table 1-3, noted works have been published on detection of metal ions, chemical warfare agents, and reactive oxygen species using colorimetric,^{16, 162, 197-200} electrochemical,⁵⁹ fluorescent,²⁰¹ and other analytical approaches.²⁰² Samples were sourced from water, soil, and air (i.e. PM, PAHs). Colorimetry is easily the most widely used analytical technique for μPADs because in many cases,

a simple “yes/no” semi-quantitative result is sufficient for a point-of-need application. For many years it was the simplest (and least expensive) analytical method for paper-based detection because the only tools required for analysis are for image capture (e.g. scanner, camera-phone) and recording image intensity. New methods have been developed recently that challenge the notion that external instrumentation is necessary for analysis; methods based on recording the distance of a colored reaction with a ruler or by the timing of a colored reaction have lowered the cost of analysis and increased device portability.^{65, 66, 68}

In this dissertation, I describe the development of two μ PADs for colorimetric and distance-based detection of Cu, Ni, Fe, and Cr from welding fumes. The work described in the following chapters represents an attempt to address the shortcomings of traditional analytical methods for measuring the chemical composition of metals in workplace aerosols, namely, the cost and timeliness of exposure assessment. Chapter 2 discusses the creation of a four-arm μ PAD that was applied for colorimetrically quantifying metals in three different welding techniques, tungsten inert gas, metal inert gas, and stick (arc) welding. Filter samples acquired from welders were subjected to acid digestion methods outlined by the Occupational Safety and Health Administration and the Environmental Protection Agency. In chapters 3 and 4, distance-based detection of metals in welding fumes is demonstrated in single and multi-channel device formats. Single channel devices were developed to demonstrate the applicability of the method for metals, small molecules, and enzymatic assays. A three-channel μ PAD is shown in chapter 4 for simultaneously measuring Fe, Cu, and Ni from a single drop. Colorimetric reagents were deposited via inkjet printing as concentration gradients to offset nonlinear flowrates observed in capillary networks. Important variables that contribute to an analytical model describing the distance-based responses of chapters

3 and 4 is described in chapter 5. The intent of this work is to establish a theoretical framework for future research on the determination of metals with distance-based detection. Finally, the progress of the field in paper sensors is detailed in chapter 6, with emphasis on where the future of the technology is headed.

REFERENCES FOR CHAPTER 1

1. Y. Lu, W. Shi, J. Qin and B. Lin, *Anal. Chem.*, 2009, **82**, 329-335.
2. Y. Lu, W. Shi, L. Jiang, J. Qin and B. Lin, *ELECTROPHORESIS*, 2009, **30**, 1497-1500.
3. K. M. Schilling, A. L. Lepore, J. A. Kurian and A. W. Martinez, *Anal. Chem.*, 2012, **84**, 1579-1585.
4. L. Ge, S. Wang, X. Song, S. Ge and J. Yu, *Lab on a Chip*, 2012, **12**, 3150-3158.
5. A. W. Martinez, *Bioanalysis*, 2011, **3**, 2589-2592.
6. X. Yang, O. Forouzan, T. P. Brown and S. S. Shevkoplyas, *Lab on a Chip*, 2012, **12**, 274-280.
7. A. W. Martinez, S. T. Phillips, Z. Nie, C.-M. Cheng, E. Carrilho, B. J. Wiley and G. M. Whitesides, *Lab on a Chip*, 2010, **10**, 2499-2504.
8. K. Abe, K. Suzuki and D. Citterio, *Anal. Chem.*, 2008, **80**, 6928-6934.
9. X. Li, J. Tian, G. Garnier and W. Shen, *Colloids and Surfaces B: Biointerfaces*, 2010, **76**, 564-570.
10. A. Määttänen, D. Fors, S. Wang, D. Valtakari, P. Ihlainen and J. Peltonen, *Sensors and Actuators B: Chemical*, 2011, **160**, 1404-1412.
11. K. Maejima, S. Tomikawa, K. Suzuki and D. Citterio, *RSC Advances*, 2013, **3**, 9258-9263.
12. J. Wang, M. R. N. Monton, X. Zhang, C. D. M. Filipe, R. Pelton and J. D. Brennan, *Lab on a Chip*, 2014, **14**, 691-695.
13. K. Yamada, S. Takaki, N. Komuro, K. Suzuki and D. Citterio, *Analyst*, 2014, **139**, 1637-1643.
14. W. K. T. Coltro, D. P. de Jesus, J. A. F. da Silva, C. L. do Lago and E. Carrilho, *Electrophoresis*, 2010, **31**, 2487-2498.
15. J. Olkkonen, K. Lehtinen and T. Erho, *Anal. Chem.*, 2010, **82**, 10246-10250.
16. M. M. Mentele, J. Cunningham, K. Koehler, J. Volckens and C. S. Henry, *Anal Chem*, 2012, **84**, 4474-4480.
17. W. Dungchai, O. Chailapakul and C. S. Henry, *Analyst*, 2011, **136**, 77-82.
18. S. Wang, L. Ge, X. Song, J. Yu, S. Ge, J. Huang and F. Zeng, *Biosensors and bioelectronics*, 2012, **31**, 212-218.
19. D. M. Cate, P. Nanthalasurasak, P. Riwkulkajorn, C. L'Orange, C. S. Henry and J. Volckens, *Annals of occupational hygiene*, 2014, met078.
20. P. Rattanarat, W. Dungchai, D. Cate, J. Volckens, O. Chailapakul and C. S. Henry, *Anal. Chem.*, 2014, **86**, 3555-3562.
21. P. Rattanarat, W. Dungchai, D. M. Cate, W. Siangproh, J. Volckens, O. Chailapakul and C. S. Henry, *Anal Chim Acta*, 2013, **800**, 50-55.
22. E. Evans, E. F. M. Gabriel, W. K. T. Coltro and C. D. Garcia, *Analyst*, 2014, **139**, 2127-2132.
23. G. E. Fridley, H. Le and P. Yager, *Anal. Chem.*, 2014, **86**, 6447-6453.
24. E. Fu, P. Kauffman, B. Lutz and P. Yager, *Sensors and Actuators B: Chemical*, 2010, **149**, 325-328.
25. J. Nie, Y. Liang, Y. Zhang, S. Le, D. Li and S. Zhang, *Analyst*, 2013, **138**, 671-676.

26. P. Spicar-Mihalic, B. Toley, J. Houghtaling, T. Liang, P. Yager and E. Fu, *Journal of Micromechanics and Microengineering*, 2013, **23**, 067003.
27. A. W. Martinez, S. T. Phillips, M. J. Butte and G. M. Whitesides, *Angew Chem Int Ed Engl*, 2007, **46**, 1318-1320.
28. E. Carrilho, A. W. Martinez and G. M. Whitesides, *Anal. Chem.*, 2009, **81**, 7091-7095.
29. A. W. Martinez, S. T. Phillips, B. J. Wiley, M. Gupta and G. M. Whitesides, *Lab on a Chip*, 2008, **8**, 2146-2150.
30. L. OuYang, C. Wang, F. Du, T. Zheng and H. Liang, *RSC Advances*, 2014, **4**, 1093-1101.
31. C. Renault, J. Koehne, A. J. Ricco and R. M. Crooks, *Langmuir*, 2014, **30**, 7030-7036.
32. Y. Wu, P. Xue, K. M. Hui and Y. Kang, *ChemElectroChem*, 2014, **1**, 722-727.
33. C. L. Cassano and Z. H. Fan, *Microfluid. Nanofluid.*, 2013, **15**, 173-181.
34. E. M. Fenton, M. R. Mascarenas, G. P. López and S. S. Sibbett, *ACS Applied Materials & Interfaces*, 2008, **1**, 124-129.
35. D. L. Giokas, G. Z. Tsogas and A. G. Vlessidis, *Anal. Chem.*, 2014, **86**, 6202-6207.
36. A. C. Glavan, R. V. Martinez, E. J. Maxwell, A. B. Subramaniam, R. M. Nunes, S. Soh and G. M. Whitesides, *Lab Chip*, 2013, **13**, 2922-2930.
37. C. Renault, X. Li, S. E. Fosdick and R. M. Crooks, *Anal. Chem.*, 2013, **85**, 7976-7979.
38. J. Noiphung, T. Songjaroen, W. Dungchai, C. S. Henry, O. Chailapakul and W. Laiwattanapaisal, *Anal Chim Acta*, 2013, **788**, 39-45.
39. T. Songjaroen, W. Dungchai, O. Chailapakul and W. Laiwattanapaisal, *Talanta*, 2011, **85**, 2587-2593.
40. B. Chen, P. Kwong and M. Gupta, *ACS applied materials & interfaces*, 2013, **5**, 12701-12707.
41. G. Demirel and E. Babur, *Analyst*, 2014, **139**, 2326-2331.
42. P.-K. Kao and C.-C. Hsu, *Microfluid. Nanofluid.*, 2014, **16**, 811-818.
43. U. Pöschl, *Angewandte Chemie International Edition*, 2005, **44**, 7520-7540.
44. P. de Tarso Garcia, T. M. Garcia Cardoso, C. D. Garcia, E. Carrilho and W. K. Tomazelli Coltro, *RSC Advances*, 2014, **4**, 37637-37644.
45. Y. Zhang, C. Zhou, J. Nie, S. Le, Q. Qin, F. Liu, Y. Li and J. Li, *Anal. Chem.*, 2014, **86**, 2005-2012.
46. V. F. Curto, N. Lopez-Ruiz, L. F. Capitan-Vallvey, A. J. Palma, F. Benito-Lopez and D. Diamond, *RSC Adv.*, 2013, **3**, 18811-18816.
47. B. M. Jayawardane, d. L. Coo, W. R. Cattrall and D. S. Kolev, *Analytica chimica acta*, 2013, **803**, 106-112.
48. C. Samara and D. Voutsas, *Chemosphere*, 2005, **59**, 1197-1206.
49. M. Chin, *Atmospheric aerosol properties and climate impacts*, DIANE Publishing, 2009.
50. L. Feng, X. Li, H. Li, W. Yang, L. Chen and Y. Guan, *Anal Chim Acta*, 2013, **780**, 74-80.
51. A. Apilux, W. Siangproh, N. Praphairaksit and O. Chailapakul, *Talanta*, 2012, **97**, 388-394.
52. G.-H. Chen, W.-Y. Chen, Y.-C. Yen, C.-W. Wang, H.-T. Chang and C.-F. Chen, *Anal. Chem.*, 2014, **86**, 6843-6849.
53. P. Nath, R. K. Arun and N. Chanda, *RSC Advances*, 2014, **4**, 59558-59561.
54. J. Shi, F. Tang, H. Xing, H. Zheng, B. Lianhua and W. Wei, *Journal of the Brazilian Chemical Society*, 2012, **23**, 1124-1130.
55. C. I. Davidson, R. F. Phalen and P. A. Solomon, *Aerosol Science and Technology*, 2005, **39**, 737-749.

56. C. Monn, A. Fuchs, D. Högger, M. Junker, D. Kogelschatz, N. Roth and H.-U. Wanner, *Science of the Total Environment*, 1997, **208**, 15-21.
57. A. Apilux, W. Dungchai, W. Siangproh, N. Praphairaksit, C. S. Henry and O. Chailapakul, *Anal. Chem.*, 2010, **82**, 1727-1732.
58. S. Vedral, *Journal of the Air & Waste Management Association*, 1997, **47**, 551-581.
59. Z. Nie, C. A. Nijhuis, J. Gong, X. Chen, A. Kumachev, A. W. Martinez, M. Narovlyansky and G. M. Whitesides, *Lab on a Chip*, 2010, **10**, 477-483.
60. G. Lisak, J. Cui and J. Bobacka, *Sensors and Actuators B: Chemical*, 2015, **207**, 933-939.
61. W. Hinds, *Aerosol Technology*, John Wiley & Sons, Inc., 1999.
62. M. Zhang, L. Ge, S. Ge, M. Yan, J. Yu, J. Huang and S. Liu, *Biosensors and Bioelectronics*, 2013, **41**, 544-550.
63. J. Brown, K. Cook, F. G. Ney and T. Hatch, *American Journal of Public Health and the Nations Health*, 1950, **40**, 450-480.
64. G. Oberdörster, Z. Sharp, V. Atudorei, A. Elder, R. Gelein, W. Kreyling and C. Cox, *Inhalation toxicology*, 2004, **16**, 437-445.
65. D. M. Cate, W. Dungchai, J. C. Cunningham, J. Volckens and C. S. Henry, *Lab on a Chip*, 2013, **13**, 2397-2404.
66. D. M. Cate, S. D. Noblitt, J. Volckens and C. S. Henry, *Lab on a Chip*, 2015.
67. R. F. Dodson, M. A. Atkinson and J. L. Levin, *American journal of industrial medicine*, 2003, **44**, 291-297.
68. G. G. Lewis, J. S. Robbins and S. T. Phillips, *Chemical Communications*, 2014, **50**, 5352-5354.
69. R. M. Harrison and J. Yin, *Science of The Total Environment*, 2000, **249**, 85-101.
70. D. L. Costa and K. L. Dreher, *Environmental health perspectives*, 1997, **105**, 1053.
71. D. Voutsas and C. Samara, *Atmospheric Environment*, 2002, **36**, 3583-3590.
72. A. J. Fernández Espinosa, M. Ternero Rodríguez, F. J. Barragán de la Rosa and J. C. Jiménez Sánchez, *Atmospheric Environment*, 2002, **36**, 773-780.
73. R. E. Arku, K. L. Dionisio, A. F. Hughes, J. Vallarino, J. D. Spengler, M. C. Castro, S. Agyei-Mensah and M. Ezzati, *J Expo Sci Environ Epidemiol*, 2014, DOI: 10.1038/jes.2014.56.
74. D. I. Nelson, M. Concha-Barrientos, T. Driscoll, K. Steenland, M. Fingerhut, L. Punnett, A. Prüss-Üstün, J. Leigh and C. Corvalan, *American journal of industrial medicine*, 2005, **48**, 400-418.
75. A. K. Cho, C. Sioutas, A. H. Miguel, Y. Kumagai, D. A. Schmitz, M. Singh, A. Eiguren-Fernandez and J. R. Froines, *Environmental Research*, 2005, **99**, 40-47.
76. R. Quansah and J. J. Jaakkola, *International archives of occupational and environmental health*, 2009, **82**, 529-537.
77. J. M. Antonini, N. J. Lawryk, G. K. Murthy and J. D. Brain, *Journal of Toxicology and Environmental Health Part A*, 1999, **58**, 343-363.
78. I. J. Yu, K. J. Kim, H. K. Chang, K. S. Song, K. T. Han, J. H. Han, S. H. Maeng, Y. H. Chung, S. H. Park and K. H. Chung, *Toxicology letters*, 2000, **116**, 103-111.
79. J. Lockey, M. Schenker, D. Howden, M. Desmeules, R. Saracci, N. Sprince and P. Harber, *The American review of respiratory disease*, 1988, **138**, 1047.
80. A. Erdely, R. Salmen-Muniz, A. Liston, T. Hulderman, P. C. Zeidler-Erdely, J. M. Antonini and P. P. Simeonova, *Toxicology*, 2011, **287**, 153-159.

81. American Welding Society, Effects of Welding on Health VIII, <http://www.aws.org/w/a/>, (accessed 2015).
82. M. El-Zein, J. Malo, C. Infante-Rivard and D. Gautrin, *European Respiratory Journal*, 2003, **22**, 513-518.
83. M. El-Zein, J. Malo, C. Infante-Rivard and D. Gautrin, *Occupational and environmental medicine*, 2003, **60**, 655-661.
84. J. M. Antonini, A. B. Lewis, J. R. Roberts and D. A. Whaley, *American journal of industrial medicine*, 2003, **43**, 350-360.
85. J. J. Moulin, P. Wild, J. M. Haguenoer, D. Faucon, R. De Gaudemaris, J. M. Mur, M. Mereau, Y. Gary, J. P. Toamain and Y. Birembaut, *British journal of industrial medicine*, 1993, **50**, 234-243.
86. C. Botta, G. Iarmarcovai, F. Chaspoul, I. Sari-Minodier, J. Pompili, T. Orsiere, J. L. Berge-Lefranc, A. Botta, P. Gallice and M. De Meo, *Environmental and molecular mutagenesis*, 2006, **47**, 284-295.
87. M. R. Gomez, S. Cerutti, L. L. Sombra, M. F. Silva and L. D. Martínez, *Food and Chemical Toxicology*, 2007, **45**, 1060-1064.
88. H. Sińczuk-Walczak, M. Jakubowski and W. Matczak, *Int. J. Occup. Environ. Health*, 2001, **14**, 329-337.
89. R. M. Bowler, S. Nakagawa, M. Drezgic, H. A. Roels, R. M. Park, E. Diamond, D. Mergler, M. Bouchard, R. P. Bowler and W. Koller, *Neurotoxicology*, 2007, **28**, 298-311.
90. M. L. Newhouse, D. Oakes and A. Woolley, *British journal of industrial medicine*, 1985, **42**, 406-410.
91. B. Sjögren, T. Fossum, T. Lindh and J. Weiner, *International journal of occupational and environmental health*, 2002, **8**, 309-311.
92. B. Hilt, T. Qvenild and O. Rømyhr, *Norsk epidemiologi*, 1999, **9**.
93. E. Ibfelt, J. P. Bonde and J. Hansen, *Occupational and Environmental Medicine*, 2010, **67**, 772-777.
94. A. Sobaszek, C. Boulenguez, P. Frimat, H. Robin, J. M. Haguenoer and J.-L. Edme, *Journal of occupational and environmental medicine*, 2000, **42**, 923-931.
95. M. Abdel-Salam, *Journal of aerosol medicine*, 2006, **19**, 434-455.
96. J. H. Vincent, G. Ramachandran, Y. Thomassen and G. J. Keeler, *Journal of Environmental Monitoring*, 1999, **1**, 285-292.
97. U.S. Department of Labor, Metal and Metalloid Particulates in Workplace Atmospheres (ICP Analysis), http://www.osha.gov/dts/chemicalsampling/data/CH_276100.html, (accessed 2015).
98. Bureau of Labor Statistics, Occupational Employment and Wages, <http://www.bls.gov/oes/current/oes514121.htm>, (accessed 2015).
99. S. L. Zeger, D. Thomas, F. Dominici, J. M. Samet, J. Schwartz, D. Dockery and A. Cohen, *Environmental health perspectives*, 2000, **108**, 419.
100. J. Partington, *Journal of Roman Studies*, 1929, **19**, 267-268.
101. J. Davy, 1800.
102. M. Dou, S. T. Sanjay, M. Benhabib, F. Xu and X. Li, *Talanta*, 2015.
103. A. K. Yetisen, M. S. Akram and C. R. Lowe, *Lab on a Chip*, 2013, **13**, 2210-2251.
104. X. Li, D. R. Ballerini and W. Shen, *Biomicrofluidics*, 2012, **6**, 011301.
105. E. W. Nery and L. T. Kubota, *Analytical and bioanalytical chemistry*, 2013, **405**, 7573-7595.

106. A. W. Martinez, S. T. Phillips, E. Carrilho, S. W. Thomas III, H. Sindi and G. M. Whitesides, *Anal. Chem.*, 2008, **80**, 3699-3707.
107. J. C. Jokerst, J. A. Adkins, B. Bisha, M. M. Mentele, L. D. Goodridge and C. S. Henry, *Anal. Chem.*, 2012, **84**, 2900-2907.
108. Q. Wei, R. Nagi, K. Sadeghi, S. Feng, E. Yan, S. J. Ki, R. Caire, D. Tseng and A. Ozcan, *ACS nano*, 2014, **8**, 1121-1129.
109. P. W. West, *Industrial & Engineering Chemistry Analytical Edition*, 1945, **17**, 740-741.
110. H. Rheinboldt, *Die Methoden der Organischen Chemie*, Thieme Publishers, Leipzig, 3 edn., 1925.
111. H. G. Kunkel and A. Tiselius, *The Journal of general physiology*, 1951, **35**, 89-118.
112. 1902.
113. 1938.
114. H. Yagoda, *Industrial & Engineering Chemistry Analytical Edition*, 1937, **9**, 79-82.
115. M. H. Hashmi, F. Chughtai, N. A. Chughtai, A. Rashid and M. Shahid, *Mikrochim Acta*, 1968, **56**, 712-718.
116. R. H. Müller and D. L. Clegg, *Anal. Chem.*, 1949, **21**, 1123-1125.
117. H. Weil, *Kolloid-Zeitschrift*, 1953, **132**, 149-162.
118. H. Weisz, *Analyst*, 1976, **101**, 152-160.
119. D. A. Bruzewicz, M. Reches and G. M. Whitesides, *Anal. Chem.*, 2008, **80**, 3387-3392.
120. K. Abe, K. Kotera, K. Suzuki and D. Citterio, *Analytical and bioanalytical chemistry*, 2010, **398**, 885-893.
121. A. Böhm, M. Gattermayer, C. Trieb, S. Schabel, D. Fiedler, F. Miletzky and M. Biesalski, *Cellulose*, 2013, **20**, 467-483.
122. A. W. Martinez, S. T. Phillips and G. M. Whitesides, *Proceedings of the National Academy of Sciences*, 2008, **105**, 19606-19611.
123. J. Comer, *Anal. Chem.*, 1956, **28**, 1748-1750.
124. S. A. Butler, S. A. Khanian and L. A. Cole, *Clinical Chemistry*, 2001, **47**, 2131-2136.
125. N. Latman and B. Bruot, *Biomedical instrumentation & technology/Association for the Advancement of Medical Instrumentation*, 1988, **23**, 144-149.
126. K.-K. Fung, C. P.-Y. Chan and R. Renneberg, *Analytica chimica acta*, 2009, **634**, 89-95.
127. G. A. Posthuma-Trumpie, J. Korf and A. van Amerongen, *Analytical and bioanalytical chemistry*, 2009, **393**, 569-582.
128. J. Wu, Z. Fu, F. Yan and H. Ju, *TrAC Trends in Analytical Chemistry*, 2007, **26**, 679-688.
129. A. H. Ng, U. Uddayasankar and A. R. Wheeler, *Analytical and bioanalytical chemistry*, 2010, **397**, 991-1007.
130. P.-J. Tsai, T.-S. Shih, H.-L. Chen, W.-J. Lee, C.-H. Lai and S.-H. Liou, *Atmospheric Environment*, 2004, **38**, 333-343.
131. A. W. Martinez, S. T. Phillips, M. J. Butte and G. M. Whitesides, *Angewandte Chemie International Edition*, 2007, **46**, 1318-1320.
132. H. Tao, L. R. Chieffo, M. A. Brenckle, S. M. Siebert, M. Liu, A. C. Strikwerda, K. Fan, D. L. Kaplan, X. Zhang and R. D. Averitt, *Advanced Materials*, 2011, **23**, 3197-3201.
133. N. Ruecha, N. Rodthongkum, D. M. Cate, J. Volckens, O. Chailapakul and C. S. Henry, *Analytica chimica acta*, 2015, **874**, 40-48.
134. K. Bal, J. Fan, M. Sarkar and L. Ye, *International Journal of Heat and Mass Transfer*, 2011, **54**, 3096-3099.
135. D. R. Ballerini, X. Li and W. Shen, *Microfluid. Nanofluid.*, 2012, **13**, 769-787.

136. J. Cai and B. Yu, *Transport in porous media*, 2011, **89**, 251-263.
137. E. Fu, B. Lutz, P. Kauffman and P. Yager, *Lab Chip*, 2010, **10**, 918-920.
138. E. Fu, S. A. Ramsey, P. Kauffman, B. Lutz and P. Yager, *Microfluid. Nanofluid.*, 2011, **10**, 29-35.
139. K. T. Hodgson and J. C. Berg, *Journal of colloid and interface science*, 1988, **121**, 22-31.
140. J. Hu, S. Wang, L. Wang, F. Li, B. Pingguan-Murphy, T. J. Lu and F. Xu, *Biosensors and Bioelectronics*, 2014, **54**, 585-597.
141. D. Tanyolaç, B. I. Yürüksoy and A. R. Özdural, *Biochemical engineering journal*, 1998, **2**, 179-186.
142. P. Nibbering, J. Marijnen, A. Rapp, P. Leijh and R. Van Furth, *Histochemistry*, 1986, **84**, 538-543.
143. G. P. Jonsson, A. B. Hedin, P. L. Hakansson, B. U. Sundqvist, B. G. S. Saeve, P. F. Nielsen, P. Roepstorff, K. E. Johansson, I. Kamensky and M. S. Lindberg, *Anal. Chem.*, 1986, **58**, 1084-1087.
144. J. J. Leary, D. J. Brigati and D. C. Ward, *Proceedings of the National Academy of Sciences*, 1983, **80**, 4045-4049.
145. C. B. Harley, *Gene analysis techniques*, 1987, **4**, 17-22.
146. F. T. Carson, *MICROSCOPE*, 1940, **9**, 1.
147. A. Vesel, M. Mozetic, A. Hladnik, J. Dolenc, J. Zule, S. Milosevic, N. Krstulovic, M. Klanjšek-Gunde and N. Hauptmann, *Journal of Physics D: Applied Physics*, 2007, **40**, 3689.
148. A. W. Martinez, S. T. Phillips, G. M. Whitesides and E. Carrilho, *Anal. Chem.*, 2009, **82**, 3-10.
149. E. W. Washburn, *Physical review*, 1921, **17**, 273.
150. C. Reed and N. Wilson, *Journal of Physics D: Applied Physics*, 1993, **26**, 1378.
151. D. Shou, L. Ye, J. Fan and K. Fu, *Langmuir*, 2013, **30**, 149-155.
152. H. S. Wiklund and T. Uesaka, *Physical Review E*, 2013, **87**, 023006.
153. J. Li, F. Rossignol and J. Macdonald, *Lab on a chip*, 2015.
154. K. Yamada, T. G. Henares, K. Suzuki and D. Citterio, *Angewandte Chemie International Edition*, 2015, **54**, 5294-5310.
155. H. P. Le, *Journal of Imaging Science and Technology*, 1998, **42**, 49-62.
156. J. C. BISCHOF and X. HE, *Annals of the New York Academy of Sciences*, 2006, **1066**, 12-33.
157. A. W. Vermeer and W. Norde, *Biophysical Journal*, 2000, **78**, 394-404.
158. S. Z. Hossain, R. E. Luckham, A. M. Smith, J. M. Lebert, L. M. Davies, R. H. Pelton, C. D. Filipe and J. D. Brennan, *Anal. Chem.*, 2009, **81**, 5474-5483.
159. J. Wang, D. Bowie, X. Zhang, C. Filipe, R. Pelton and J. D. Brennan, *Chemistry of Materials*, 2014, **26**, 1941-1947.
160. S. Z. Hossain, R. E. Luckham, M. J. McFadden and J. D. Brennan, *Anal. Chem.*, 2009, **81**, 9055-9064.
161. S. Z. Hossain, C. Ozimok, C. Sicard, S. D. Aguirre, M. M. Ali, Y. Li and J. D. Brennan, *Analytical and bioanalytical chemistry*, 2012, **403**, 1567-1576.
162. S. M. Hossain and J. D. Brennan, *Anal Chem*, 2011, **83**, 8772-8778.
163. T. Soga, Y. Jimbo, K. Suzuki and D. Citterio, *Anal. Chem.*, 2013, **85**, 8973-8978.
164. B. Yoon, I. S. Park, H. Shin, H. J. Park, C. W. Lee and J. M. Kim, *Macromolecular rapid communications*, 2013, **34**, 731-735.

165. R. S. J. Alkasir, M. Ornatska and S. Andreescu, *Anal. Chem.*, 2012, **84**, 9729-9737.
166. H. Kwon, F. Samain and E. T. Kool, *Chemical Science*, 2012, **3**, 2542-2549.
167. J. Wang, L. Yang, B. Liu, H. Jiang, R. Liu, J. Yang, G. Han, Q. Mei and Z. Zhang, *Anal. Chem.*, 2014, **86**, 3338-3345.
168. Y. Zhang, F. Lyu, J. Ge and Z. Liu, *Chemical Communications*, 2014, **50**, 12919-12922.
169. C. Zhao, M. M. Thuo and X. Liu, *Science and Technology of Advanced Materials*, 2013, **14**, 054402.
170. A. A. Rowe, A. J. Bonham, R. J. White, M. P. Zimmer, R. J. Yadgar, T. M. Hobza, J. W. Honea, I. Ben-Yaacov and K. W. Plaxco, *PLoS ONE*, 2011, **6**, e23783.
171. I. Ramfos, N. Vassiliadis, S. Blionas, K. Efstathiou, A. Fragoso, C. K. O'Sullivan and A. Birbas, *Biosensors and Bioelectronics*, 2013, **47**, 482-489.
172. U. Kim, S. Ghanbari, A. Ravikumar, J. Seubert and S. Figueira, *IEEE Journal of Translational Engineering in Health and Medicine*, 2013, **1**, 1-7.
173. R. V. Taudte, A. Beavis, L. Wilson-Wilde, C. Roux, P. Doble and L. Blanes, *Lab on a Chip*, 2013, **13**, 4164-4172.
174. W. Dungchai, O. Chailapakul and C. S. Henry, *Analytica chimica acta*, 2010, **674**, 227-233.
175. E. H. Doeven, G. J. Barbante, E. Kerr, C. F. Hogan, J. A. Endler and P. S. Francis, *Anal. Chem.*, 2014, **86**, 2727-2732.
176. M. Funes-Huacca, A. Wu, E. Szepesvari, P. Rajendran, N. Kwan-Wong, A. Razgulin, Y. Shen, J. Kagira, R. Campbell and R. Derda, *Lab Chip*, 2012, **12**, 4269-4278.
177. B. Veigas, J. M. Jacob, M. N. Costa, D. S. Santos, M. Viveiros, J. Inacio, R. Martins, P. Barquinha, E. Fortunato and P. V. Baptista, *Lab Chip*, 2012, **12**, 4802-4808.
178. T. S. Park, W. Li, K. E. McCracken and J. Y. Yoon, *Lab Chip*, 2013, **13**, 4832-4840.
179. T.-T. Tsai, S.-W. Shen, C.-M. Cheng and C.-F. Chen, *Science and Technology of Advanced Materials*, 2013, **14**, 044404.
180. Q. Wei, H. Qi, W. Luo, D. Tseng, S. J. Ki, Z. Wan, Z. n. Göröcs, L. A. Bentolila, T.-T. Wu and R. Sun, *ACS nano*, 2013, **7**, 9147-9155.
181. S. Lee, V. Oncescu, M. Mancuso, S. Mehta and D. Erickson, *Lab on a Chip*, 2014, **14**, 1437-1442.
182. A. A. Weaver, H. Reiser, T. Barstis, M. Benvenuti, D. Ghosh, M. Hunckler, B. Joy, L. Koenig, K. Raddell and M. Lieberman, *Anal Chem*, 2013, **85**, 6453-6460.
183. A. K. Yetisen, J. L. Martinez-Hurtado, A. Garcia-Melendrez, F. da Cruz Vasconcellos and C. R. Lowe, *Sensors and Actuators B: Chemical*, 2014, **196**, 156-160.
184. V. Oncescu, D. O'Dell and D. Erickson, *Lab on a Chip*, 2013, **13**, 3232-3238.
185. A. F. Coskun, R. Nagi, K. Sadeghi, S. Phillips and A. Ozcan, *Lab on a Chip*, 2013, **13**, 4231-4238.
186. V. Oncescu, M. Mancuso and D. Erickson, *Lab on a Chip*, 2014, **14**, 759-763.
187. L. P. Cardoso, R. F. Dias, A. A. Freitas, E. M. Hungria, R. M. Oliveira, M. Collovati, S. G. Reed, M. S. Duthie and M. M. Stefani, *BMC infectious diseases*, 2013, **13**, 497.
188. M. Salles, G. Meloni, W. de Araujo and T. Paixão, *Analytical Methods*, 2014, **6**, 2047-2052.
189. J. L. Delaney, E. H. Doeven, A. J. Harsant and C. F. Hogan, *Anal Chim Acta*, 2013, **790**, 56-60.
190. L. Shen, J. A. Hagen and I. Papautsky, *Lab Chip*, 2012, **12**, 4240-4243.
191. N. K. Thom, G. G. Lewis, K. Yeung and S. T. Phillips, *RSC Adv*, 2014, **4**, 1334-1340.

192. X. Fang, S. Wei and J. Kong, *Lab Chip*, 2014, **14**, 911-915.
193. Y. Hao, W. Chen, L. Wang, B. Zhou, Q. Zang, S. Chen and Y.-N. Liu, *Analytical Methods*, 2014, **6**, 2478.
194. S. C. Lou, C. Patel, S. Ching and J. Gordon, *Clinical chemistry*, 1993, **39**, 619-624.
195. G. G. Lewis, M. J. DiTucci and S. T. Phillips, *Angewandte Chemie*, 2012, **124**, 12879-12882.
196. R. F. Zuk, V. Ginsberg, K. , T. Houts, R. Judith, H. Merrick, E. F. Ullman, M. M. Fischer, C. C. Sizto, S. N. Stiso and D. J. Litman, *Clinical Chemistry*, 1985, **31**, 1144-1150.
197. C. Díez-Gil, A. Caballero, I. Ratera, A. Tárraga, P. Molina and J. Veciana, *Sensors*, 2007, **7**, 3481-3488.
198. L. Li, H. Xiang, X. Zhou, M. Li and D. Wu, *Journal of Chemical Education*, 2012, **89**, 559-560.
199. D. Pardasani, V. Tak, A. K. Purohit and D. K. Dubey, *Analyst*, 2012, **137**, 5648-5653.
200. Y. Sameenoi, P. Panymeesamer, N. Supalakorn, K. Koehler, O. Chailapakul, C. S. Henry and J. Volckens, *Environmental Science & Technology*, 2013, **47**, 932-940.
201. Z. Gu, M. Zhao, Y. Sheng, L. A. Bentolila and Y. Tang, *Anal Chem*, 2011, **83**, 2324-2329.
202. C. H. Lee, L. Tian and S. Singamaneni, *ACS Appl Mater Interfaces*, 2010, **2**, 3429-3435.

CHAPTER 2: RAPID DETECTION OF TRANSITION METALS IN WELDING FUMES USING PAPER-BASED ANALYTICAL DEVICES

Chapter Overview

The overall goal of the research presented in this dissertation is to reduce the cost and timeliness of personal exposure assessment to metal-containing PM in welding fumes. One step towards that goal is described in this chapter with the development of a four-zone μ PAD for quantifying the content of Fe, Ni, Cu, and total Cr in welding fumes. Samples were acquired from various sources, analyzed, and results verified independently by ICP-OES. The work was published in *The Annals of Occupational Hygiene* and is reproduced here.¹ The color intensities of formation complexes between the metal analyte and detection reagents were analyzed by integrating the grayscale color intensity of the complex via desktop scanner. This demonstrated that inexpensive analysis of metals was feasible using paper-based analytic devices.

Metals in particulate matter (PM) are considered a driving factor for many pathologies. Despite the hazards associated with particulate metals, personal exposures for at-risk workers are rarely assessed due to the cost and effort associated with monitoring. As a result, routine exposure assessments are performed for only a small fraction of the exposed workforce. The objective of this research was to evaluate a relatively new technology, microfluidic paper-based analytical devices (μ PADs), for measuring the metals content in welding fumes in an occupational health setting. Fumes from three common welding techniques (shielded metal arc, metal inert gas, and tungsten inert gas welding) were sampled in two welding shops. Concentrations of acid extractable Fe, Cu, Ni, and Cr were measured and independently verified using inductively coupled - optical

emission spectrometry (ICP-OES). Results from the μ PAD sensors agreed well with ICP-OES analysis; the averages of the two methods agreed within 25% for all samples analyzed. Analytical costs for the μ PAD technique were approximately 50 times lower than market-rate costs with ICP-OES. Furthermore, the μ PAD method was capable of providing same-day results (as opposed to several weeks for ICP laboratory analysis). Results of this work suggest that μ PAD sensors are a viable and inexpensive alternative to traditional analytic methods for transition metals in welding fume particulate matter. These sensors have potential to enable substantially higher levels of hazard surveillance for a given resource cost, especially in resource-limited environments.

Introduction

Human exposure to metal-containing particulate matter (PM) in industries such as mining, construction, and manufacturing significantly impacts worker health. Occupational respiratory diseases cost approximately \$10B each year in the United States and result in approximately 425,000 premature deaths annually world-wide, though it is unknown the direct impact that metal exposures have on these figures.² Known pathologies include pneumoconiosis,^{3, 4} respiratory impairment and cardiovascular disease,⁵⁻⁸ ‘metal fume fever’,⁹⁻¹¹ and lung cancer.¹²⁻¹⁴ Of particular concern is exposure to welding fumes, known to contain hazardous levels of particulate metals such as hexavalent chromium, nickel, copper, nitrous oxide, manganese, and lead.¹⁵ Despite the risks posed by these inhalation hazards, welders’ exposure to particulate metals is infrequently assessed due to the high cost and effort associated with personal exposure measurement.⁶ Regulatory compliance monitoring for welding fumes calls for an 8-hr filter sample (collected within the worker’s breathing zone) followed by chemical analysis via flame atomic absorption or inductively coupled plasma emission spectrometry.¹⁶ Both of these techniques require large and

expensive instrumentation and highly trained staff, resulting in analysis costs of over \$100 per sample (depending on the number of analytes measured). These costs include sample preparation, sample analysis, and personnel time. In the developed world, such costs tend to preclude routine exposure assessments; in the developing world, these costs render the exposure assessment practically impossible. Furthermore, because collected samples must be shipped to a central laboratory for analysis, the time from sample collection to reporting (i.e., hazard communication) is typically on the order of several weeks. Consequently, there is a need for simple, sensitive, and cost-friendly alternatives for monitoring workers' exposure to PM metals that would enable broader screening of occupational exposures.^{17, 18} This need is particularly evident since such exposures tend to be spatiotemporally variable and log-normally distributed.¹⁹

There is growing demand for new exposure measurement approaches that are both affordable and available for use at the point-of-need. An emerging technology that may address this demand is microfluidic paper-based analytical devices (μ PADs),²⁰⁻²² a new technology platform for extremely low-cost sensing applications. The μ PAD concept is similar to 'lab-on-a-chip' technology, but in this case the 'chip' consists of cellulosic paper. In a typical μ PAD, hydrophobic barriers, printed onto the paper, define fluidic circuits that control liquid (sample) transport. These fluidic circuits are chemically modifiable and are therefore amenable to a variety of physical, chemical, and biological measurement applications.²³ Relative to traditional chemical assays, μ PADs require low reagent volumes (typically microliters), are simple to operate, portable, and inexpensive.²⁴⁻²⁷ Even at low production numbers, these devices often cost less than \$0.05 to produce. As a consequence of using small sample volumes, mass-based detection sensitivities in

paper devices are often comparable to or better than analogous detection moieties in traditional assays.^{28, 29}

One of the most common techniques for quantifying analytes on paper is colorimetry. Colorimetric sensors are attractive for analytical measurements because they offer a high-contrast signal that is easy to quantify with an external optical reader such as a scanner, camera, or smartphone.³⁰⁻³⁵ Several reports have focused on the detection of metals in water using nanoparticle aggregation³⁶⁻⁴⁰ and enzymatic action.⁴⁰ Our group was one of the first to extend colorimetry to paper devices for the measurement of Fe, Cu, and Ni in combustion ash samples.⁴¹ Functionalized AgNPs have been used to measure Cu on paper substrates with a reported linear detection range of $0.5 - 4 \times 10^{-6} \mu\text{g mL}^{-1}$.⁴⁰ Lateral flow chromatography systems have also been developed for measuring Cu, Cr, and Ni with 0.02, 0.15, and $0.23 \mu\text{g mL}^{-1}$ detection sensitivities respectively.³⁶

The objective here is to extend the application of colorimetric μ PADs to welding fumes and to the detection of total Cr. To demonstrate the utility of our method a paper sensor capable of measuring concentrations of acid-soluble Fe, Ni, Cu, and Cr with punches taken from air sampling filters was developed. A series of filter samples was taken at several welding facilities and analyzed concurrently using the μ PAD method and a standard technique: inductively coupled plasma – optical emission spectrometry (ICP-OES). Samples were collected from three separate welding processes (Tungsten Inert Gas [TIG], Metal Inert Gas [MIG], and Shielded Metal Arc Welding [SMAW]) with several common SAE stainless steel (SS) grades (304, 308, 309, and 17-4 PH). Analytical costs to quantify concentrations of 28 analytes and samples, combined, were on the order of \$20 for the μ PAD, compared to ~\$1000 using laboratory ICP-OES.

Methods

Chemicals and Materials

All chemicals were analytical grade and used as received without further purification. Iron(III) chloride hexahydrate, nickel(II) sulfate hexahydrate, aluminum(III) sulfate hydrate, copper(II) sulfate pentahydrate, phthalic anhydride, dimethylglyoxime (DMG), sodium acetate trihydrate, sodium fluoride, cerium (IV) ammonium nitrate, 1,5-diphenylcarbazide (1,5-DPC), and polydiallyldimethylammonium chloride (PDDA, medium molecular weight) were purchased from Sigma-Aldrich (St. Louis, MO, USA). Tris-hydrochloride and ammonium hydroxide were purchased from Mallinckrodt Baker, Inc. (Phillipsburg, NJ, USA). Glacial acetic acid was purchased from Fisher Scientific (Pittsburgh, PA, USA). Nitric acid (18.4 M) was purchased from EMD Millipore (Billerica, MA, USA). Milli-Q water from a Millipore deionized water generator ($R \geq 18.2 \text{ M}\Omega \text{ cm}^{-1}$) was used for all experiments. Mixed cellulose ester (MCE) filters were purchased from Fisher Scientific Company (Pittsburgh, PA, USA). Whatman No. 1 qualitative-grade filter paper was purchased from General Electric Company (Schenectady, New York).

Welding Fume Sampling

Samples were collected from SMAW, MIG, and TIG welding processes. Each welding technique used a different stainless steel alloy of varying composition of Cr, Fe, Cu, and Ni (Table 2-1). Information from the table comes from the manufacturer. Specifically, 304 SS was used for TIG welding, alloys of 304, 309-EL, and 17-4 PH were used for SMAW, and 304, 308, and 17-4 PH SS alloys were used for MIG welding. Area samples were taken on multiple days in the vicinity of each welding operation. Aerosol was sampled onto 37 mm mixed cellulose ester (MCE) filters (0.8 μm pore size) using a size-selective sampler (PM₁₀ PEM, SKC, Fullerton, CA, USA) designed

Table 2-1 | Percent composition of Ni, Cr, Cu, and Fe in the stainless steel alloys (SAE grade) used for collecting of welding fumes. Table information was provided from the manufacturer.

Alloy	% Nickel	% Chromium	% Copper	% Iron
304	8-10.5	18-20	0-1	> 50
308	10-12	19-21	Trace	> 50
309-EL	12-15	22-24	Trace	> 50
17-4 PH	3-5	15-17.5	3-5	> 50

to collect particles less than 10 µm in aerodynamic diameter. The sample air flow rate was 4 L min⁻¹ and sampling duration lasted approximately eight hours. In total, 15 filters were collected, extracted, and analyzed. Method validation was performed independently by ICP-OES on seven 10 mm punches taken from 37 mm diameter filters (Technology Laboratories, Fort Collins, CO, USA). To compare both µPAD and ICP-OES methods, filter punches were analyzed from the same filter. One of our assumptions was that PM was homogeneously distributed across the filter because two filter punch samples from the same filter (tested by ICP-OES) differed by less than 0.02 µg for each metal. For example, the measured levels of Cr, Ni, Fe, and Cu were 0.43 and 0.42, 0.17 and 0.19, 0.85 and 0.86, and less than 0.05 µg, respectively. Sample preparation and ICP-OES analysis followed EPA Methods 3050B and 6010B respectively. Metal content on the field blank filters was below the detection limit of the ICP instrument.

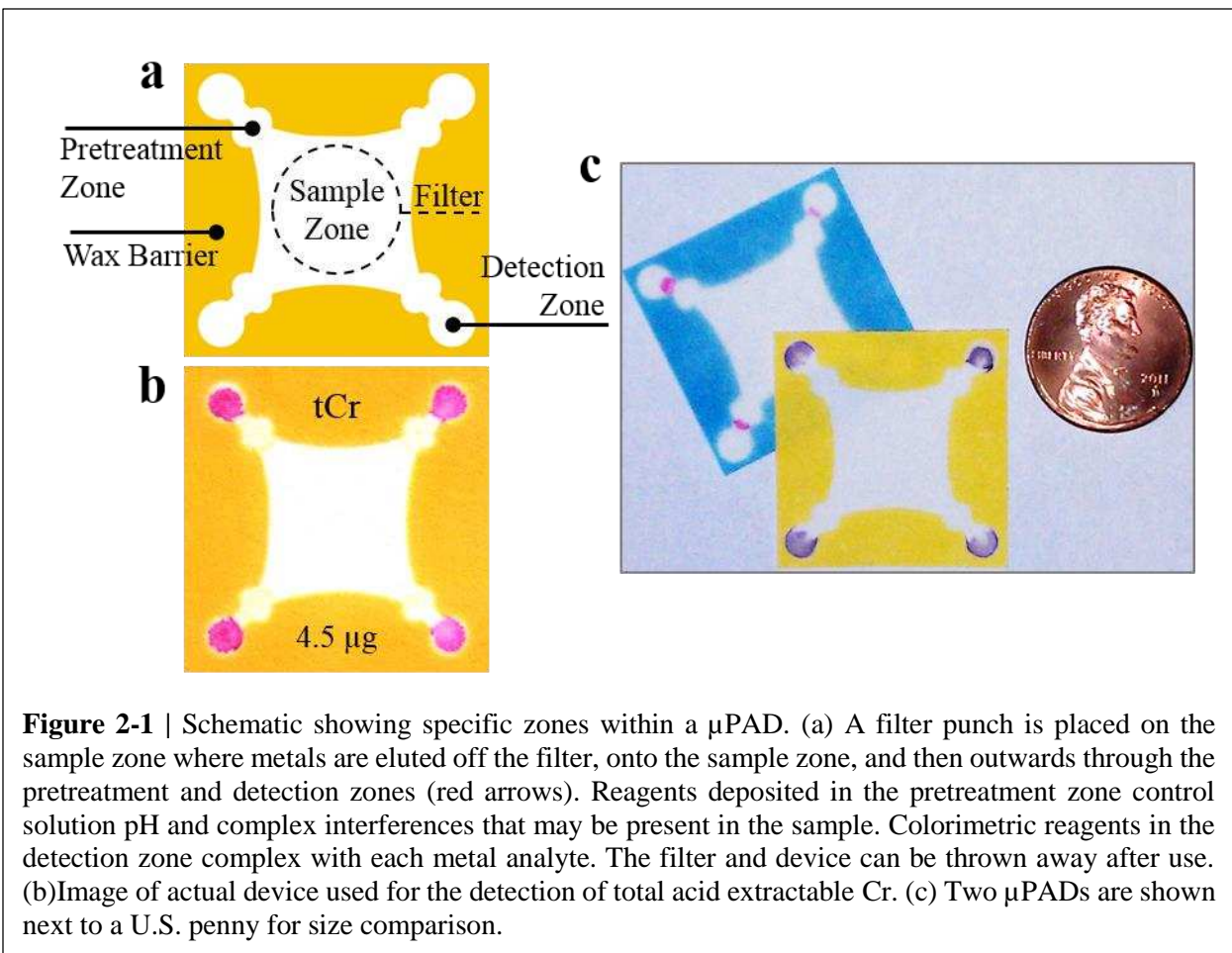
µPAD Fabrication and Colorimetric Assay

Paper devices were designed in CorelDraw and Adobe Illustrator and fabricated as shown in Figure 2-1a. Briefly, wax barriers were printed onto filter paper using a commercial wax printer (Xerox Colorqube 8870); these barriers were then melted into the paper (creating a 3D hydrophobic channel) by placing the paper onto a 150°C hotplate for 60 s.^{42, 43} After cooling, packing tape was

applied to one side of the filter paper to prevent reagents from leaking through the device. A picture of the device is provided (Figure 2-1c). Previously described reagent deposition protocols for detection of Fe, Ni, and Cu were followed.⁴¹ For determination of total acid extractable Cr, 0.5- μ L ceric (IV) ammonium nitrate (0.35 mM) was first added to the pretreatment zone twice, followed by 0.5 μ L of PDDA (5% w/v) which stabilized the Cr-1,5-DPC reaction product and decreased the mobility of the product complex in the detection zone.⁴⁴ A mixture of 15 mg mL⁻¹ 1,5-DPC and 40 mg mL⁻¹ phthalic anhydride was prepared in acetone and deposited once on the detection zone (0.5 μ L). The pretreatment and detection zones were dried between additions of reagent. In the presence of Cr (VI), the colorimetric reagent 1,5-DPC oxidizes to form diphenylcarbazone (DPCO); this compound then reacts with trivalent Cr to produce an intensely purple-hued complex, which easily discernable from the paper background. (Figure 2-1b).^{45, 46}

Filter Extraction and μ PAD Analysis

Following sample collection, 10 mm punches were taken from each filter and subjected to microwave-assisted acid digestion (Figure 2-2). Wetting and extraction efficiency was enhanced by pipetting 20 μ L of surfactant (SDS, 5 mM) onto each punch followed by air drying prior to sample digestion. To digest the metals in the welding fume, 5 μ L of concentrated HNO₃/SDS (5 mM) was added to the punch along with 30 μ L deionized water. Each punch was placed in a microwave (1100 W) for 15 s. A second water/SDS (5 mM) mixture (30 μ L) was again added to the punch (to keep the filter wet), followed by another 15 s in the microwave; this wetting/microwave step was repeated twice. After digestion, the filter punch was neutralized by adding 10 μ L of sodium bicarbonate (0.5 M, pH 9.5), dried, and placed on the sample zone of the μ PAD. For each test, a PDMS lid, designed to reduce eluent evaporation and to distribute pressure



evenly across the paper surface, was placed on top of filter-punch/ μ PAD. The lid also contained openings above the sample (3 mm diameter) and detection (5 mm diameter) zones for solvent/buffer addition. Acetate buffer (40 μ L, 0.1 M, pH 4.5) was next added to the sample zone and a 300 g weight was placed on the PDMS lid to help stabilize flow across the device. Metal detection was accomplished in approximately 20 minutes after the eluent had completely dried. Devices were then analyzed using a common flatbed scanner.

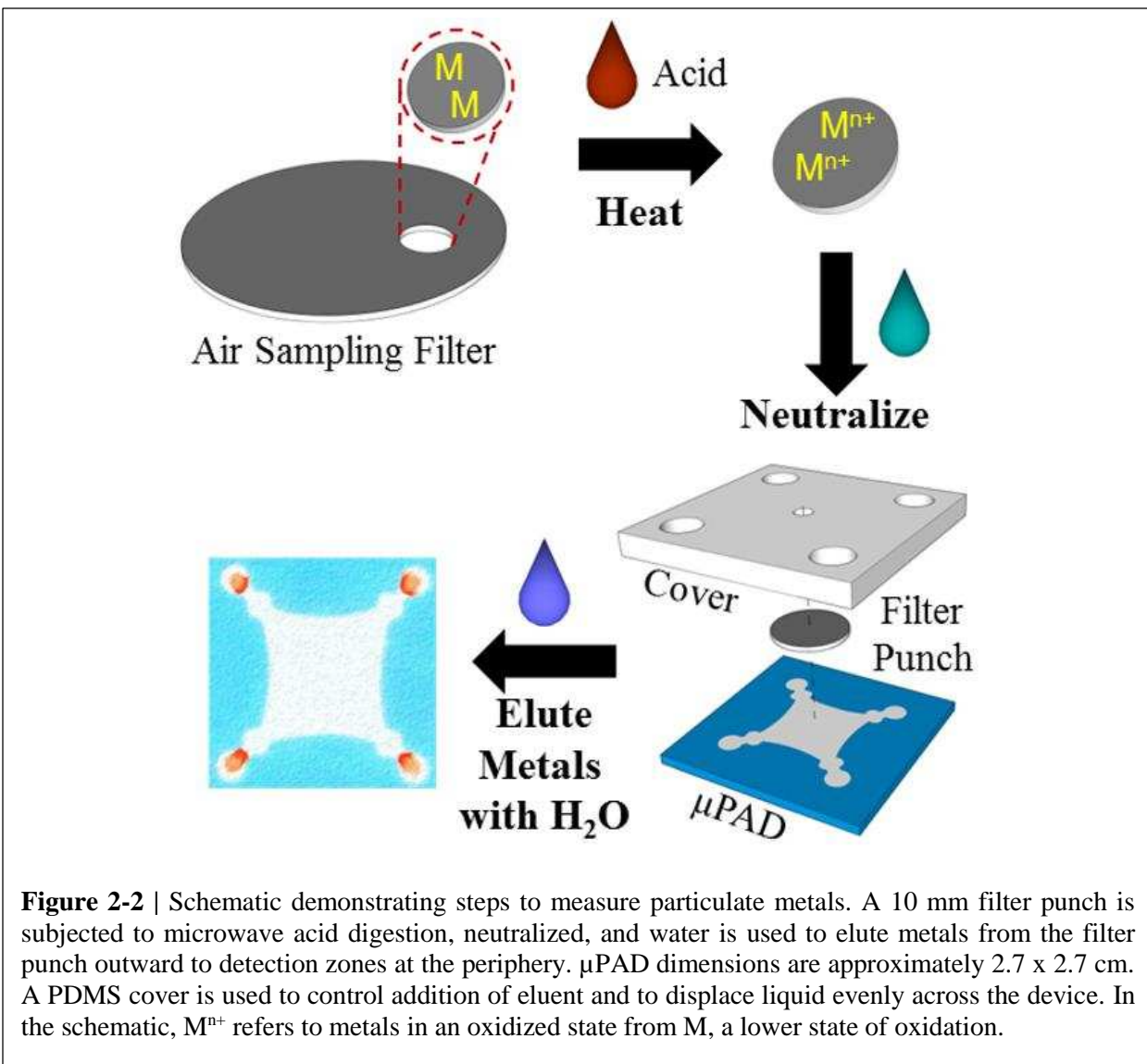


Image Processing

For quantitation, devices were scanned using a desktop flatbed scanner (XEROX DocuMate 3220), providing a high resolution, well-focused image. This detection method was chosen because office scanners are available worldwide and because scanned images are typically unaffected by external lighting conditions. A color thresholding window was applied to each image using Image J software⁴⁷ to remove background interferences from the paper. Wax backgrounds were chosen to

be the complementary color of the hue of the analyte complex being measured. A complementary colored background was easiest to remove using the thresholding window. Image intensity units selected for the thresholding window for each metal were: Fe (18-230), Ni (10-210), Cu (35-225), and Cr (0-180). Pure white and black backgrounds were considered 255 and 0 pixel intensity, respectively. After thresholding, images were inverted and the color intensity at each detection zone was measured as the arithmetic mean of pixel intensity. Measurements from all four detection zones were then averaged to yield a single result for each metal of interest. The process used for image analysis is detailed in Appendix 1.

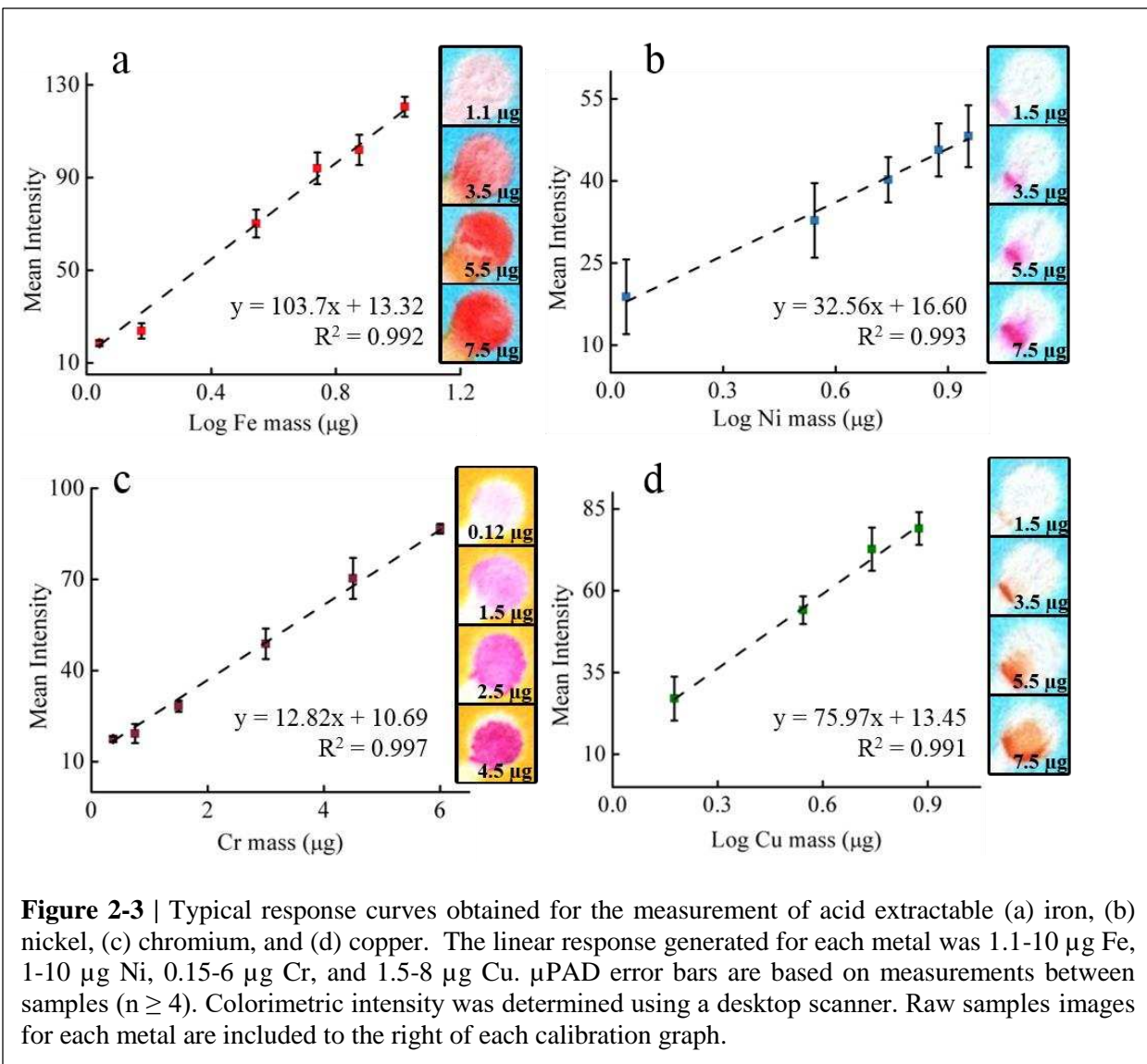
Data Analysis

Outliers were discarded when identified using Grubb's test for outliers.⁴⁸ Assumptions of normality and unequal variance were verified using chi-squared and F distribution tests. Minimum sample sizes for establishing calibration curves were determined using a power analysis ($1-\beta \geq 0.75$, $\alpha = 0.05$, using G*Power v3.1.9.2 software). Weighted linear regression was used to fit calibration curve data ($N \geq 4$). Deming regression was used to account for error for both μ PAD and ICP-OES detection methods; a software add-on package was installed for fitting the data (Excel 2010). Three filter punch samples were analyzed when comparing both methods.

Results

Metal Determination Using μ PADs

Calibration curves and analytic figures of merit were generated for each metal of interest. Iron was measured by the intensity of the reddish ferroin complex $[\text{Fe}(\text{phen})_3]^{2+}$ after complexation with 1,10-phenanthroline.⁴⁹ The detection limit for Fe was 1.1 μg with a linear range between 1.1 – 10



μg (Figure 2-3a) with a relative standard deviation of 7.7% (number of samples $N \geq 4$). Above 10 μg Fe, the color signal begins to saturate and a detection threshold is reached around 15 μg. Further increases in linear range could be achieved using different sized detection zones but this step was not required here. The range of measurement for μPAD-based quantification of Fe is 7.8 - 107 μg m⁻³ as a time weighted average (TWA) air concentration (based on a 4 L min⁻¹ sample collected over 8 hours). We also tested the inter-device variability of our method with Fe and Ni as the analyte (Figure 2-4). Over the course of nine days, calibration curves were generated across the

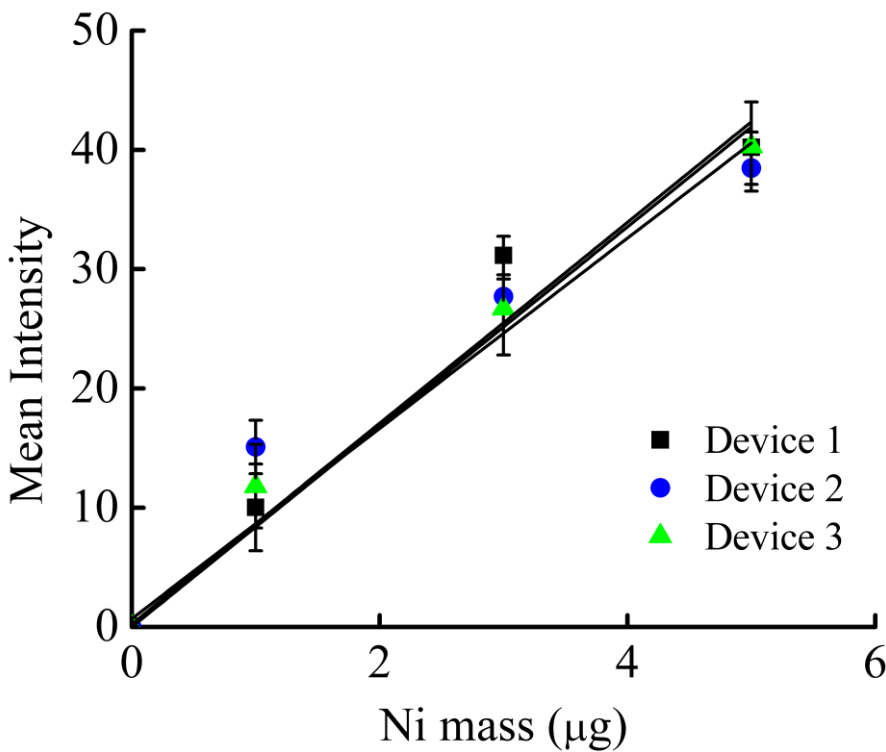


Figure 2-4 | Inter-device variability for Fe (top) and Ni (bottom) detection over three to four weeks. Intensity values are background subtracted. For Fe and Ni, the average difference in the slope for all linear regressed fits was $4.8 \pm 4.4\%$ and $9.7 \pm 5.2\%$ respectively. The average difference in measured intensity per mass of metal for Fe and Ni was 5.6 ± 5.7 and 1.5 ± 0.59 respectively.

working range of the assay. Reagents were made fresh each time. For Fe and Ni, the average difference in the slope for all linear regressed fits was $4.8 \pm 4.4\%$ and $9.7 \pm 5.2\%$ respectively. The average difference in measured intensity per mass of metal for Fe and Ni was 5.6 ± 5.7 and 1.5 ± 0.59 respectively.

Nickel was measured by recording the intensity of the magenta-colored complex formed by reaction with DMG (Figure 2-3b).⁵⁰ Acetic acid and NaF were added to the pretreatment zone as masking agents for Fe, Cu, and Co; as a result, these metals are sequestered upstream of the Ni detection zone. Analyte intensity was log linear with respect to Ni mass with a dynamic range of $1.1 - 9.0 \mu\text{g}$ ($7.8 - 64.2 \mu\text{g m}^{-3}$ TWA) and a relative standard deviation of 17.9% ($N = 4$). There

Table 2-2 | Chemical validation by ICP-OES compared to μ PAD measured metal content for each 10 mm filter punch. Particulate metal samples from three different welding processes (TIG, SMAW, and MIG) were collected and evaluated. Cu was not detected in any sample with either the μ PAD or the ICP instrument (0.05 μ g limit of detection). The content of all four transition metals of a filter blank was below ICP detection limits.

Metal	Welding Type	ICP-OES \pm SD (μ g)	μ PAD \pm SD (μ g)	Recovery %	Relative Standard Deviation _{μPAD} %
Fe	SMAW	9.52 \pm 1.43	9.45 \pm 1.00	99.3	10.6
	MIG	2.77 \pm 0.42	2.25 \pm 0.07	81.2	3.15
	TIG	1.55 \pm 0.23	1.21 \pm 0.11	78.1	9.42
Ni	MIG ^c	1.53 \pm 0.23	1.50 \pm 0.39	98.0	25.7
Cr	SMAW 1 ^b	2.01 \pm 0.30	1.81 \pm 0.44	90.0	24.4
	SMAW 2	0.86 \pm 0.13	0.81 \pm 0.35	94.0	43.8
	MIG	0.36 \pm 0.05	0.41 \pm 0.06	115.0	13.8
Cu		< 0.05	Too low	-	-

^b Three filter punches used for analysis

^c Two filter punches used for analysis

was no discernible color produced when a single filter punch was analyzed, so two punches were stacked, placed in the sample zone of the device and analyzed (Table 2-2). While this method decreases analytical precision somewhat, the inter-device relative standard deviation remains less than 20%. The largest detectable mass prior to color intensity saturation was 20 μ g, however this upper limit was outside the dynamic linear range of the test.

Total, acid-extractable Cr was measured using 1,5-DPC as the detection reagent (Figure 2-3c).⁵¹ The measured intensity was linear with respect to Cr mass with a range between 0.37 and 6 μ g and a relative standard deviation of 8.2% among repeated measurements. Three filter punches were stacked and analyzed simultaneously for one of the SMAW samples (Table 2-2), but only one punch was used for each of the other two welding fume samples for which Cr was measured. This method provided quantitative measurements of Cr air concentrations (based on an 8-hr TWA at a

4 L min^{-1} sample flow) in the range of $2.6 - 42.8 \mu\text{g m}^{-3}$. The detection limit was almost an order of magnitude lower for Cr than for Fe, due in part to the larger molar absorptivity of the Cr-1,5-DPC product ($4.6 \times 10^4 \text{ L mol}^{-1} \text{ cm}^{-1}$) compared to Fe-1,10-Phen ($1.1 \times 10^4 \text{ L mol}^{-1} \text{ cm}^{-1}$).^{52, 53}

For the detection of copper, bathocuproine was used to produce an orange-brown complex with Cu^{2+} (Figure 2-3d).^{41, 54, 55} We were able to detect Cu reproducibly at masses as low as $1.5 \mu\text{g}$. The dynamic range for analyte measurement as a TWA is $10.7 - 121.2 \mu\text{g m}^{-3}$. The PEL for Cu exposure is $100 \mu\text{g m}^{-3}$, which is within the dynamic range of the test. However, Cu was not detected on any field samples by either the ICP-OES or paper-based methods. The PAD sensors are stable when stored (in the dark and at 25°C) for $7 - 30$ days, depending on which reagents are added to the PAD. The PADs for detection of Cr can be stored and used for up to 30 days, whereas the PADs for Cu can be stored for up to seven days without significant loss of functionality.⁵⁶

Method Validation

Filter samples were collected from three SS welding processes (TIG, MIG, and SMAW) using three of the most commonly used SS alloys (304, 309, and 17-4 PH) in the welding industry. Levels of Fe, Ni, Cu, and total (acid extractable) Cr were then quantified using both μPAD and ICP-OES methods. In total, 28 analytes were measured from seven filter punches. Results of these tests are presented in Table 2-2 and shown in a 1:1 plot in Figure 2-5. For all seven punches analyzed, the average metal mass determined by μPAD detection was within 25% of the ICP-OES-determined average. According to the National Institute for Safety and Health handbook of analytical methods, a viable method for determining concentrations of airborne metals must have over 75% accuracy for 95% of samples measured, for which the paper sensing method is in compliance.⁵⁷ Detectable

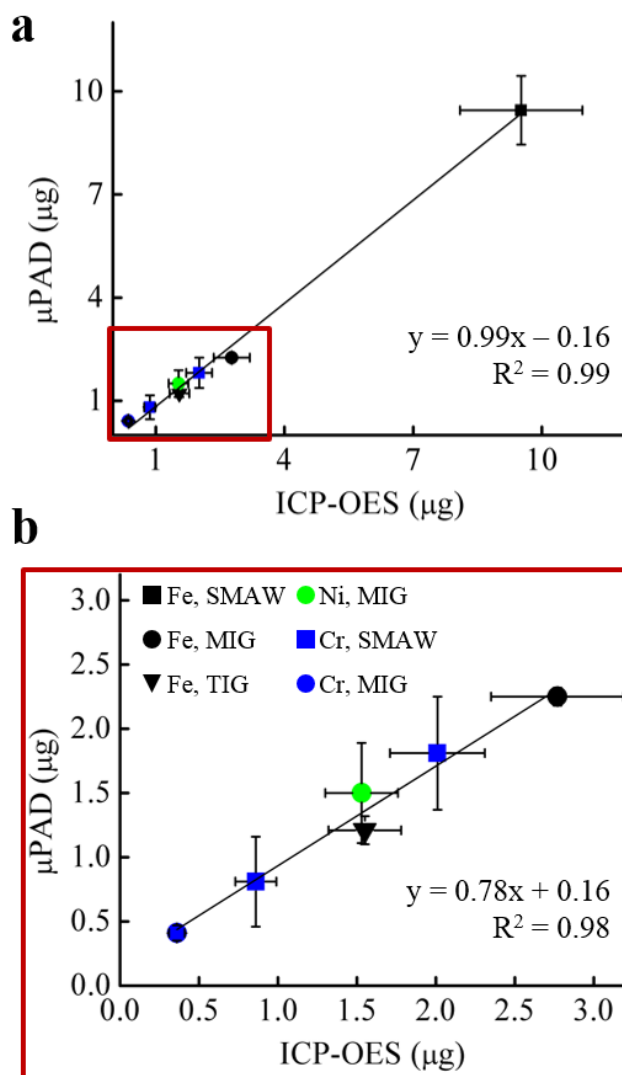


Figure 2-5 | (a) Paper-based measurement of Fe, Ni, and Cr compared with independent validation by ICP-OES. Cu was present below the detection limit of both measurement methods and was thus not presented. (b) An expanded view of the graph above shows that on small a smaller mass scale, method correlation is slightly worse ($R^2 \sim 0.98$), however this value is still within acceptable limits according to the NIOSH manual of analytical methods.

levels of Cu were not seen using either method, indicating that Cu levels were below the detection limit of the ICP instrument ($0.4 \mu\text{g L}^{-1}$). This result was not surprising because Cu is only present in significant quantity in few SS alloys and as a result, personal exposure to Cu is not considered a primary danger to welders.

Discussion

This is the first reported method, to our knowledge, for speciating metal aerosols quickly and at low-cost. Similar to gas detector tubes, our method requires little lab turnaround time, is simple to operate, and was developed specifically to make exposure assessment quicker, easier, and cost effective. The dynamic range of our screening method (two orders of magnitude) does not yet match traditional instrumentation such as ICP, however there remains great potential for μ PAD techniques to offer rapid, on-site analysis (similar to gas detection tubes) enabling more frequent and thorough monitoring of occupational environments.

Currently, the cost and time associated with occupational exposure assessment represent a significant impediment towards adequate hazard surveillance. According to the Department of Labor, in 2012 there were approximately 329,710 welders, cutters, solderers, and brazers in the U.S.⁵⁸ The analytical costs (not including personnel time and equipment) to assess each individual's exposure just once and to a single metal species would exceed \$33,000,000 per year. In contrast, the μ PAD method described here has the potential to reduce analytical costs by a factor of 50. This method is also amenable for rapid, on-site detection immediately following sample collection. Results presented here are encouraging, from the standpoints of detection sensitivity and method repeatability.

The linear detection range for Fe is sufficient for occupational exposure assessment, given that the personal exposure limit (PEL) stipulated by the OSHA is 10,000 $\mu\text{g m}^{-3}$ for Fe. Because each test uses a single 10 mm filter punch, several assays can be performed from a single 37 mm MCE filter should it be necessary to re-evaluate filter samples (or send samples to a lab for independent

validation). We were not able to assess method accuracy for Cu, since all samples were below the detection limit. For Fe, Ni, and Cu, the relationship between colorimetric intensity and analyte mass is presented as log-linear due to the characteristics of color saturation on paper. It is important to note that the dynamic ranges reported in Figure 2-3 do not represent the entire dynamic range of the method, but only the range necessary for the processed samples.

The dynamic range of the μ PAD method (for all four analytes) reported here is constrained by molar absorptivity of the colorimetric reagent (lower end) and signal saturation (upper end), highlighting a limitation of colorimetric sensing on paper. When the paper surface becomes saturated with analyte (as is the case in the detection zones), the resulting intensity reaches a threshold limit. Although the detection limits reported here are adequate for monitoring personal exposure at levels below the OSHA regulated limits, a larger dynamic detection range may be desired, especially for short-term sampling. The upper end of the dynamic range may be extended by increasing the size of the detection zone; larger paper surface area equates to slower surface saturation (more area for color development). In addition, multiple punches may be analyzed simultaneously (i.e., stacked onto the μ PAD) to extend the detection limit to lower masses.⁵⁶ Yet another option for improving device sensitivity is to design a μ PAD with multiple detection zones of varying size.

Although we report total Cr mass here, the 1,5-DPC reagent is specific to hexavalent chromium (Cr-VI) and thus, future application of this technology could assess exposures to the more toxic Cr-VI. Unfortunately, the ICP validation method we chose could not speciate between different Cr oxidation states. To measure Cr(VI) via μ PAD, the same protocol could be followed, but

tetravalent cerium (Ce(IV)) could be excluded from the pretreatment zone. Tetravalent cerium oxidizes soluble Cr(III) to Cr(VI) for complexation with 1,5-DPC, and thus, in the absence of Ce(IV), only Cr(VI) from the original sample is measured.⁵¹ As a result, this method shows promise for measurement of total soluble Cr or soluble Cr(VI). Future work will investigate Cr speciation using μPADs.

Several interfering metals present in welding fumes have the ability to complex with the chromophores in the detection zones. In previous work, we discussed our approach to ‘masking’ these interferences on paper using pre-treatment zones.⁴¹ For Cr VI, we investigated potential interferences from Mg, Mn, Zn, Al, Ba, V, Co, Cu, Fe, and Ni, and found that there was no significant effect for determination of Cr VI when other metals were present in metal:Cr VI ratios less than 4:1.⁵⁶ This concentration ratio is reasonable for welding fume because Fe is usually the largest constituent in most welding fumes and is almost never present at four times the concentration of Cr, which typically represents 15-22% of welded metals. Examination of the 1:1 plot in Figure 2-5 indicates that interferences from other metals presented only a minor influence for analyte detection on paper, if at all.

Conclusions

The μPAD presented here offers a much simpler and less expensive alternative for measuring human exposure to toxic metals than current methods. Colorimetric detection provides a convenient, portable, and rapid way to quantify exposure at the point of need, whereas current methods require more expensive and lengthy, offsite analyses. This μPAD sensor enables sensitive determination of Fe, Cu, Ni, and Cr for ~50 times less cost than ICP-based methods. Consequently,

μ PADs show great potential as an enabling technology for low-cost, high throughput sensing. Future work will focus on method modifications to improve sensitivity, quantitative range, and functionality, in addition to extending this method to other species. Ultimately, paper-based sensors may enable more comprehensive hazard recognition and surveillance worldwide. This technology appears well suited for resource limited environments, where improvements in workplace safety can be challenging. However, several obstacles must be overcome before exposure assessment costs are low enough for more widespread sampling and analysis; for example, the costs associated with personal sampling pumps and size-selective inlets are still relatively high. Additionally, sample preparation included microwave-assisted acid digestion which, in its current state of development, is not field-ready. Future improvements must be made to control liquid handling of strong bases and acids such that a minimally trained individual in the field can perform all sample preparation processes without undue risk to themselves. The vision for the future of μ PAD-based assessment of airborne metals is that field analysis of metal analytes on filters could be performed by industrial hygienists having little technical training in chemistry or microfluidic fields.

Closing Comments

Further efforts were made after the completion of this work on the development of detection chemistry for manganese (Mn), a metal toxic in high doses, commonly found both in aquatic and occupational environments.⁵⁹ Welding is a recognized source of exposure to Mn. Although Mn is an essential trace metal, elevated concentrations ($> 5 \text{ mg m}^{-3}$) of Mn are associated with neurotoxicity and diseases with Parkinson's-like symptoms.⁶⁰ Even low exposure levels ($< 0.5 \text{ mg m}^{-3}$) have been linked with some systematic neurological changes in individuals like mood swings,

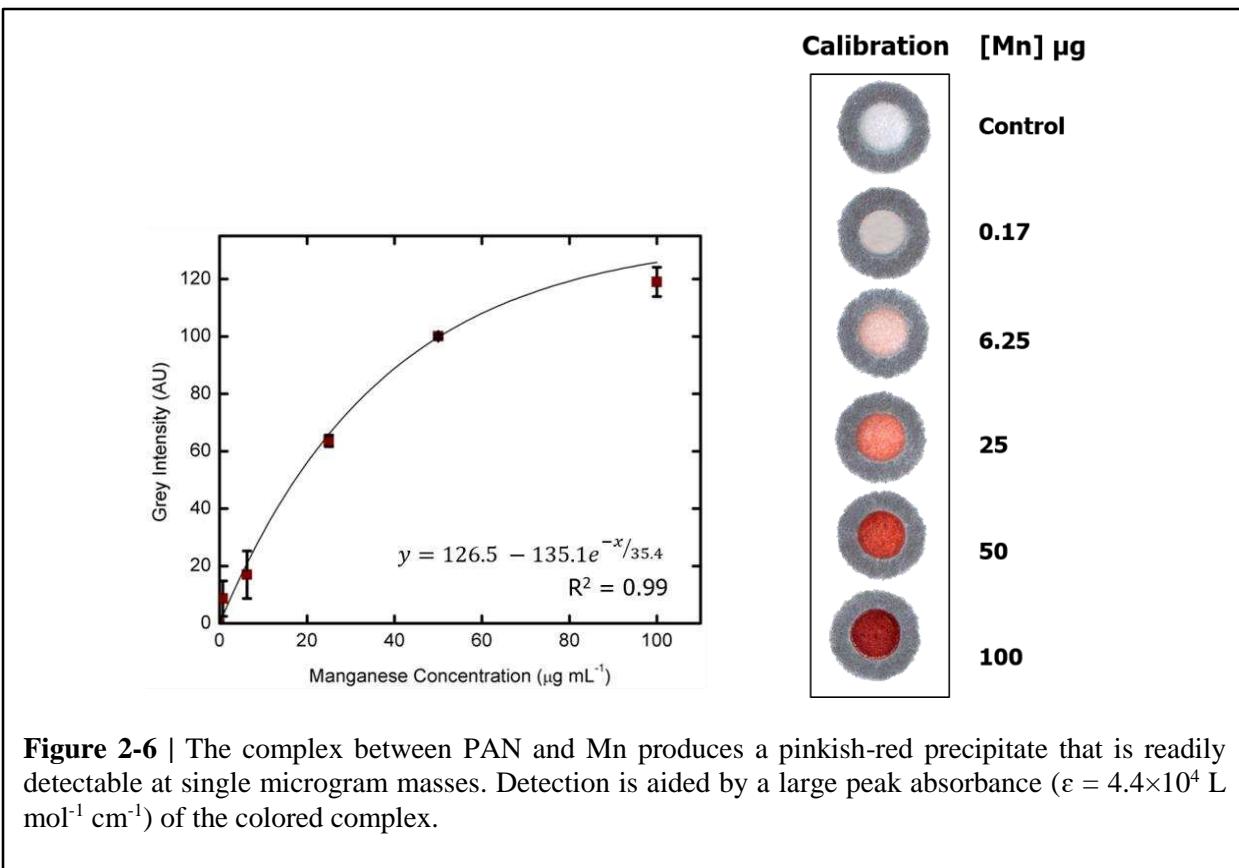


Figure 2-6 | The complex between PAN and Mn produces a pinkish-red precipitate that is readily detectable at single microgram masses. Detection is aided by a large peak absorbance ($\epsilon = 4.4 \times 10^4 \text{ L mol}^{-1} \text{ cm}^{-1}$) of the colored complex.

short term memory loss, and lower hand-eye coordination/ reaction time. Establishing a causative link between Mn exposure and associated health effects has proven difficult because resource and fiscal costs associated with workplace sampling are simply too high for large-scale studies. For this work, spot tests on paper were developed for measuring soluble Mn in aqueous media using 1-(2-pyridylazo)-2-naphthol (PAN), a colorimetric reagent known to chelate Co, Cu, Pd, V, U, and Mn (Figure 2-6).⁶¹ With this method, as little as 5 μg Mn was detectable via the desktop scanner.

REFERENCES FOR CHAPTER 2

1. D. M. Cate, P. Nanthalasurasak, P. Riwkulkajorn, C. L'Orange, C. S. Henry and J. Volckens, *Annals of occupational hygiene*, 2014, **58**, 413-423.
2. D. I. Nelson, M. Concha-Barrientos, T. Driscoll, K. Steenland, M. Fingerhut, L. Punnett, A. Prüss-Üstün, J. Leigh and C. Corvalan, *American Journal of Industrial Medicine*, 2005, **48**, 400-418.
3. H. Frank, R.-H. Monika, W. Tobias, L. Martin, G. Katarzyna, K. Benjamin, H. Volker, H. Jana, P. Beate, B. Thomas and W. S. G. the, *Journal of Breath Research*, 2012, **6**, 027105.
4. F. Della Torre, M. Cassani, M. Segale, G. Scarpazza, R. Pietra and E. Sabbioni, *Respiration*, 1990, **57**, 248-253.
5. J. I. Phillips, F. Y. Green, J. C. A. Davies and J. Murray, *American Journal of Industrial Medicine*, 2010, **53**, 763-767.
6. S. H. Gavett and H. S. Koren, *International Archives of Allergy and Immunology*, 2001, **124**, 109-112.
7. E. Ibfelt, J. P. Bonde and J. Hansen, *Occupational and Environmental Medicine*, 2010, **67**, 772-777.
8. J. Szram, S. J. Schofield, M. P. Cosgrove and P. Cullinan, *European Respiratory Journal*, 2012, DOI: 10.1183/09031936.00206011.
9. S. Mehta, R. Shende and B. Sampat, *CHEST Journal*, 2012, **142**, 1002A-1002A.
10. K. Kunimasa, M. Arita, H. Tachibana, K. Tsubouchi, S. Konishi, Y. Korogi, A. Nishiyama and T. Ishida, *Internal Medicine*, 2011, **50**, 2035-2038.
11. J. R. Cain and R. M. Fletcher, *Occupational Medicine*, 2010, **60**, 398-400.
12. K. Jomova and M. Valko, *Toxicology*, 2011, **283**, 65-87.
13. P. C. Zeidler-Erdely, L. A. Battelli, R. Salmen-Muniz, Z. Li, A. Erdely, M. L. Kashon, P. P. Simeonova and J. M. Antonini, *Journal of Toxicology and Environmental Health, Part A*, 2011, **74**, 728-736.
14. A. Mannetje, P. Brennan, D. Zaridze, N. Szeszenia-Dabrowska, P. Rudnai, J. Lissowska, E. Fabiánová, A. Cassidy, D. Mates, V. Bencko, L. Foretova, V. Janout, J. Fevotte, T. Fletcher and P. Boffetta, *American Journal of Epidemiology*, 2012, **175**, 706-714.
15. R. Quansah and J. K. Jaakkola, *Int Arch Occup Environ Health*, 2009, **82**, 529-537.
16. K. Abe, K. Suzuki and D. Citterio, *Analytical Chemistry*, 2008, **80**, 6928-6934.
17. M. Fierz, C. Houle, P. Steigmeier and H. Burtscher, *Aerosol Science and Technology*, 2011, **45**, 1-10.
18. A. Leman, A. Omar and M. Yusof, *International Journal of Research and Reviews in Applied Sciences (IJRRAS)*, 2010, **5**, 18-26.
19. M. R. Flynn and P. Susi, *Journal of occupational and environmental hygiene*, 2009, **7**, 115-126.
20. M. S. Khan, G. Thouas, W. Shen, G. Whyte and G. Garnier, *Analytical Chemistry*, 2010, **82**, 4158-4164.
21. M. Li, J. Tian, M. Al-Tamimi and W. Shen, *Angewandte Chemie International Edition*, 2012, **51**, 5497-5501.
22. J. Su, M. Al-Tamimi and G. Garnier, *Cellulose*, 2012, **19**, 1749-1758.

23. M. N. Belgacem, M. C. Salon-Brochier, M. Krouit and J. Bras, *Journal of Adhesion Science and Technology*, 2011, **25**, 661-684.
24. A. W. Martinez, S. T. Phillips, G. M. Whitesides and E. Carrilho, *Analytical Chemistry*, 2009, **82**, 3-10.
25. A. M. López Marzo, J. Pons, D. A. Blake and A. Merkoçi, *Analytical Chemistry*, 2013, **85**, 3532-3538.
26. D. Ballerini, X. Li and W. Shen, *Microfluid Nanofluid*, 2012, **13**, 769-787.
27. P. Zwanenburg, X. Li and X. Y. Liu, 2013.
28. S. Wang, L. Ge, X. Song, M. Yan, S. Ge, J. Yu and F. Zeng, *Analyst*, 2012, **137**, 3821-3827.
29. X. Y. Liu, C. M. Cheng, A. W. Martinez, K. A. Mirica, X. J. Li, S. T. Phillips, M. Mascaren and G. M. Whitesides, 2011.
30. J. C. Jokerst, J. A. Adkins, B. Bisha, M. M. Mentele, L. D. Goodridge and C. S. Henry, *Analytical Chemistry*, 2012, **84**, 2900-2907.
31. Y. Sameenoi, P. Panymeesamer, N. Supalakorn, K. Koehler, O. Chailapakul, C. S. Henry and J. Volckens, *Environmental Science & Technology*, 2012, **47**, 932-940.
32. W. Zhao, M. M. Ali, S. D. Aguirre, M. A. Brook and Y. Li, *Analytical Chemistry*, 2008, **80**, 8431-8437.
33. A. K. Ellerbee, S. T. Phillips, A. C. Siegel, K. A. Mirica, A. W. Martinez, P. Striehl, N. Jain, M. Prentiss and G. M. Whitesides, *Analytical Chemistry*, 2009, **81**, 8447-8452.
34. A. W. Martinez, S. T. Phillips, E. Carrilho, S. W. Thomas, H. Sindi and G. M. Whitesides, *Analytical Chemistry*, 2008, **80**, 3699-3707.
35. Y.-K. Yang, K.-J. Yook and J. Tae, *Journal of the American Chemical Society*, 2005, **127**, 16760-16761.
36. S. M. Z. Hossain and J. D. Brennan, *Analytical Chemistry*, 2011, **83**, 8772-8778.
37. A. R. Ferhan, L. Guo, X. Zhou, P. Chen, S. Hong and D.-H. Kim, *Analytical Chemistry*, 2013, **85**, 4094-4099.
38. X. Yang and E. Wang, *Analytical Chemistry*, 2011, **83**, 5005-5011.
39. J. P. Lafleur, S. Senkbeil, T. G. Jensen and J. P. Kutter, *Lab on a Chip*, 2012, **12**, 4651-4656.
40. N. Ratnarathorn, O. Chailapakul, C. S. Henry and W. Dungchai, *Talanta*, 2012, **99**, 552-557.
41. M. M. Mentele, J. Cunningham, K. Koehler, J. Volckens and C. S. Henry, *Analytical Chemistry*, 2012, **84**, 4474-4480.
42. S. Ge, L. Ge, M. Yan, X. Song, J. Yu and J. Huang, *Chemical Communications*, 2012, **48**, 9397-9399.
43. L. Ge, J. Yan, X. Song, M. Yan, S. Ge and J. Yu, *Biomaterials*, 2012, **33**, 1024-1031.
44. J. Xiao, Y. Y. Meng, P. L. Zhang, W. Wen, Z. M. Liu and T. Zhang, *Laser Phys.*, 2012, **22**, 1481-1488.
45. F. Kong, *Water science and technology*, 2009, **60**, 3083-3089.
46. F. Kong, *BioResources*, 2009, **4**, 1088.
47. W. S. Rasband, U. S. National Institutes of Health, Bethesda, Maryland, USA, 2009, vol. <http://rsb.info.nih.gov/ij/>.
48. F. E. Grubbs, *The Annals of Mathematical Statistics*, 1950, 27-58.
49. W. W. Brandt, F. P. Dwyer and E. D. Gyarfas, *Chemical Reviews*, 1954, **54**, 959-1017.

50. E. Booth and J. Strickland, *Journal of the American Chemical Society*, 1953, **75**, 3017-3019.
51. A. Farag, A. El-Wakil and M. El-Shahawi, *Analyst*, 1981, **106**, 809-812.
52. H. Filik, M. Doğutan and R. Apak, *Anal Bioanal Chem*, 2003, **376**, 928-933.
53. J. Xu, P. Che and Y. Ma, *Journal of Chromatography A*, 1996, **749**, 287-294.
54. D. H. Wilkins and G. Frederick Smith, *Analytica Chimica Acta*, 1953, **9**, 338-348.
55. E. M. Penner and W. R. Inman, *Talanta*, 1963, **10**, 407-412.
56. P. Rattanarat, W. Dungchai, D. M. Cate, W. Siangproh, J. Volckens, O. Chailapakul and C. S. Henry, *Analytica Chimica Acta*, 2013, **800**, 50-55.
57. Center for Disease Control, NIOSH Manual of Analytical Methods, <http://www.cdc.gov/niosh/docs/2003-154/chaps.html>, (accessed 2015).
58. Bureau of Labor Statistics, Occupational Employment and Wages, <http://www.bls.gov/oes/current/oes514121.htm>, (accessed 2013).
59. W. Yue, A. Bange, B. L. Riehl, B. D. Riehl, J. M. Johnson, I. Papautsky and W. R. Heineman, *Electroanalysis*, 2012, **24**, 1909-1914.
60. R. Witholt, R. Gwiazda and D. Smith, *Neurotoxicology and teratology*, 2000, **22**, 851-861.
61. S. Shibata, *Analytica Chimica Acta*, 1960, **23**, 367-369.

CHAPTER 3: SIMPLE, DISTANCE-BASED MEASUREMENT FOR PAPER ANALYTICAL DEVICES

Chapter Overview

The paper-based device described in Chapter 2 required external equipment (e.g. scanner, computer, camera) for quantitative analysis of metals, adding cost, complexity, and inhibiting sensor portability. Furthermore, intensity-based measurements were limited for even semi-quantitative detection (in the absence of optical instrumentation) because color hue was interpreted differently from person-to-person. Here, a new method for quantitative measurement of metals (and other analytes) using paper-based sensors is described wherein analysis is performed based on visual determination of color *distance*. Contrary to other visual techniques based on metal-ligand complex color changes, distance-based detection is open to less interpretation and is applicable to a wide range of analytes, both organic and inorganic. The work described in this chapter was published in *Lab on a Chip* and is reproduced here with minor modifications and updates.¹ The results presented in this chapter were developed with Wijitar Dungchai, a visiting scholar in the Henry laboratory. I developed the methods for measuring nickel and assisted Wijitar with method development for measuring glucose and reduced glutathione.

Paper-based analytical devices (PADs) represent a growing class of elegant, yet inexpensive chemical sensor technologies designed for point-of-need applications. Most PADs, however, still utilize some form of instrumentation such as a camera for quantitative detection. We describe here a simple technique to render PAD measurements more quantitative and straightforward using the distance of color development as a detection motif. The so-called distance-based detection enables

PAD chemistries that are more portable and less resource intensive as compared to classical approaches that rely on the use of peripheral equipment for quantitative measurement. We demonstrate the utility and broad applicability of this technique with measurements of glucose, nickel, and glutathione using three different detection chemistries: enzymatic reactions, metal complexation, and nanoparticle aggregation, respectively.

Introduction

Methods to measure chemical composition, a fundamental need in virtually all science and engineering disciplines, have undergone rapid technological development in recent years. For example, single gene analyses that once took days to complete can now be conducted in minutes using instruments that quantify thousands of genes simultaneously. Most technological advancements in the field of measurement science focus on increasing sample throughput, and/or reducing sample detection limit.²⁻⁸ Although such technological advancements have enhanced our understanding of chemistry and biology, they are often limited to laboratory use by highly trained scientists. Consequently, there is a growing recognition of the need to augment contemporary analytical tools with low-cost methods designed for point-of-need applications.⁹⁻¹²

Point-of-need measurement technologies are often simple and inexpensive but sacrifice detection limit and operating range for sensitivity, specificity, and speed.¹³⁻¹⁷ Point-of-need technologies are also attractive because they are low cost and require minimal user training. Such technologies can have great impact on science and also in society. Examples include litmus paper and the home pregnancy test, both of which have diffused far into everyday societal contexts. Common to each of these point-of-need devices is their reliance on simple capillary-based flow for the analytics.

Paper-based analytical devices (PADs), first introduced by the Whitesides group in 2007, are a type of point-of-need technology that uses porous cellulose (i.e., common filter paper) to store reagents and the addition of water to generate flow via capillary action.¹⁸ Hydrophobic materials printed onto the paper define circuits that control flow path.^{17, 19-22} Unlike traditional analytical techniques making use of paper as a substrate, the use of patterning in these devices increases the overall functionality. To conduct chemical analysis, colorimetric reagents are added to specific zones within the paper, with analyte detection and quantification carried out by changes in color hue and/or intensity.¹⁷ Although straightforward, this detection method has limitations, including user variability when distinguishing changes in reagent hue and intensity.²³⁻²⁷ Consequently, even with PADs, precise and accurate quantification can require the use of peripheral technologies such as digital scanners, cameras, or other optical techniques.^{17, 27, 28} Instrumented techniques, such as electrochemistry, can also help improve PAD performance.²⁹⁻³¹ Ladder-based barcode assays have also been developed which reduce the requirement for color differentiation by the user.³²⁻³⁵

Presented here is a simplified technique for quantitative PAD detection with broad chemical applicability, referred to as distance-based detection or chemometer. In this approach, colorimetric reagents, designed to precipitate or aggregate on reaction with the analyte, are deposited along the capillary flow path. Consequently, as flowing analyte reacts with reagent, color develops along the flow line until all of the analyte is consumed. Quantification is achieved by measuring color length, thus eliminating the need to differentiate hues and intensities by the user (as is typical with existing PAD devices). Measuring length instead of color intensity produces fewer user errors from device to device and renders the analytical measurement largely independent of the operator.

Distance-based detection on paper has been demonstrated previously. Zuk et al. quantified theophylline levels in whole blood and serum by distance-based detection using antibody-activated chromatography paper.^{36, 37} Since then, few applications have been reported using this detection motif.^{38, 39} In 1990, Allen and co-workers developed a similar enzyme-based method for measuring cholesterol levels on paper.⁴⁰ Chatterjee et al. developed a PDMS microfluidic device using biotin-modified channels and flow distance as the detection motif for fluorescently labelled streptavidin.²⁸ A complimentary strategy was recently demonstrated by Lewis et al. for point-of-care (POC) paper-based detection using individual strips of paper that turn color in response to the presence of an analyte. Quantification is determined by counting the number of strips that turn color.⁴¹

The method described here extends distance-based detection on paper beyond the use of immobilized enzymes and antibodies. The technique is simplified and broadened in scope, requiring fewer steps to complete the analysis and can be applied to a broader class of analytes. In addition, device fabrication with via wax printing (vs. paper strips) is amenable to multiplexing. The sensor presented here couples the cost effectiveness and simplicity of printed hydrophobic barriers, which scales well for mass fabrication. This form of distance-based PAD detection can be applied to analytes beyond the biotinylation and immunoassays described previously.

In this work, non-instrumented analysis is demonstrated using distance-based detection of a broad range of analytes using three different detection motifs: nanoparticle aggregation, metal complexation, and enzymatic activity. To demonstrate the utility of the method, assays for detection of nickel, reduced glutathione (GSH), and glucose were developed. These three analytes represent compounds found in environmental (Ni) and biological (GSH, glucose) samples. Chronic

or even acute exposure to Ni is associated with a number of toxic effects.⁴²⁻⁴⁵ Glutathione is an endogenous marker of oxidative stress and can impart useful information about the health of an individual.⁴⁶⁻⁵⁰ Glucose monitoring is essential for controlling blood sugar levels in diabetic patients. Analyte measurements were accurate and precise, with detection sensitivities for Ni, GSH, and glucose of $0.7 \mu\text{g m}^{-3}$, 0.12 nmol, and 11 mg dL^{-1} respectively. Once developed, the distance-based PADs were used to quantify each analyte in a relevant biological (serum) or environmental (incineration ash) sample. We found no significant difference between values measured using device and known levels demonstrating the applicability of this method to real-world samples.

Experimental Methods

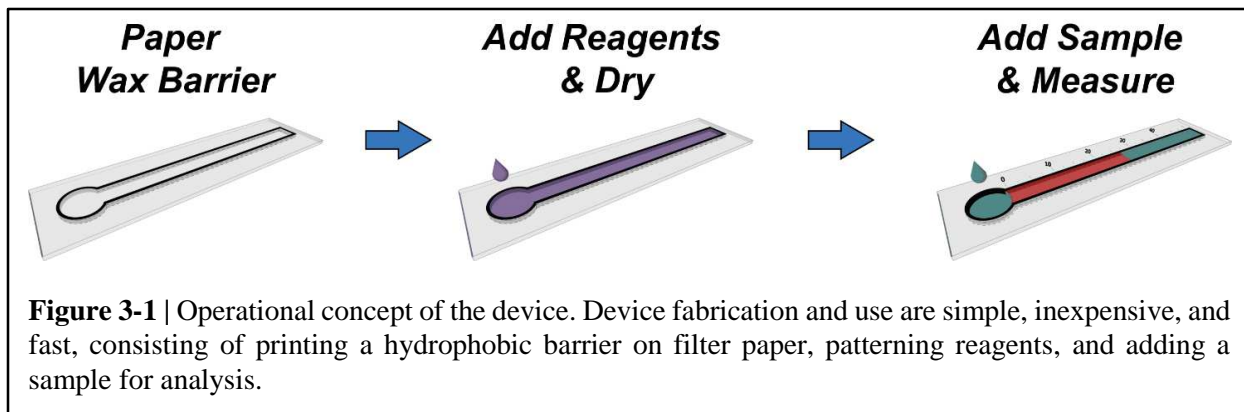
Materials and Equipment

Glutathione (reduced form), glutathione disulfide, cysteine, cysteine, and homocysteine, dimethylglyoxime (DMG, 50 mM), sodium acetate trihydrate, and sodium fluoride (0.5 M), D-(+)-glucose, glucose oxidase (GOx, from *Aspergillus niger*, 5 U mg⁻¹) and peroxidase Type I (HRP, from *Horseradish*, 100 U/mg) were purchased from Sigma-Aldrich (St. Louis, MO). The silver nanoparticle solution (AgNPs) was obtained from the Sensor Research Unit at the Department of Chemistry, Chulalongkorn University, Thailand. Tris-hydrochloride and ammonium hydroxide were purchased from Mallinckrodt Baker, Inc. (Phillipsburg, NJ). Glacial acetic acid and potassium phosphate were purchased from Fisher Scientific (Pittsburgh, PA). Nitric acid (18.4 M) was purchased from EMD Millipore (Billerica, MA, USA). The 3, 3'-diaminobenzidine (DAB) in peroxidase substrate kit was obtained from Vector Laboratories, Inc. (Burlingame, CA). All chemicals were used as received without further purification. An

industrial incineration ash sample (RTC-CRM012-100) certified for heavy metals content was obtained from LGC Standards (Teddington, UK). Whatman No. 1 qualitative-grade filter paper was purchased from General Electric Company (Schenectady, New York). CorelDraw and Adobe Illustrator software were used to design the hydrophobic wax barrier for all three assay types. Hydrophobic wax barriers were printed on filter paper using a commercial wax printer (Xerox Colorqube 8870).

Device Operation

The operational concept is shown in Figure 3-1 along with three detection chemistries selected to demonstrate application pathways. The microfluidic flow circuit, which closely resembles a thermometer, was designed using graphics software and printed onto cellulosic filter paper using wax ink. A circular reservoir at the bottom accommodates sample addition; filter paper in the reservoir may be retained (e.g., to hold reagents for sample pre-treatment) or removed to facilitate sample transfer into the detection zone. Colorimetric detection reagents were deposited along the flow channel by spray application or pipetting. Spray application used a nebulizer to deposit reagent droplets uniformly along the channel. This process was fast but inefficient, as significant amounts of reagent were deposited onto the surrounding paper (outside the flow circuit). Reagents in the surrounding paper did not, however, affect experimental results because they were separated from the flow channel by a wax barrier. Alternatively, reagents may be pipetted onto the paper in minute ($0.5 \mu\text{L}$) increments. This process consumed less reagent but was somewhat tedious and time-intensive. Once the reagents were dry, the device was ready for use. An aqueous sample extract was added to the sample reservoir and then carried by capillary action along the flow channel. As the analyte reacted with its reagent, a colored product developed. Once all of the



analyte was consumed, the color development stopped (even though eluent proceeded to wick along the channel). Analyte quantification is as simple as measuring the length of the colored region in the flow channel, typically with a ruler either be held up to or printed directly along the channel. No computer software was required for analyte quantification. A desktop scanner and computer software (Xerox DocuMate 3220 Scanner, color photo setting, 600 dpi) were also used to quantify color distance but only for the purpose of experimental validation.

After adding an analyte/eluent mixture to the sample zone of the device, assay measurement was performed once the eluent completely evaporated (~15–20 min), however a reading could be accomplished in less than 10 min once the channel became completely saturated and the flow velocity approached zero. In the 10 min needed for the eluent to reach the end of the channel, all upstream color formation (i.e. analyte complexes with reagents) had already occurred.

The flow Reynolds number along the sample channel was low (~10), favouring laminar flow. Color distance was measured from the beginning of the channel near the sample zone to the most downstream tip of detectable color (i.e., the apex of the parabolic flow profile). Albeit somewhat arbitrary, the tip of color was chosen for detection instead of the farthest color region spanning the

width of the channel because both methods provided approximately the same level of reproducibility (6.1 and 6.5% RSD respectively), and the difference in analyte concentration (< 3 µg) in choosing one method over the other was lower than the limit of quantification (5-10 µg) for each assay. We chose to measure to the tip of color formation because this procedure improved detection sensitivity.

Glutathione Detection

The paper assay for glutathione detection consisted of a circular reservoir for sample addition (6 mm diameter) and a baffled flow channel (3×60 mm) divided into 14 equal sections (0.3×2mm). The flow baffles were used to decrease the capillary flow velocity along the channel, maximizing reaction time between glutathione and the AgNPs. The AgNP solution (0.5 µL) was spotted onto each of the 14 sections along the channel. For each assay, 20 µL of sample solution was added to the sample reservoir. Complete sample analysis took approximately 10 minutes. Assay selectivity was investigated by addition of 20 µL of standard thiol solution (0.5 nmol), which did not form a colored reaction product along the paper channel.

Glucose Detection

The paper-based assay for glucose detection consisted of a wax-printed circular reservoir (5 mm diameter) for GOx and HRP enzyme modification and a straight channel (2×40 mm) for measuring glucose reaction with peroxidase and DAB. Aliquots (0.5 µL) of 600 U mL⁻¹ GOx and 500 U mL⁻

¹ HRP were spotted on the sample reservoir and 0.5 µL of DAB was pipetted onto the straight channel every five millimeters to account for reagent spreading along the channel length. For each assay, 20 µL of the standard or sample solution was added to the sample reservoir.

Analysis of Glutathione and Glucose in Human Serum

Human control serum samples (levels I and II) for both GSH and glucose were obtained from Pointe Scientific (Canton, MI). Levels of analytes were provided by the supplier. Before analysis, unwanted protein was removed by filtration (10 KDa MWCO) and centrifugation at 10,000 rpm for 20 and 10 minutes, respectively, for glucose and GSH. A solution of 5% 5-sulfosalicylic acid was added prior to centrifugation for GSH.

Nickel Detection

A nebulizer was used to saturate the paper surface with DMG (50 mM). The deposited reagents were then air dried. The paper was uniformly coated with ammonium hydroxide (pH 9.5) because the rate and extent of Ni^{2+} -DMG complexation are pH dependent with the fastest rate occurring at pH 9. To prevent user contamination and excess solvent evaporation, the filter paper was passed through a desktop laminator at 150°C (Model No. 92499, Gordon) twice on each side. Laminating the paper also provided better mechanical stability for assay handling. A 6.4mm (ID) hole was punched through the sample reservoir and masking tape was applied to one side to prevent sample loss from leakage during use. For analysis, 20 μL of a Ni standard solution (1000 ppm) was deposited onto the sample reservoir. The Ni-DMG complex is reddish pink and precipitates upon formation. Color development is rapid and total sample analysis was performed in <10 min.

Analysis of Ni in Combustion Incineration Ash

An incineration ash sample was purchased for assay validation. Briefly, incineration ash along with 1 mL concentrated nitric acid was heated in a 20 mL scintillation vial for 5 min at ~250°C on a hotplate until complete acid evaporation. A 262 μL solution containing deionized water (250

μL), sodium fluoride, acetic acid (2:1:1 v/v %), and 12 μL sodium hydroxide (12 M) was added to the vial. After homogenous mixing with a pipette for several seconds, the solution was centrifuged for 10 min at 14,000 RPM. For each assay, 20 μL of the supernatant was added to the sample reservoir.

Results and Discussion

Glucose Quantification

Detection of glucose is shown in Figure 3-2a using glucose oxidase, 3,3'-diaminobenzidine (DAB) and peroxidase. In this reaction, glucose oxidase produces hydrogen peroxide that further reacts with DAB in the presence of peroxidase to form a brown, insoluble product (polyDAB). DAB is colorless but forms a highly colored and easily visualized product after reacting with the analyte. To demonstrate method viability, levels of glucose in a serum standard were quantified. Test results, along with device photographs, are shown in Figure 3-2b (calibration data is shown as blue squares). The plot depicts sample reaction length as a logarithmic function of the known analyte concentration. For glucose detection, the length of the colored range is proportional to the amount of glucose added over the range of 7 to 200 nmol. Negative controls (zero sample concentration) produced no discernible color change. The linear range obtained for glucose in our system is approximately $11\text{--}270 \text{ mg dL}^{-1}$, having a slightly lower detection limit than commercially available point-of-care blood glucose meters ($\sim 20 \text{ mg dL}^{-1}$).⁵¹ The upper range in our system is limited however, and is approximately half the level of commercial systems (500 mg dL^{-1}).

Method variability is relatively low as seen by the small error bars (representing standard deviations of repeat measures) around each datum. We tested this system using serum samples

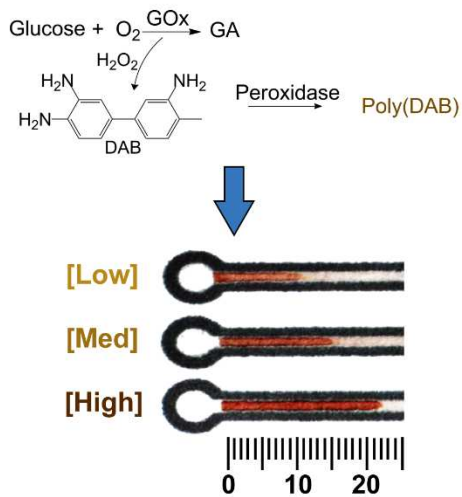
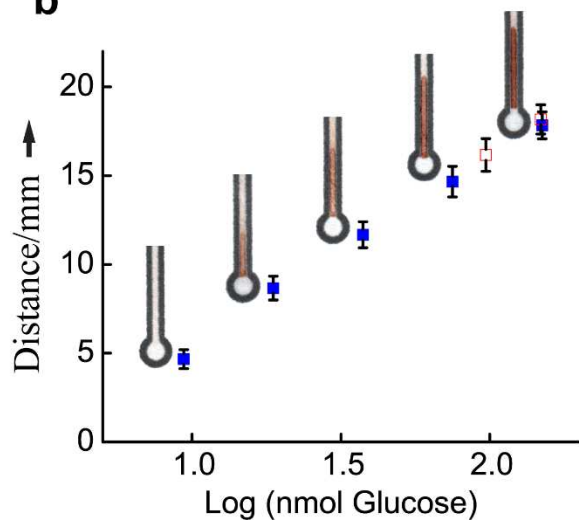
a**b**

Figure 3-2 | (a) Glucose oxidase reacts with DAB and peroxidase to form a brown precipitate in approximately five minutes. (b) Analyte flow of standard solutions compared with real (complex) serum samples. Standard curves show the distance of color development is proportional to the amount of glucose added (closed blue squares). The extent of the reaction is easily visualized within the linear range of the reaction. Photos of the complete reaction are included for each calibration data point. Reaction distance for complex serum samples (open red squares) show good agreement with standard calibration curves (closed blue squares). Error bars represent one standard deviation ($n = 6$).

known to contain either normal or abnormal glucose levels. Such commercially-available control samples are widely used for assay validation because they have all the complexity of normal serum without the worry of blood-borne pathogens. Glucose concentrations within the control serum samples are shown as open red squares; their alignment with the calibration curve shows the ability of this method to measure glucose accurately and precisely in a relatively complex sample matrix.

Quantification of Nickel in a Combustion Ash Sample

Detection of nickel (Ni^{2+}) using dimethylglyoxime (DMG) as an example assay for toxic metals is shown in Figure 3-3a. In this assay, DMG is placed in the channel and reacts with Ni^{2+} to form a pinkish-red product. $\text{Ni}(\text{DMGH})_2$ is poorly soluble and immediately precipitates from solution. Solutions containing Ni^{2+} are colorless in the absence of DMG. For Ni detection, the concentration that linearly corresponds to color length is $0.7\text{--}92 \mu\text{g m}^{-3}$. The legal limit for exposure to Ni in occupational settings is $1,000 \mu\text{g m}^{-3}$, for which our detection limits are clearly sufficient.³⁵ We are continuing to investigate methods for improving the dynamic range of the assay. We envision this test could develop into a very cost effective, ‘first-pass’ evaluation tool for personal exposure to aerosol pollution containing Ni compounds. We next established the sensitivity of the assay to the amount of DMG deposited on the device (Figure 3-3b). As the amount of DMG increases, the sensitivity of the assay decreases. The assay can detect nmol levels of Ni^{2+} in the presence of other transition and heavy metals making it useful for a range of application areas from water analysis to particulate matter composition studies.⁵²

Levels of aqueous Ni^{2+} concentrations were evaluated in a certified combustion incineration ash sample as part of an on-going program to develop fast, inexpensive environmental measurement

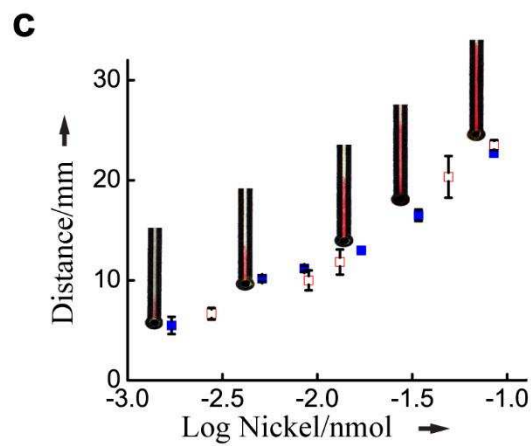
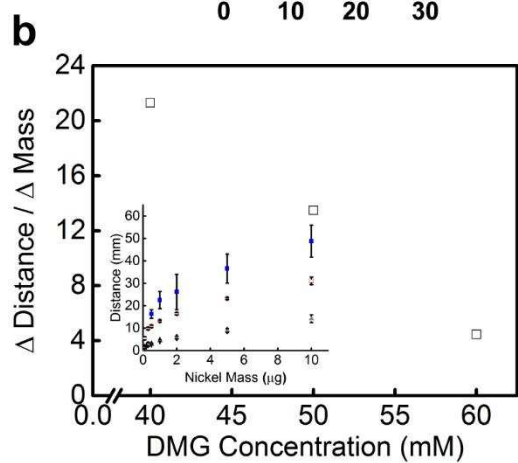
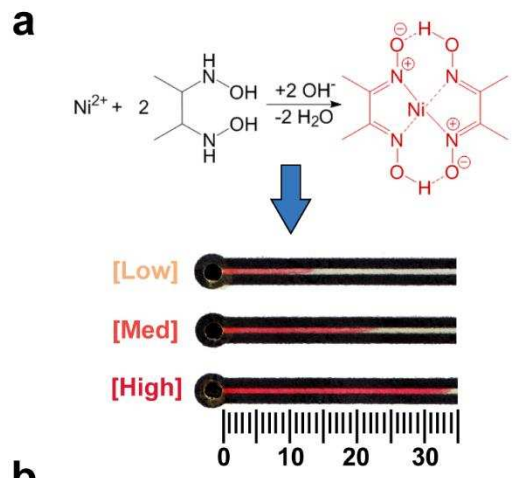


Figure 3-3 | (a) Formation of a bright red precipitate is easily visualized when DMG- Ni^{2+} complexation occurs. The reaction product is formed immediately, and complete analysis in the concentration range studied took approximately 15 minutes. (b) Assay sensitivity decreases as the concentration of DMG increases. [Insert] The limit-of-detection (LOD) for the Ni assay increases as the concentration of DMG increases from 40mM (closed blue squares) to 50mM (open red squares) to 60mM (closed grey triangles). (c) Standard curves show the distance of color development is proportional to the amount of Ni added (closed blue squares). A sample of incineration ash was tested for method validation (open red squares). Error bars represent one standard deviation ($n = 8$).

tools. Combustion incineration ash is a by-product of medical, municipal, and industrial incineration processes and can be a significant contributor to local and regional air, water, and soil pollution. For this assay, DMG was deposited uniformly along the flow channel and solutions containing known amounts of nickel (in 20 μ L aliquots), first dissolved in concentrated HNO₃, were added to the inlet to prepare calibration curves. The Ni-DMG complex gave a highly colored product that was readily distinguished from the clear sample solution.⁵³ Various dilutions of the resulting solution were analyzed and the results shown as open red squares in Figure 3-3c. Good agreement was obtained between measured and known Ni concentrations, demonstrating the ability of the chemometer method to carry out these measurements in complex sample matrices.⁴¹ Our lab continues to evaluate strategies for mobilizing the acid digestion process. The color intensity that developed down the paper channel remained essentially constant. This was unexpected since we assumed the color intensity would soften as the Ni remaining in solution reacted with DMG. One possible explanation for this phenomenon is that Ni(DMGH)₂ becomes highly concentrated in a confined space on the paper (solvent evaporation drives this process) causing irregular particle clusters to form, which saturates the surface. No discernible color changes or reaction products were observed in negative controls.

GSH Quantification Assay

Detection of GSH using a silver nanoparticle (AgNP) aggregation assay is shown in Figure 3-4a. In this assay, AgNPs aggregate in the presence of GSH to form a reddish-brown product that is distinguished from the orange color of the AgNPs in the absence of glutathione. AgNPs (11 nm diameter) were spotted onto the detection channel, turning it a dark orange color. These nanoparticles aggregate in the presence of glutathione, which causes a color shift from orange to

deep red on the paper (Figure 3-4b).⁵⁴ The filled blue squares represent calibration data of known GSH concentration. A color change from orange to light orange was also observed when only buffer was added. The buffer effect, however, was easily distinguished from the dark red of the glutathione specific product. The shift in absorbance maximum in the presence of buffer is hypothesized to result from weak non-specific aggregation of the AgNPs.

The ability to measure glutathione spiked in serum samples (open red squares in Figure 3-4b) was also determined. As can be seen, the distances measured with serum samples (4.2 and 5.7 mm) agree well with those of the standard solutions (3.7 and 5.3 mm) for glutathione concentrations 0.25 and 0.5 nmol, respectively (Table 3-1). Detection of glutathione was log-linear for the concentration range tested (0.12–2.0 nmol). The detection limits for this assay are on the same order as conventional measurement methods for GSH, however the dynamic range for the most sensitive assays extends a few orders of magnitude higher. The assay selectivity against other thiols (cysteine and homocysteine) and disulfides (cystine, homocystine, and glutathione disulfide) was also investigated (Figure 3-5).

Cysteine and homocysteine did cause a similar color change but the length of color development was much less than for glutathione. None of the disulfides tested produced any color change. For all three assays, color formation and bulk flow along the channel was observed to follow the Lucas-Washburn equation for flow in capillary tubes (Figure 3-6). Reaction kinetics for each assay were assumed to be rapid compared with solvent flow rate, so the length of color production along a channel should be driven predominantly by flow rate.

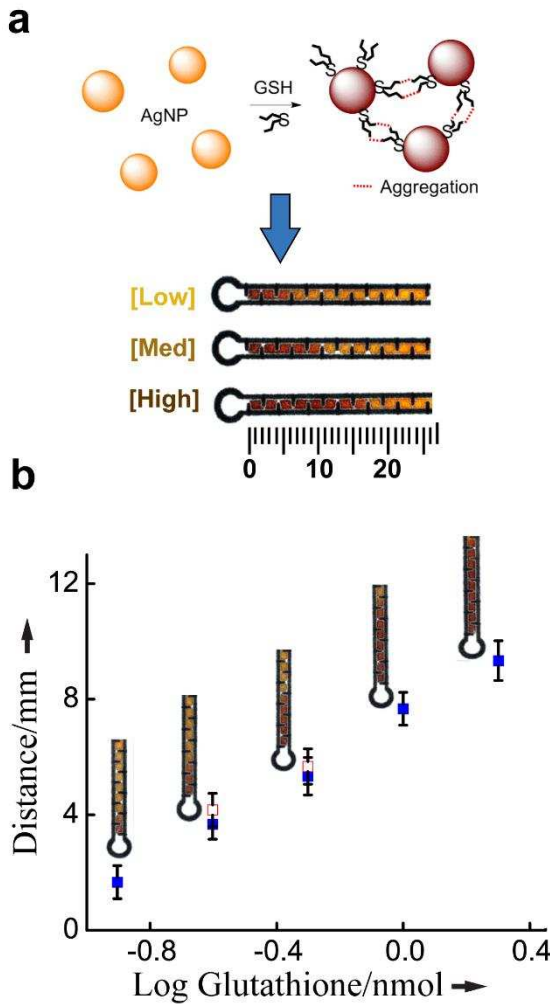


Figure 3-4 | (a) AgNPs aggregate in the presence of glutathione and produce a reddish-brown color, easily distinguishable by the naked eye. Reaction kinetics were slow, so wax baffles were used to divert flow in a serpentine pattern as capillary action flowed liquid through the channel. For one assay, the detection of glutathione within the concentration range tested took approximately 10 minutes. (b) Standard curves show the distance of color development is proportional to the amount of glutathione added (blue squares). Spiked serum samples were evaluated for method validation (open red squares). Error bars represent one standard deviation ($n = 4$).

We have demonstrated this method using three representative compounds commonly found in environmental and biological matrices, but this method should be easily extendable to a much larger range of analytes because of the possibility for cellulose modification.⁵⁵ Even without substrate modification, our detection motif is applicable for analysis of a variety of transition and

Table 3-1 | Determination of glucose and glutathione in human serum (^aSD: standard deviation, n = 3).

Real Samples	Concentration (^a SD, standard deviation (n = 3))		% Recovery
Glucose	Certified value (mM ± SD ^a)	Measured (mM ± SD ^a)	
Serum Level 1	5.6 ± 0.4	6.1 ± 0.2	108.7
Serum Level 2	16.8 ± 1.7	18.6 ± 0.3	110.8
Glutathione	Added (μM)	Measured (μM ± SD ^a)	% Recovery
Spiked Serum 1	6.2	7.1 ± 2.5	112.9
Spiked Serum 2	12.5	13.4 ± 0.0	107.3
Spiked Serum 3	25.0	21.1 ± 2.9	84.2

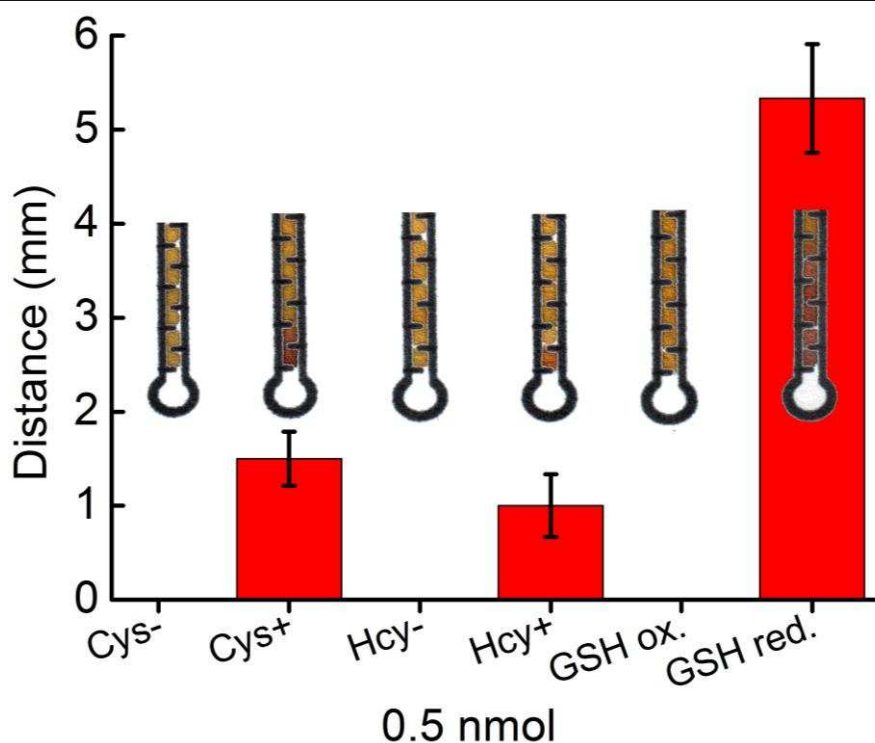


Figure 3-5 | Selectivity study of AgNPs aggregation for glutathione determination against other thiols: cystine (Cys-), cysteine (Cys+), homocystine (Hcy-), homocysteine (Hcy+), and glutathione oxidized form at 0.5 nmol. Error bars represent one standard deviation (n = 3).

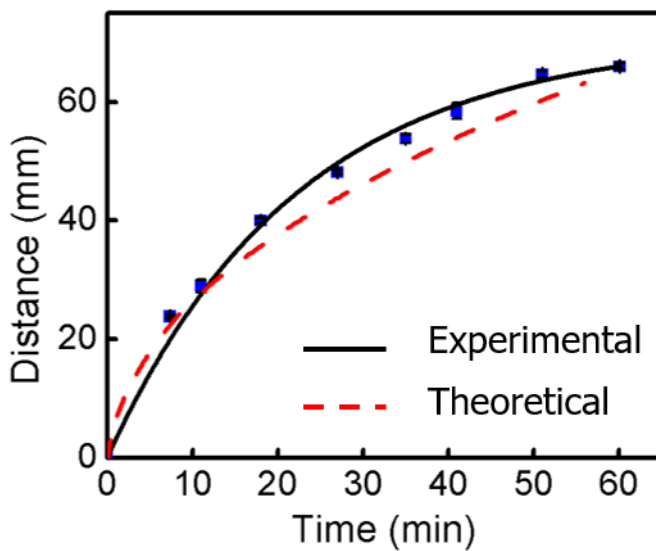


Figure 3-6 | Fluid wicking in porous networks is modeled by the Lucas Washburn equation which states that wicking distance is proportional to $t^{1/2}$. Experimental data ($n \geq 3$) shows that flow velocity can be approximated by the LW equation.

heavy metals, including Fe, Mn, Cr, Cu, Hg, and Pb. Many biological compounds should also be quantifiable with this method via nanoparticle aggregation, including lysine, heparin, thrombin, and DNA.⁵⁶⁻⁶⁰

Conclusions

The distanced-based detection concept represents a new and dramatically simplified technique for quantitative PAD detection that eliminates peripheral instrumentation during sample analysis. This technology is adaptable to suit different detection chemistries and multiple analytes, including those from complex environmental and biological matrices where analyte specificity is critical. One challenge that must be overcome with our method is the current requirement for the sample to be solubilized; however we are developing new methods of analysis that will accommodate samples in multiple formats and with various solvents. The assays described herein were developed in controlled laboratory conditions with small variability in temperature and relative

humidity (25 °C and ~30 % relative humidity), however if studies were conducted in a less controlled environment (i.e. for environmental monitoring), large changes in ambient conditions could affect wicking velocity and alter results. We plan to investigate these and other variables further to improve assay reproducibility in a wider range of ambient conditions.

Paper-based analytical devices hold great potential for application at the point-of-need. The analytical technique presented here is minimally instrumented for device portability and is highly cost effective; excluding fabrication equipment (computer, drawing software, printer, pipette), a single assay costs approximately \$0.04.⁵² Since analyte quantification is immediate and can be performed on-site, processing time is dramatically reduced when compared to other centralized measurement techniques, which often sacrifice processing speed for detection sensitivity. Like most PAD technologies, this technique sacrifices dynamic range for cost, speed, and ease of use. However, we have shown that devices can be tuned to detect different analyte concentration ranges by modulating reagent concentrations in the flow channel, thus, accommodating different reaction stoichiometries.

REFERENCES FOR CHAPTER 3

1. D. M. Cate, W. Dungchai, J. C. Cunningham, J. Volckens and C. S. Henry, *Lab on a Chip*, 2013, **13**, 2397-2404.
2. E. Bakker and E. Pretsch, *TrAC Trends in Analytical Chemistry*, 2005, **24**, 199-207.
3. B. S. Broyles, S. C. Jacobson and J. M. Ramsey, *Analytical Chemistry*, 2003, **75**, 2761-2767.
4. R. Fan, O. Vermesh, A. Srivastava, B. K. H. Yen, L. Qin, H. Ahmad, G. A. Kwong, C.-C. Liu, J. Gould, L. Hood and J. R. Heath, *Nat Biotech*, 2008, **26**, 1373-1378.
5. S. P. FitzGerald, J. V. Lamont, R. I. McConnell and E. O. Benchikh, *Clinical Chemistry*, 2005, **51**, 1165-1176.
6. J. A. Hansen, J. Wang, A.-N. Kawde, Y. Xiang, K. V. Gothelf and G. Collins, *Journal of the American Chemical Society*, 2006, **128**, 2228-2229.
7. G. Huang, Z. Ouyang and R. G. Cooks, *Chemical Communications*, 2009, 556-558.
8. A. H. Merrill Jr, M. C. Sullards, J. C. Allegood, S. Kelly and E. Wang, *Methods*, 2005, **36**, 207-224.
9. T. Dworak, C. Gonzalez, C. Laaser and E. Interwies, *Environmental Science & Policy*, 2005, **8**, 301-306.
10. A. E. Herr, A. V. Hatch, W. V. Giannobile, D. J. Throckmorton, H. M. Tran, J. S. Brennan and A. K. Singh, *Annals of the New York Academy of Sciences*, 2007, **1098**, 362-374.
11. N. Maisonneuve, M. Stevens, M. E. Niessen, L. Steels, I. N. Athanasiadis, A. E. Rizzoli, P. A. Mitkas and J. M. Gómez, Springer Berlin Heidelberg, 2009, DOI: 10.1007/978-3-540-88351-7_16, pp. 215-228.
12. P. von Lode, *Clinical Biochemistry*, 2005, **38**, 591-606.
13. S. J. Barnes and E. Scornavacca, *International Journal of Mobile Communications*, 2004, **2**, 128-139.
14. S. F. Clarke and J. R. Foster, *British Journal of Biomedical Science*, 2012, **69**, 83-93.
15. S. Kanji, J. Buffie, B. Hutton, P. S. Bunting, A. Singh, K. McDonald, D. Fergusson, L. A. McIntyre and P. C. Hebert, *Critical Care Medicine*, 2005, **33**, 2778-2785.
16. I. Korhonen, J. Parkka and M. Van Gils, *Engineering in Medicine and Biology Magazine, IEEE*, 2003, **22**, 66-73.
17. A. W. Martinez, S. T. Phillips, E. Carrilho, S. W. Thomas, H. Sindi and G. M. Whitesides, *Analytical Chemistry*, 2008, **80**, 3699-3707.
18. A. W. Martinez, S. T. Phillips, M. J. Butte and G. M. Whitesides, *Angewandte Chemie International Edition*, 2007, **46**, 1318-1320.
19. D. A. Bruzewicz, M. Reches and G. M. Whitesides, *Analytical Chemistry*, 2008, **80**, 3387-3392.
20. E. Carrilho, A. W. Martinez and G. M. Whitesides, *Analytical Chemistry*, 2009, **81**, 7091-7095.
21. W. K. T. Coltro, D. P. de Jesus, J. A. F. da Silva, C. L. do Lago and E. Carrilho, *Electrophoresis*, 2010, **31**, 2487-2498.
22. Y. Lu, W. Shi, L. Jiang, J. Qin and B. Lin, *Electrophoresis*, 2009, **30**, 1497-1500.

23. T. Songjaroen, W. Dungchai, O. Chailapakul, C. S. Henry and W. Laiwattanapaisal, *Lab on a Chip*, 2012, **12**, 3392-3398.
24. A. K. Ellerbee, S. T. Phillips, A. C. Siegel, K. A. Mirica, A. W. Martinez, P. Striehl, N. Jain, M. Prentiss and G. M. Whitesides, *Analytical Chemistry*, 2009, **81**, 8447-8452.
25. J. C. Jokerst, J. A. Adkins, B. Bisha, M. M. Mentele, L. D. Goodridge and C. S. Henry, *Analytical Chemistry*, 2012, **84**, 2900-2907.
26. M. P. Allen, A. DeLizza, U. Ramel, H. Jeong and P. Singh, *Clinical Chemistry*, 1990, **36**, 1591-1597.
27. W. Zhao, M. M. Ali, S. D. Aguirre, M. A. Brook and Y. Li, *Analytical Chemistry*, 2008, **80**, 8431-8437.
28. D. Chatterjee, D. S. Mansfield, N. G. Anderson, S. Subedi and A. T. Woolley, *Analytical Chemistry*, 2012, **84**, 7057-7063.
29. A. Apilux, W. Dungchai, W. Siangproh, N. Praphairaksit, C. S. Henry and O. Chailapakul, *Anal Chem*, 2010, **82**, 1727-1732.
30. W. Dungchai, O. Chailapakul and C. S. Henry, *Anal Chem*, 2009, **81**, 5821-5826.
31. Z. Nie, C. A. Nijhuis, J. Gong, X. Chen, A. Kumachev, A. W. Martinez, M. Narovlyansky and G. M. Whitesides, *Lab on a Chip*, 2010, **10**, 477-483.
32. J.-H. Cho and S.-H. Paek, *Biotechnology and Bioengineering*, 2001, **75**, 725-732.
33. C. Fang, Z. Chen, L. Li and J. Xia, *Journal of Pharmaceutical and Biomedical Analysis*, 2011, **56**, 1035-1040.
34. K.-K. Fung, C. P.-Y. Chan and R. Renneberg, *Analytica Chimica Acta*, 2009, **634**, 89-95.
35. K.-K. Fung, C.-Y. Chan and R. Renneberg, *Anal Bioanal Chem*, 2009, **393**, 1281-1287.
36. R. F. Zuk, V. Ginsberg, K. , T. Houts, R. Judith, H. Merrick, E. F. Ullman, M. M. Fischer, C. C. Sizto, S. N. Stiso and D. J. Litman, *Clinical Chemistry*, 1985, **31**, 1144-1150.
37. R. Chen, T. M. Li, H. Merrick, R. F. Parrish, V. Bruno, A. Kwong, C. Stiso and D. J. Litman, *Clin Chem*, 1987, **33**, 1521-1525.
38. L. M. Vaughan, M. M. Weinberger, G. Milavetz, S. Tillson, E. Ellis, J. Jenne, S. J. Szeffler, M. B. Wiener, K. Conboy, T. Shaughnessy and et al., *Lancet*, 1986, **1**, 184-186.
39. V. Y. Liu, T. Y. Lin, W. Schrier, M. Allen and P. Singh, *Clin Chem*, 1993, **39**, 1948-1952.
40. M. P. Allen, A. DeLizza, U. Ramel, H. Jeong and P. Singh, *Clin Chem*, 1990, **36**, 1591-1597.
41. G. G. Lewis, M. J. DiTucci and S. T. Phillips, *Angewandte Chemie International Edition*, 2012, **51**, 12707-12710.
42. R. Hayes, *Cancer Causes Control*, 1997, **8**, 371-385.
43. T. Menné and E. Nieboer, *Endeavour*, 1989, **13**, 117-122.
44. L. Järup, T. Bellander, C. Hogstedt and G. Spång, *Occupational and Environmental Medicine*, 1998, **55**, 755-759.
45. S.-C. Xu, M.-D. He, Y.-H. Lu, L. Li, M. Zhong, Y.-W. Zhang, Y. Wang, Z.-P. Yu and Z. Zhou, *Journal of Pineal Research*, 2011, **51**, 426-433.
46. G. K. Balendiran, R. Dabur and D. Fraser, *Cell Biochemistry and Function*, 2004, **22**, 343-352.
47. I. Ceballos-Picot, V. Witko-Sarsat, M. Merad-Boudia, A. T. Nguyen, M. Thévenin, M. C. Jaudon, J. Zingraff, C. Verger, P. Jingers and B. Descamps-Latscha, *Free Radical Biology and Medicine*, 1996, **21**, 845-853.

48. L. A. Herzenberg, S. C. De Rosa, J. G. Dubs, M. Roederer, M. T. Anderson, S. W. Ela, S. C. Deresinski and L. A. Herzenberg, *Proceedings of the National Academy of Sciences*, 1997, **94**, 1967-1972.
49. J. P. Richie Jr, *Experimental Gerontology*, 1992, **27**, 615-626.
50. D. M. Townsend, K. D. Tew and H. Tapiero, *Biomed Pharmacother*, 2003, **57**, 145-155.
51. R. Ng, *Point of Care*, 2008, **7**, 161.
52. M. M. Mentele, J. Cunningham, K. Koehler, J. Volckens and C. S. Henry, *Analytical Chemistry*, 2012, **84**, 4474-4480.
53. D. B. Gazda, J. S. Fritz and M. D. Porter, *Analytica Chimica Acta*, 2004, **508**, 53-59.
54. M. Stobiecka, K. Coopersmith and M. Hepel, *Journal of Colloid and Interface Science*, 2010, **350**, 168-177.
55. A. Yu, J. Shang, F. Cheng, B. A. Paik, J. M. Kaplan, R. B. Andrade and D. M. Ratner, *Langmuir : the ACS journal of surfaces and colloids*, 2012, **28**, 11265-11273.
56. Li and L. J. Rothberg, *Journal of the American Chemical Society*, 2004, **126**, 10958-10961.
57. H. Li and L. Rothberg, *Proceedings of the National Academy of Sciences of the United States of America*, 2004, **101**, 14036-14039.
58. J.-S. Lee, M. S. Han and C. A. Mirkin, *Angewandte Chemie*, 2007, **119**, 4171-4174.
59. H. Wei, B. Li, J. Li, E. Wang and S. Dong, *Chemical communications (Cambridge, England)*, 2007, DOI: 10.1039/b707642h, 3735-3737.
60. Y. Zhou, Z. Yang and M. Xu, *Analytical Methods*, 2012, **4**, 2711-2714.

CHAPTER 4: MULTIPLEXED PAPER ANALYTICAL DEVICE FOR QUANTIFICATION OF METALS USING DISTANCE-BASED DETECTION

Chapter Overview

The purpose of chapter 3 was to demonstrate the viability of and highlight the range of uses for distance-based detection as an analytical tool. In this chapter, distance-based detection is investigated specifically for determining the content of metals present in welding fume samples. Furthermore, reagent deposition techniques are investigated not only as a means for precisely defining the placement of reagents but also as a method for tailoring the output of distance-based detection. The concentration of colorimetric reagents/buffers/masking agents can be deposited as a function (1st, 2nd, 3rd order, etc.) of distance to alter the response curve according to the point-of-need application. For instance, if the concentration of analyte is expected to vary widely (over several orders of magnitude), a log-linear response curve can be established to cover this need. Work from this chapter was published in *Lab on a Chip* and reproduced here with minor modifications and updates.¹

Exposure to metal-containing aerosols has been linked with adverse health outcomes for almost every organ in the human body. Commercially available techniques for quantifying particulate metals are time-intensive, laborious, and expensive; often sample analysis exceeds \$100. We report a simple technique, based upon a distance-based detection motif, for quantifying metal concentrations of Ni, Cu, and Fe in airborne particulate matter using microfluidic paper-based analytical devices. Paper substrates are used to create sensors that are self-contained, self-timing, and require only a drop of sample for operation. Unlike other colorimetric approaches in paper

microfluidics that rely on optical instrumentation for analysis, distance-based detection provide quantification visually based on the distance of a colorimetric reaction, similar to reading temperature on a thermometer. To demonstrate the effectiveness of this approach, Ni, Cu, and Fe were measured individually in single-channel devices; detection limits as low as 0.1, 0.1, and 0.05 µg were reported for Ni, Cu, and Fe. Multiplexed analysis of all three metals was achieved with detection limits of 1, 5, and 1 µg for Ni, Cu, and Fe. The dynamic range for multi-analyte detection was also extended by printing concentration gradients of colorimetric reagents using an off-the-shelf inkjet printer. Analyte selectivity was demonstrated for common interferences. To prove method utility, Ni, Cu, and Fe were measured from samples of certified welding fume; levels measured with paper sensors matched known values determined gravimetrically.

Introduction

Human exposure to metal-containing particulate matter (PM) has been studied extensively. Epidemiological studies of metal exposure in the workplace have found that occupations such as metalworking, construction, transportation, and mining place individuals at increased risk to numerous cardiovascular and respiratory health issues, even to early death.² For example, inhalable aerosols containing Ni are listed by the International Agency for Research on Cancer as probably carcinogenic (Group 2B) to humans and animals.³ Tens of thousands of individuals are exposed to metal-containing PM in their workplace, yet relatively few are routinely monitored for their exposure due to the time-intensive sampling and cost-prohibitive analytical methods currently available.⁴ Common measurement methods for metals include inductively coupled plasma optical emission spectroscopy, mass spectrometry, and atomic absorption spectroscopy.^{5,6} These analytic

methods have high precision, sensitivity, and low detection limits, but they are expensive (> \$100 per sample) and require trained specialists for operation.

Low-cost, point-of-need sensors have been highlighted as key for improving exposure assessment.⁷ Towards this goal, microfluidic paper-based analytical devices, or μ PADs, show promise for overcoming technical and financial obstacles that, traditionally, have impeded more widespread exposure assessment. One major limitation of current exposure analysis methodologies is cost; therefore, detection strategies need to be minimally instrumented to enable routine monitoring. Paper sensors are attractive as an analytical tool because sample flow is passively driven by capillary action, microliter sample and reagent volumes are needed, and devices (typically) are disposable. To date, paper sensors have been developed for environmental exposure analysis of various agents, including: metals,⁸⁻¹² pesticides,¹³ explosive residues,^{14, 15} and reactive oxygen species,^{16, 17} among others. However, μ PADs still have limitations; they often require external equipment, trained personnel, and are not geared for multiplexed analyses.

To date, the most common detection motif for paper sensors has been colorimetry.^{18, 19} Although straightforward, accurate quantification of color intensity on paper requires an external optical detector (e.g. camera, scanner, etc.) and image quality has been known to vary based on lighting conditions.²⁰ Alternatively, visual detection using a color/intensity comparator can be used; however, color hue and brightness perception may differ from person to person, complicating analysis and increasing measurement uncertainty. Several groups have made attempts to simplify quantitative readout by removing all external instrumentation. One strategy employed by Lou et al.²¹ involved counting the number of segments (along a flow path) that reacted with analyte, where

the number of segments was proportional to analyte concentration. This detection motif has since been applied for measuring hydrogen peroxide.^{22, 23} Using time as an analytical readout has also been explored.²⁴ A timing element (e.g. stopwatch, phone app) measured the time elapsed for a chemical reaction that took place between an analyte and indicator. A complementary approach originally developed by Zuk et al. in 1985,²⁵ and later expanded by our group, is distance-based detection.¹ This technique relies on reading the length of a colored reaction product along a paper channel with the unaided eye. Each device essentially contains one sample reservoir and a flow channel patterned with a colorimetric indicator specific for an analyte of interest. As analyte flows down the channel, complexes formed between analyte and indicator precipitate, generating a color band with length that is proportional to the amount of analyte. Visual quantification is aided by a ruler printed alongside each device, similar to reading temperature on a thermometer. In this approach, analyte is measured completely with the unaided eye; no electronic readers or timers are necessary.

A key step in consistent color formation on paper is reagent deposition. In porous networks, color formation is dependent on wicking rate, which decreases nonlinearly with both time and penetration distance across the paper substrate.^{26, 27} In distance-based detection, analytical dynamic range is heavily influenced by wicking behavior. Slower flow rates allow more time for reaction in a given zone, ultimately leading to a shorter band of color along the detection channel and a smaller dynamic range. To address this limitation, concentration gradients of a chromophoric indicator were printed along the channel using a modified piezoelectric printer.^{28, 29} Inkjet printing has become a common fabrication technique for defining the location and concentration of chemical reagents on paper surfaces.³⁰ Many of the reported printing techniques for μPADs use

hydrophobic barriers for confining reagents,³¹⁻³⁴ though it is becoming more common to pattern reagents directly on the substrate surface.³⁵⁻³⁷ Reagent printing is advantageous because it greatly improves device reproducibility, functionality, and flexibility compared to manual deposition methods such as pipetting, nebulizing, or dip coating. Small droplet volumes from the printer (~1.5 pL) lead to high patterning resolution and little reagent is wasted in the manufacturing process. Moreover, inkjet printing is scalable for mass production.

In this work, a distance-based μPAD was developed for simultaneous measurement of Fe(II), Ni(II), and Cu(II) from aerosolized particulate matter. These metals were selected due to their high prevalence in welding fumes. Typically, metals are extracted from filter samples for chemical speciation, but in this work we utilized certified welding fumes in powder form. Hydrophobic barriers and colorimetric reagents were printed for controlling fluid transport and for quantifying metals. Reagent deposition by inkjet printing provided better assay reproducibility than manual deposition (6.3% vs. 11.4% relative standard deviation). The limit of detection for Ni, Cu, and Fe in single and multi-channel devices was 0.1, 0.1, 0.05 μg (6.7, 6.7, 3.3 ppm) and 5, 5, 1 μg (100, 100, 20 ppm), respectively. Chemical gradients were printed to extend the dynamic range of each assay; improvements of 50.0% and 41.2% were observed for Ni and Cu. Signal interference from non-target metals was also investigated. Metal constituents common to most welding alloys (e.g. stainless and mild steel) had minimal impact on results. Finally, a welding fume standard certified for Fe, Ni, Zn, and Mn was used to demonstrate the efficacy of distance-based detection for measuring metal particulates in samples with complex matrices. Concentrations of Zn and Mn were not evaluated here.

Experimental Methods

Materials and Equipment

All reagents were analytical grade. Ultrapure water ($18.2 \text{ M}\Omega\cdot\text{cm}$) from a Mill-Q system (Merck Millipore, Darmstadt, Germany) was used throughout. Laboratory containers were rinsed with H_2O prior to use. Standard solutions of all metals (lead(II) nitrate, cadmium(II) nitrate tetrahydrate, potassium dichromate(VI), iron(III) chloride hexahydrate, nickel(II) sulfate hexahydrate, copper(II) sulfate pentahydrate, manganese(II) chloride tetrahydrate, magnesium(II) chloride hexahydrate, iron(II) sulfate heptahydrate, aluminum(III) sulfate hydrate, barium(II) chloride, vanadium(III) chloride, and cobalt(II) sulfate pentahydrate) were purchased from Sigma-Aldrich (St. Louis, MO, USA). L-ascorbic acid (97%), L-cysteine, Tris base (99.9%), bathophenanthroline (97%), dimethylglyoxime (99%), dithiooxamide (98.5%), and sodium fluoride were purchased from Sigma-Aldrich. Sodium acetate, ammonium acetate, hydrochloric acid, sodium hydroxide, and glacial acetic acid were obtained from Fisher Scientific (Pittsburgh, PA, USA). Whatman (grade 1) filter paper was purchased from Apollo Presentation Products (Booneville, MS, USA).

Device Fabrication and Operation

Distance-based detection with μ PADs has been described previously.¹ The operational concept for multiplexed distance-based detection is shown in Figure 4-1. Briefly, a wax barrier designed in a shape resembling a thermometer was printed onto Whatman 1 filter paper. To preserve channel resolution, wax barriers were printed on both sides of the filter paper. Each flow lane of the device served as a detection channel for a single metal. Analyte was added to the device at a circular reservoir at the bottom of the device, which formed a common flow inlet for all three channels. Filter paper containing either pretreatment reagents or the analyte may also be added to the

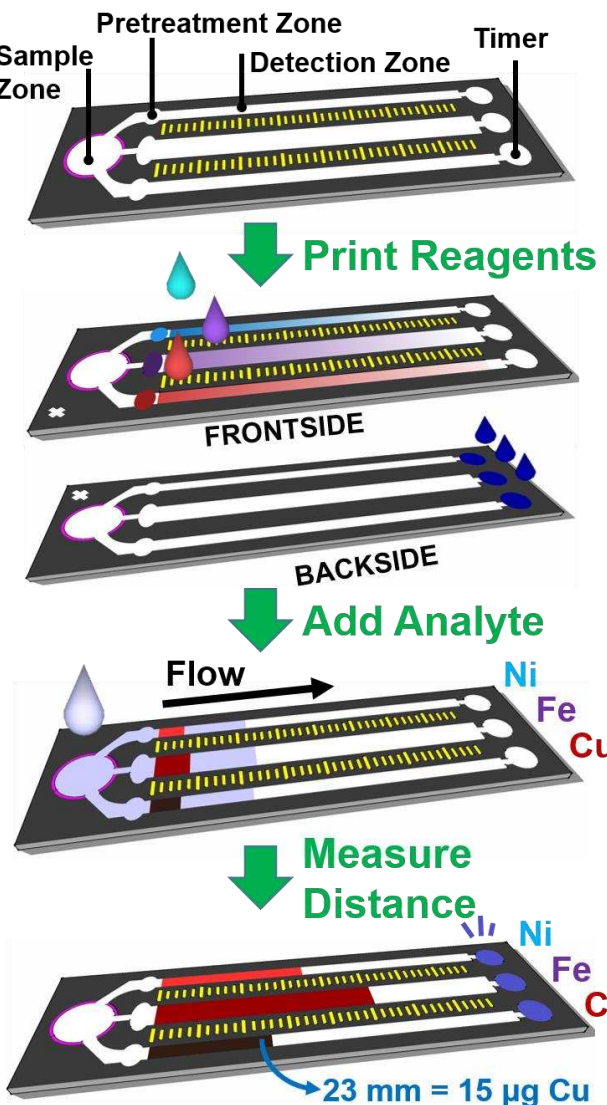


Figure 4.1 | Schematic of distance-based detection in a multi-layer device. Colorimetric reagents, buffers, and masking agents are inkjet printed in the detection and pretreatment zones. A colorimetric indicator was printed on the back of the device, functioning as a passive timer. Analyte mass was quantified when a metal-ligand complex precipitated on the substrate, generating a band of color with a length proportional to the amount of metal present. Quantification in single and multi-channel devices was achieved in ~30 and ~40 min, respectively.

reservoir to facilitate sample transfer into the detection zone. In this work, a piezoelectric printer (Epson R280) was used to deposit colorimetric detection reagents along the flow channel homogeneously or as a gradient. The primary component of the printed ink solution was isopropanol, so evaporation after printing was nearly instantaneous at the small volumes printed.

Before adding sample, the devices were laminated (Apache AL13P) at 170 °C to create an encapsulating hydrophobic barrier to prevent solvent evaporation along the channel during analysis. A sample reservoir was punched using an 8-mm biopsy punch (Robbins Instruments, Chatham, NJ, USA) and backed with transparent tape to prevent leakage of solvent. As aqueous sample (50 µL) was added to the device via the sample reservoir, capillary action carried solution along the flow channel (the 3D wax barrier served to confine and direct sample flow). As analyte reacted with the colorimetric reagent deposited along the flow channel, a colored precipitate formed. Color development ceased once all the analyte had been consumed, though the eluent continued to proceed along the flow channel. Analyte quantification was achieved by measuring the distance of color development along the flow channel using a ruler printed beside each channel. A desktop scanner and computer software (Xerox DocuMate 3220 Scanner, color photo setting, 600 dpi) were also used to quantify color distance for experimental validation.

After sample addition, the eluent flowed along each channel until reaching a circular indicator zone at the end of the channel. Each indicator zone was pre-patterned with blue dye on the bottom of the device. When dry, the dye was not visible from the top of the sensor. Once wetted, dye in the indicator zone migrated from the bottom of the device to the top, indicating assay completion. The time from sample addition to appearance of the indicator dye was 40 ± 6 min ($n = 10$).

As described previously, the Reynolds number along the sample channel was low (~10), indicating laminar flow.¹ Color distance was measured from the beginning of the ruler printed beside each channel to the most downstream tip of detectable color (i.e., the apex of the colored flow profile). The tip of color was chosen for detection rather than the furthest region spanning the width of the

channel because both methods provided approximately the same level of reproducibility (6.1 and 6.5% RSD respectively), and the difference in analyte concentration in choosing one method over the other was lower than the limit of quantification for each assay.¹

Inkjet Cartridge Modification and Reagent Printing

A piezoelectric inkjet printer (Epson Model R280) was selected for reagent printing, as described earlier, with modifications.^{28, 38} The purpose of inkjet printing was twofold: 1) printing offered superior control (vs. spraying) over the volume and droplet resolution of deposited material, and 2) this method enabled printing of non-uniform reagent concentrations onto the paper substrate. To modify the printer, stock Epson ink cartridges were replaced with third-party refillable cartridges (Inkproducts.com) which had been modified to fit 200 µL (non-filtered) pipette tips. For the cartridges, a Dremel® tool was first used to cut off the plastic-covered outlet protruding from the cartridge. A hole was then drilled from the bottom of the cartridge towards the top with bits of increasing size (1/4" and 19/64"); care was taken not to extend the bit beyond the top of the cartridge. The sides of the cartridge remained intact. Compressed air was used to remove plastic remnants from inside the cartridge. Pipette tips used as ink reservoirs were cut to fit on nozzles over the print head (Figure 4-2). The tips were designed to fit tightly over the nozzles (i.e. without leaking). Inkjet reservoirs were cleaned with filtered H₂O, methanol, ethanol, and isopropanol, according to previous reports.³⁸ Approximately 100 µL of reagent solution (the composition varied according to each metal species) was injected into the pipette reservoir and pushed through the print head via pipette until solution was dispensed onto a paper towel placed below the print head. After this 'priming step', another 180 µL of reagent solution was added to the reservoir. Adobe Illustrator CS3 software was used for device design and printing control. For reagent printing, the

1. Cut end off 200 μ L pipette tip



2. Fill pipette reservoirs with reagents



3. Drill holes in inkjet cartridge to fit over pipette reservoirs

Figure 4-2 | To create a reservoir for inkjet printing, the end of a 200 μ L pipette tip was cut and placed over a nozzle for each color channel. Third-party refillable cartridges were cored to create space for the pipette tip. The reservoir holds approximately 180 μ L of printable liquid.

highest available print quality was selected, and high-speed printing, edge-smoothing, and grayscale printing were deselected. Adobe RGB 2.2 was used for color control.

For each metal, reagent concentration gradients were printed along the channel according to an empirically derived equation. Reagent concentration (i.e., the number of successive overprints across a substrate) varied for each metal; for gradients, the concentration of reagent deposited was highest near the sample zone and decreased along the channel's longitudinal axis. A consequence of gradient printing was that the response curve for each metal was more linear, according to a residual sum of squares regression. As reagent concentration increased, the slope of the response

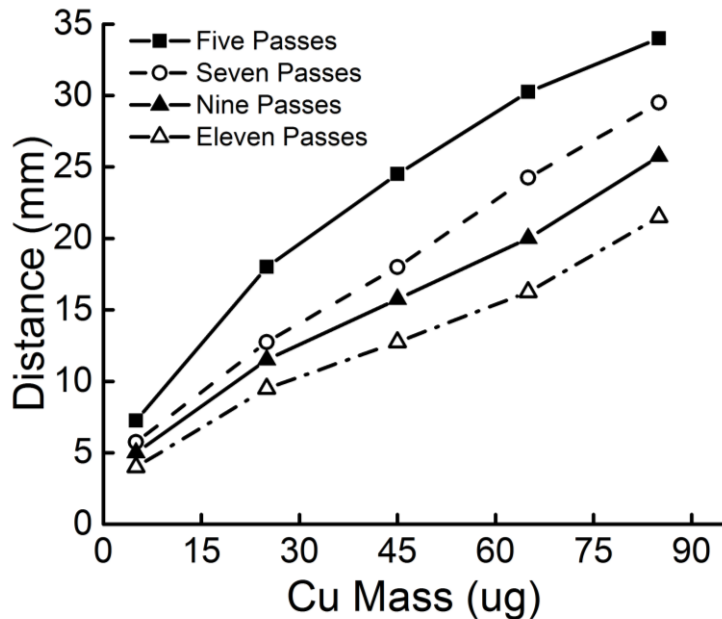


Figure 4-3 | Operational concept of the device. Device fabrication and use are simple, inexpensive, and fast, consisting of printing a hydrophobic barrier on filter paper, patterning reagents, and adding a sample for analysis.

curve (i.e. sensitivity) decreased (Figure 4-3). For each metal, the concentration of printed reagents were chosen to provide the highest linear dynamic range according to Tukey's range test and a test of non-linearity at 95% confidence. After reagents were added, each print head reservoir was flushed with ≥ 10 mL of H₂O, methanol, ethanol, and isopropanol to ensure complete removal of residual reagent.

Ink Formulation and Gradient Creation

A solution composed of 95/5% (w/v) isopropyl alcohol/H₂O was used for all experiments as the solvent for colorimetric reagents, buffers, masking agents, and the indicator dye. Solution formulation was based on the reciprocal of the Ohnesorge number Z = Oh⁻¹:

$$Oh = \frac{(d\rho\gamma)^{1/2}}{\eta}$$

which is a function of the print head diameter d , and the fluid properties of surface tension γ , density ρ , and dynamic viscosity η . Much of the literature agrees that a Z value from 1-10 is ideal for producing consistent drops with minimal satellite spray, though debate persists about how large Z can be while maintaining high-quality droplet formation.³⁹ In this work, several organic solvents (isopropanol, ethanol, methanol, dimethylsulfoxide, xylene) were evaluated as candidates for printing; their Z values are listed in Table A2-1. The Z value of isopropanol (16.4) was closest to ideal and was selected for printing. H_2O (5% w/v) was added to the isopropanol ink to increase solution surface tension.

Fluid velocity in porous networks is nonlinear, and because distance-based detection is velocity-dependent, the response (i.e., color distance) generated for a range of metal masses is also non-linear. To counter this non-linearity in response, we developed equations for printing concentration gradients of colorimetric reagents on paper. The general process for creating a printed reagent gradient for detection of each metal was as follows: 1) measure the location of the eluent flow front, x_i , as a function time, t , along the longitudinal flow axis, 2) create a curve fit of x_i vs. t , 3) non-dimensionalize flow distance vs. time by creating parameters $x_i^* = \frac{x_i}{x_f}$ and $t^* = \frac{t}{t_f}$, where the variables x_f and t_f represent the maximum recorded distance x_f , of the fluid front at time t_f , 4) develop a new function representing the change in pixel intensity vs. distance (in pixels) along the channel [$I(D) = 255 \times x^*$] where $D = 215 \times t^*$ represents the distance of the fluid front in pixels. The coefficients 255 and 215 represent the maximum pixel intensity (in RGB space) and channel distance (in our system), respectively, 5) generate a counter function, $G = 255 - I(D)$, to be the complement of $I(D)$, 6) convert the counter function into a colored image using a custom-designed LabVIEW VI, and 7) print the gradient on the substrate at the desired concentration

determined by the counter function (Figure A2-1). For gradient deposition, intensity equations used to create the gradients are provided in Appendix 2. Colorimetric reagent concentration was optimized for each metal to produce the greatest linear dynamic range and lowest limit of detection. Statistical treatment of the data excluded outliers; a weighted linear regression was applied to each response curve due to unequal variance present in the sample measurement (Excel and LabVIEW software).

Nickel Detection

Detection chemistry for Ni was used as previously reported, with modifications.¹ A solution composed of dimethylglyoxime (100 mM) and Tris base (50 mM, pH 10.2) was made in 95/5% isopropanol/H₂O solvent. Masking agents (1 M NaF and 6 M ammonium acetate) were mixed 2:1 (%w/v) and applied to the pretreatment zone of the Ni detection channel five times via pipette (0.35 μL increments). The presence of sodium and ammonium acetate helped create a more visible color band in the channel and also served to mask potential interferences from Co and Fe.⁸ The DMG solution was printed six times on each device (~3 μmol DMG per 20 devices) for both gradient and non-gradient reagent deposition. Sample volumes of 15 and 50 μL were deposited in the sample zone for analysis of Ni using the single-channel and multi-channel devices, respectively. For analysis, 1000 or 2000 ppm solutions of Ni(II), Cu(II), or Fe(II) were made and diluted with H₂O to appropriate concentrations. The Ni(DMG)H₂ complex is reddish pink and precipitates upon formation.

Copper Detection

Measurement of Cu was carried out using dithiooxamide, a common ligand used for complexing Co, Ni, and Cu.⁴⁰ For detection, a solution composed of dithiooxamide (30 mM), sodium acetate buffer (pH 4.0, 20 mM), and 1% (w/w) hydroxylamine was made in 95/5% (w/v) IPA/H₂O solvent. For masking, a solution of higher hydroxylamine concentration (10% w/w in H₂O) was made and added via pipette to the pretreatment zone of the Cu detection channel once (0.35 µL). At low pH, the binding constant for Ni to dithiooxamide was reduced, preventing much of the Ni from interfering with Cu measurement. Quantitative recovery of Ni with dithiooxamide has been typically performed from pH 7-9.⁴¹ Chemical gradients for detection of Cu were printed seven times (~1 µmol dithiooxamide per 20 devices).

Iron Detection

Measurement of Fe was carried out using 4,7-diphenyl-1-1,10-phenanthroline (bathophenanthroline), a common colorimetric indicator for Fe corrosion.^{42, 43} Bathophenanthroline (Bphen) was selected as the chromogenic reagent for Fe over other common 1,10-phenanthroline derivatives because 1) Bphen is approximately two times more sensitive to Fe than 1,10-phenanthroline, 2) the ferrous-Bphen complex has low solubility in H₂O, and 3) Bphen has fewer interferences than 1,10-phenanthroline for Fe detection. A solution composed of Bphen (10 mM), sodium acetate buffer (pH 4.5, 20 mM), and 1% (w/w) L-ascorbic acid was made in 95/5% (w/v) IPA/H₂O solvent and printed twenty times along the Fe detection channel (~1 µmol Bphen per 20 devices). Ascorbic acid (5% w/w) was added to the pretreatment zone via pipette (0.5 µL) to reduce soluble Fe(III) to Fe(II) for complexation with Bphen.

Welding Fume Standard Reference Material

A reference material derived from stainless steel welding fume (HSL SSWF), certified for Fe and Ni, was obtained from the Health and Safety Laboratory (Harpur Hill, Buxton, UK). Approximately 1 mg of the HSL SSWF was weighed and added to a 1.5 mL centrifugation tube, followed by acid digestion under 10 µL HCl (15.4 M) and 15 µL H₂O. Each aliquot was then microwaved (1100 W) for 6 min, before adding 25 µL NaOH (3 M). Aliquots were centrifuged for 3 min at 10,000 RPM. Extracted supernatant (volume varied) was diluted with H₂O to a total volume of 50 µL prior to use. Control tests were conducted in parallel using standard metal solutions.

Data Analysis

Measurements were recorded with half-millimeter resolution using rulers printed beside each detection channel; distances measured visually were later verified with Image J software using images obtained from a scanner. Outliers were discarded when identified using Grubb's test for outliers.⁴⁴ Assumptions of normality and unequal variance were verified using chi-squared and F distribution tests. Minimum sample sizes for testing were determined using a power analysis ($1-\beta \geq 0.8$, $\alpha = 0.05$, using G*Power v3.1.9.2 software). Due to the presence of increasing variance with metal mass, we applied a weighting factor to each linear model (Figure A-2). In this work, weighting (w) was given according to inverse distance (y_i^{-1}), according to the equation:

$$wi = \frac{ny_i^{-1}}{\sum_{i=1}^n y_i^{-1}}$$

where n is the number of samples in the calibration data set. Further details on the weighting statistics used for analysis are provided in Appendix 2.

Results and Discussion

Detection of Fe, Ni, and Cu in Single Channels

For each metal, single-channel devices were fabricated and patterned with reagents to determine detection sensitivity, detection limits, and operating range. Quantitative values are provided in units of mass because the target sample comes from air pollution; equivalent concentration units are provided in parenthesis throughout the paper. Initial studies were performed by nebulizing colorimetric reagents on the paper substrate, as described previously,¹ to ensure uniform coverage along the detection channel. Standard metal solutions from 0.01-100 µg ($0.7\text{-}7 \times 10^3$ ppm) were made for each metal; for each test 15 µL was added to the sample zone of the device. The dynamic ranges for Ni, Cu, and Fe were 0.1-5, 0.1-10, and 0.05-7 µg, respectively ($n \geq 10$). The upper limit of the range for each metal was determined by applying the Tukey-Kramer range test. Limit of detection was determined by the lowest measurable distance of the color band that precipitated a minimum of 1 mm from the beginning of the detection channel (as identified by a 0 mm datum printed onto device). Relative standard deviations ranged from 9.5-13%, which is typical with µPADs.¹⁴ A higher molar extinction coefficient for the complex was hypothesized as the reason for a 50% improvement in detection limit for Fe(II)-Bphen (2.2×10^4 M⁻¹ cm⁻¹) compared to Ni(DMG)H₂ (3×10^3 M⁻¹ cm⁻¹) and Cu-dithiooxamide (750 M⁻¹ cm⁻¹).⁴⁵⁻⁴⁷ The observed solubility of the Ni(DMG)H₂ complex was higher than the Cu-dithiooxamide product, which was suspected as the reason why detection sensitivity of Ni was not higher than Cu.

Extending Dynamic Range

A constant reduction in wicking rate was a factor limiting the upper range of detection; over time, the rate of flow approached zero, ceasing new color formation along the detection channel. To

overcome this limitation, two approaches were tested: 1) control channel geometry, and 2) control colorimetric reagent concentration.

Varying Channel Width

The hydrophilic surface available for reagent-analyte complexation influenced the slope of the analyte response curve. More paper surface (per unit distance along the flow channel) led to a lower sensitivity (less positive slope) than when less paper surface was available (more positive slope). However, because the flow in the paper channel followed Lucas-Washburn theory⁴⁸, sample flow rate eventually approached zero (in our system this occurred ~60 mm down the channel). As the sample flow rate approached zero, further growth of the color band ceased. As a result, a tradeoff exists between dynamic range and sensitivity for distance-based detection with μ PADs. This tradeoff (lower dynamic range for higher sensitivity and vice versa) is depicted using two hypothetical traces in Figure 4-4. In the figure, the linear dynamic range of trace 1 (1-34 μ g) is approximately 48% smaller than the linear dynamic range of trace 2 (1-70 μ g). To minimize upper-bound losses, a study was performed with single-channel devices with widths starting at 4.7 mm and decreased in 25% increments (e.g. 4.7, 3.5, and 2.6 mm). Channel width was defined prior to melting the wax barrier (Figure 4-5). According to previous work, 2.6 mm was subjectively chosen as the narrowest channel width for which a visual reading of the color band could be accomplished without difficulty by the naked eye.¹ The maximum channel width was limited to 4.7 mm because detection range for wider channels was unacceptably low. As demonstrated in Figure 4-5, the slope of the response curve for Fe decreased in devices from the narrowest to widest channel, as anticipated. The detection limit was not influenced by channel width in this study and was equal for all three experiments. We suspect this was due to a threshold of analyte mass that

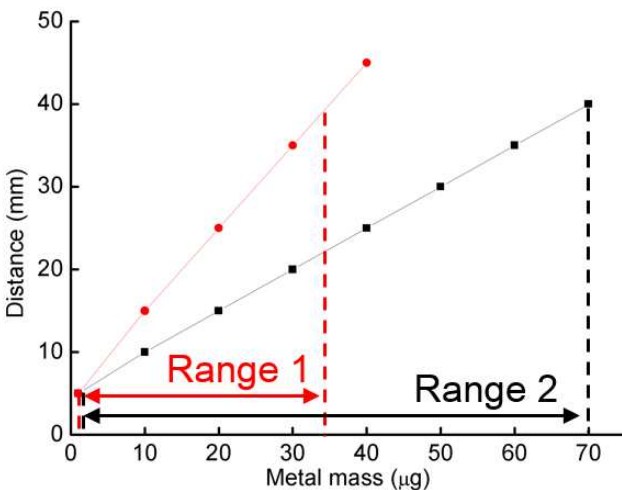


Figure 4-4 | Hypothetical curves showing changes in dynamic range as a result of slope. The lines on the horizontal were drawn to intersect the vertical axis at 40 mm, which represented the distance at which the eluent velocity was approximately zero.

must be present before color formation is visible with the unaided eye. A channel width of 3.5 mm was chosen for this study because it produced a response curve with the best sensitivity and largest dynamic range for Fe. Although the dynamic range of 4.7 mm wide channels was slightly larger (Figure 4-5b), the slope of the response curve was low, prompting our decision to pursue testing with 3.5 mm channels. Further alterations of channel geometry were not considered for this study but could potentially provide a larger overall dynamic range for metals. Narrow channels produce higher sensitivity (good for low analyte levels), but were non-ideal for larger analyte concentrations because less surface available for analyte-reagent complexation produced a longer band of color. Due to a constant reduction in eluent flow rate with penetration distance in the channel, long (i.e. > 50 mm) color bands were undesirable because eluent velocity beyond 50 mm was approximately zero.

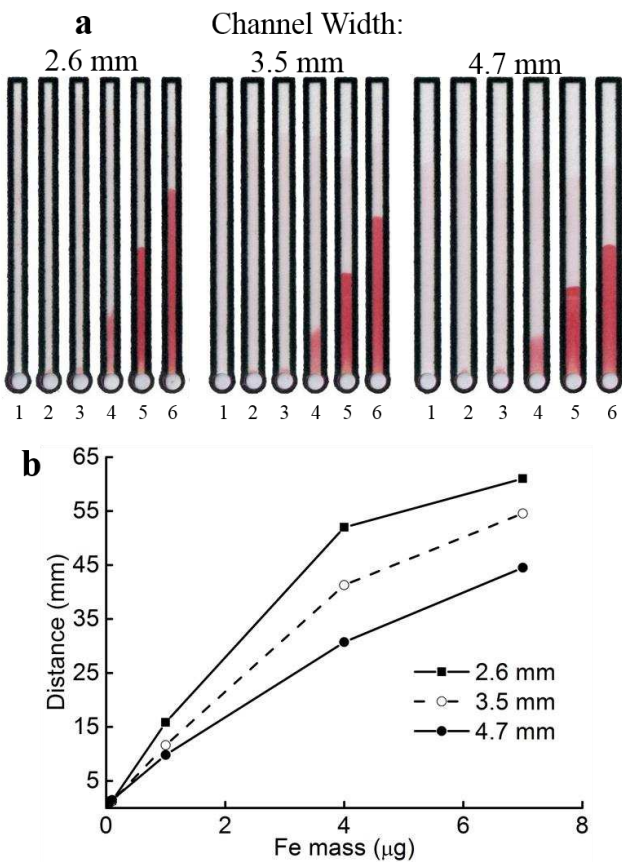


Figure 4-5 | (a) Detection sensitivity for Fe(II) varied as a function of channel width. (b) Quantitative data from (a). As channel width increased, the sensitivity (slope) of Fe(II) measurement decreased.

Distance-Based Detection of Ni, Cu, and Fe in Single Channels

Gradients of colorimetric reagents were printed 1-25 times in odd-numbered increments; devices were tested with the same analyte range (0.1-20 μg) for all three metals ($n \geq 5$). If two or more concentrations produced the same linear dynamic range, preference was given to the concentration that produced the highest sensitivity (slope). The dynamic ranges for Ni, Cu, and Fe were 0.1-10, 0.1-17, and 0.05-7 μg , respectively ($n \geq 10$). Relative standard deviations ranged from 6.0-6.6% (Figure 4-6). From an exposure perspective, these linear ranges correspond to metal aerosol concentrations (as time-weighted averages) from 1.43-143, 1.43-242, and 0.710-99.8 $\mu\text{g m}^{-3}$

assuming analysis is performed using a 10-mm filter punch extracted from a 37-mm filter operating at 2 L min^{-1} of air flow for an 8-hr workshift.⁴⁹ Time-weighted averages are used in occupational air sampling to calculate a welder's exposure to a hazardous substance, averaged over an 8-hr shift.⁴⁹ When compared to the minimum action level for a substance, the time-weighted average exposure determines if a person has been exposed to a toxic concentration of a metal species (action levels vary by metal). If the average exposure is above the action level, corrective action such as more frequent exposure monitoring and medical surveillance must be taken to mitigate undue risk.⁴⁹ A comparison between the analyte ranges that were measurable between gradient printing and manual reagent deposition (spraying) showed that printing extended the dynamic range by 50, 41, and 0% for Ni, Cu, and Fe, respectively. Results are displayed for all three metals in Figure 4-6. The difference in Fe performance compared to Ni and Cu is unclear and is under investigation. However, the linearity of the Fe assay was still improved. Response curve data near the LOD does not cross the vertical axis at zero because a band of color is not visible (and therefore measurable) when analyzing analyte masses below the LOD. By extending the dynamic ranges for Ni and Cu, a greater range of exposures can be analyzed. The TWA's for Ni, Cu, and Fe are all below the permissible exposure limits (1,000, 100, and 1,000 $\mu\text{g m}^{-3}$, respectively) established by the Occupational Safety and Health Administration.⁴⁹ This means that shorter sampling times can be used to capture task-based exposures instead of relying on an ensemble average over the course of a full day. Reagent printing also exhibited a significant improvement in relative standard deviation (from 11.4 to 6.4% on average) compared to manual deposition. Visual differences for the detection of Cu (1-13 μg) between devices in the presence and absence of a colorimetric reagent gradient are demonstrated in Figure 4-7. For a given Cu mass, the measured color band was longer in the presence of a gradient. This difference was

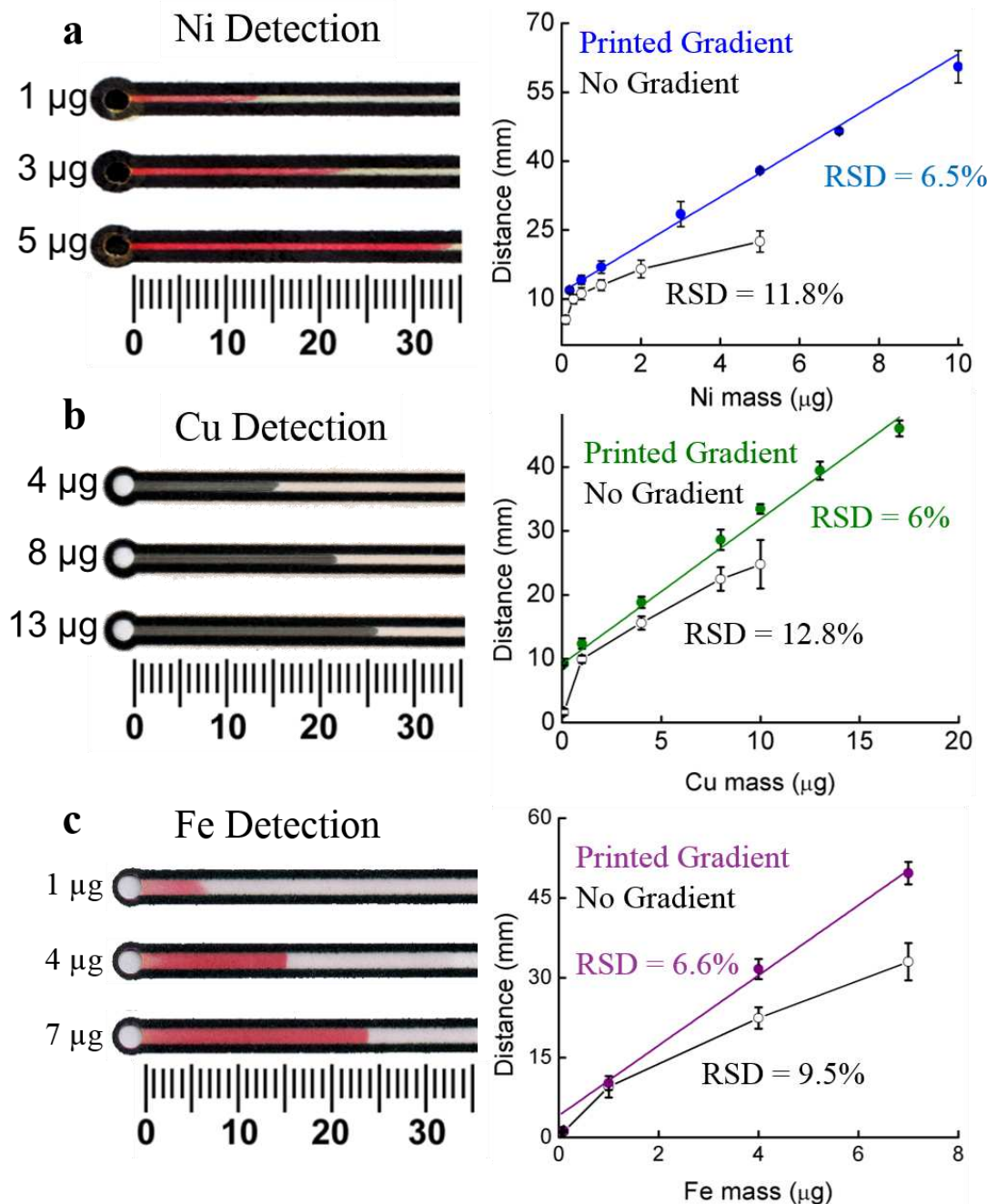


Figure 4-6 | Distance-based detection of (a) Ni, (b) Cu, and (c) Fe. Analyte was transported along the detection channel and precipitated upon complex formation with colorimetric reagents. Once analyte was consumed, color formation ceased and the distance from the beginning to the end of the color band was measured. Wicking distance was proportional to analyte mass. Printing a concentration gradient increased the linear dynamic range of Ni and Cu by 50 and 41%, respectively, than in the absence of a gradient. Inkjet printing was also more reproducible than manual reagent deposition. ($n \geq 4$).

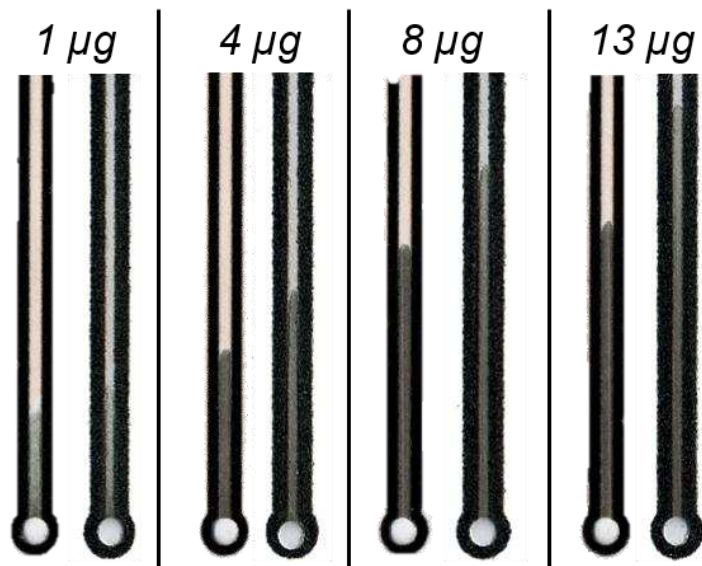


Figure 4-7 | In the presence of a reagent gradient, the distance of the color band increased as a function of the mass of Cu added. For each set of devices, the left and right images were in the absence or presence of a reagent gradient. In the absence of a gradient, reagents were deposited evenly across the substrate surface.

magnified at higher Cu masses. The average differences between band distance for devices with and without gradients for Cu masses of 1, 4, 8, and 13 µg were 3.6, 7.9, 10.7, and 15.2 mm, respectively.

For single-channel μPADs, the limit of detection is much higher for Ni, Fe, and Cu (7, 3, and 7 ppm), respectively, than for ICP-OES (1-10 ppb), which is the most common detection technique for heavy and transition metal detection. ICP-OES is certainly sensitive, however the cost of analysis (on a per-sample basis) is several orders of magnitude higher than for the μPAD technique presented here. Another common analytical method, X-ray fluorescence spectroscopy, is less expensive than ICP-OES, but detection limits are not appreciably better than with μPADs (sub 10 ppm).

Sensor performance is affected by ambient temperature and percent relative humidity (%RH). At high temperatures/low %RH, it is possible that the sample well could evaporate before most of the analyte has entered the μ PAD. Moreover, low temperatures/high %RH could pose additional complications. Experiments were performed with single-channel devices to establish conditions under which performance was unaffected by changes in temperature or %RH (Figure 4-8). For the first assay, 0.1-13 μ g Cu was measured with dithiooxamide from 23-51 °C (at 25 %RH). In the second assay, 0.1-13 μ g Cu was measured with dithiooxamide from 20-80 \pm 4% RH (at 20 °C). In both assays, solutions in devices were allowed to dry completely before analysis. Dithiooxamide was printed homogeneously along the substrate wicking channel. As demonstrated in Figure 4-8, significant differences were observed in the distance of color development between low and high temperatures at Cu masses of 8 and 13 μ g ($n = 4$). Experiments of %RH were not repeated, so definitive conclusions cannot be made based on the data shown in the figure, but it appears that significant differences in measured distance begin to appear above 60 %RH.

Simultaneous Distance-Based Detection of Ni, Cu, and Fe

Multi-Channel Device Geometry

Device inlet geometry was investigated for the multi-channel format. At neutral pH, the overall charge at the surface of cellulose was negative, which could hinder cation transport in the device through electrostatic interaction. We hypothesized that a device with more inlet surface area led to higher metal detection limits because, when present at low mass, metal analyte was sufficiently hindered by the cellulose matrix (and thus, some proportion of each sample failed to reach the detection zone). Two devices with varying inlet surface areas, A and B, were tested; reagent concentrations, solution pH, masking agents, and detection channel geometry were equivalent

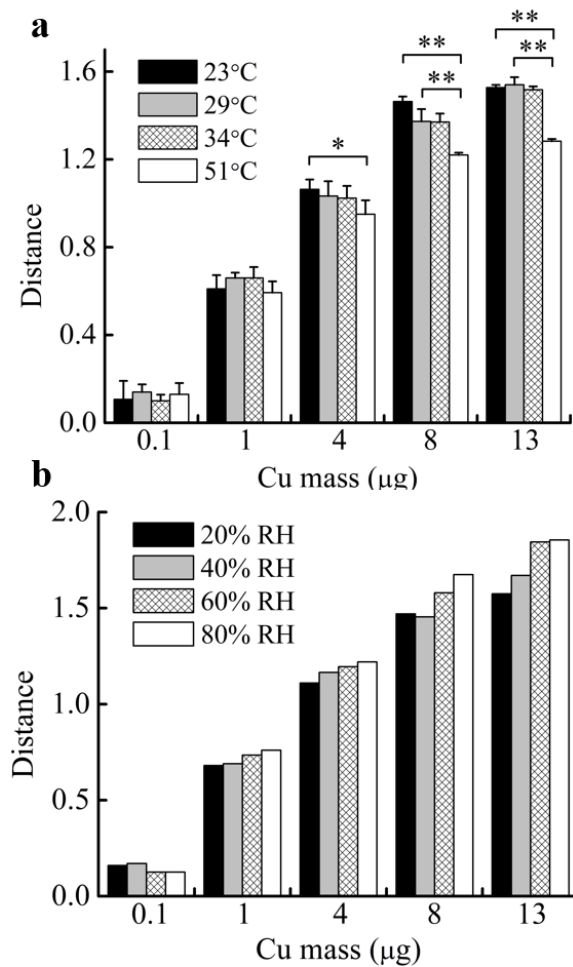


Figure 4-8 | Effect of (a) temperature and (b) percent relative humidity on measurement outcomes. * $p < 0.05$; ** $p < 0.001$.

between both devices (Figure 4-9). Device A had approximately 66% more inlet surface area than device B. The mass of Ni tested for both devices ranged from 5-80 μg . The limits of detection for devices A and B were 20 and 5 μg , respectively. Both devices responded similarly (i.e. not statistically different) above 35 μg Ni.

A droplet of solution added to the sample zone wicked towards the detection channels as a result of capillary action. The path length from the sample zone to either Ni or Cu channels was longer than for Fe. The result was that fluid fronts for Ni and Cu significantly lagged (i.e. minutes) behind

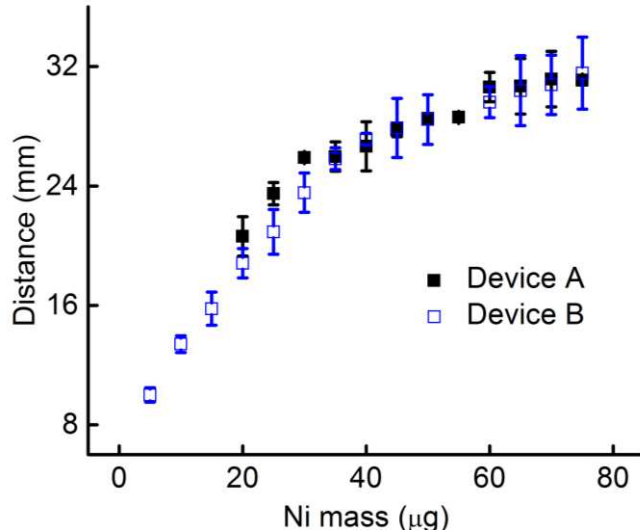


Figure 4-9 | Dynamic range increased for multi-channel detection of Ni when the inlet surface area was reduced.

the front for Fe. Two approaches were sought to produce equivalent volumetric flow rates in all channels: 1) increase the length of the flow path to the Fe channel, and 2) decrease the width of the flow path to the Fe channel, creating a constriction that limited the flow rate of eluent to the Fe channel. An elongated flow path extended the time for the fluid front to travel from the sample to detection zone; however, we observed significant analyte losses to the capillary network as a result of chemical interactions between cationic metals and cellulose. We opted for the second method, testing a variety of lengths and widths of constriction channels bounded by wax barriers, before settling on a channel $500 \times 750 \mu\text{m}$ (W×L) after melting with a laminator. Channels narrower than $500 \mu\text{m}$ were not reproducible.

Analyte Measurements

Three single-channel devices were combined in parallel for simultaneous measurement of Ni, Cu, and Fe. Design changes implemented in the multi-channel device were: dual rulers printed between detection channels for easy analyte quantitation, a larger sample well to accommodate higher-

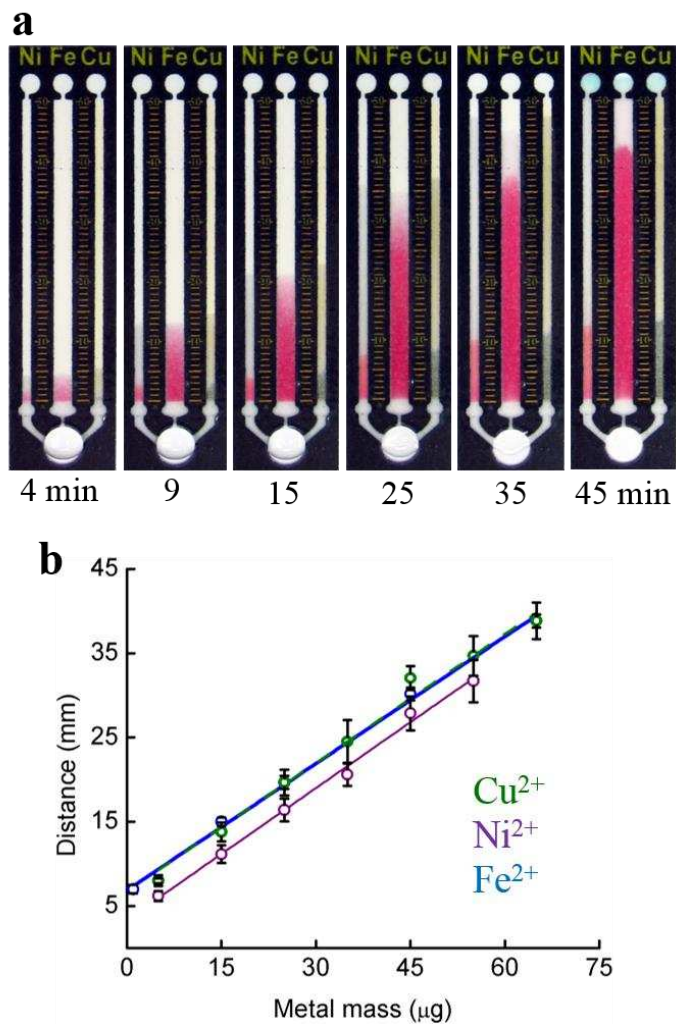


Figure 4-10 | (a) Time lapse of 15, 5, and 5 μg Fe, Ni, and Cu. (b) Response curves for Cu, Ni, and Fe in the multi-channel device.

volume droplets and larger samples (3 vs. 8 mm), wide wax barriers (4.2 mm before melting) between channels to mitigate cross-contamination, and a passive timer. The passive timer was composed of a blue dye (food coloring) printed at the end of each detection channel on the underside of the device and allowed to dry. When eluent reaches the end of the detection channel, the dye was solubilized and quickly migrated to the top of the device. Thus, the presence of blue dye indicates assay completion. A time lapse of detection is presented in Figure 4-10a for 5, 5, and 15 μg Ni, Cu, and Fe, respectively. This automated indicator system is simple, removes all external

timing mechanisms, and reduces any potential error due to assay timing. Moreover, timing for each channel is independent of the others; complications in any one channel will not impede analyte measurement in the other two.

Eluent flow rates were measured in the multi-channel system to establish empirical equations for reagent gradient printing. Future efforts will be directed towards establishing predictive flow models in these devices, eliminating the need for empirical fits. Linear dynamic range, detection limits, and device reproducibility were investigated using serially diluted analytical standards (2,000 ppm). Metal ranges varied from 1 to 100 µg. The linear dynamic ranges presented in Figure 4-10b for Ni, Cu, and Fe were 5-55, 1-65, and 5-65 µg, respectively ($20 \leq n \leq 32$ per mass). Relative standard deviations ranged from 6.7-8.4% (7.6% average). For aerosol exposure monitoring, time-weighted averages for these range values are 71.3-784, 14.3-927, and 71.3-927 µg m⁻³, respectively. The relative standard deviation was slightly higher (7.6%, up from 6.4%) for the multi-channel device than for assays conducted in single channels likely due to greater variance present in device fabrication (e.g. variation in width of constriction channel). A comparison between single- and multi-channel devices is presented in Table 4-1. The mass of analyte that was measurable was likely higher for the multi-channel device due to analyte losses from flow in paper and from analyte splitting as a result of operating parallel channels. In the multi-channel format, analyte was split between three channels. Ni and Cu channels each occupy ~25% of the available surface area for detection meaning that the mass of analyte entering either channel was decreased (vs. a single-channel device) by ~75%.

Table 4-1 | Comparison of dynamic range and percent relative standard deviation for single and multi-channel devices for analyte mass (concentration). n ≥ 100

Metal	Single Channel (μg) (ppm)	Multi-Channel (μg) (ppm)	Single-Channel (Multi-Channel) %RSD (n ≥ 10)
Ni	0.10 – 10 (6.7 – 670)	5.0 – 55 (100 – 1100)	6.5 % (6.7 %)
Fe	0.05 - 7.0 (3.3 – 470)	1.0 – 65 (20 – 1300)	6.6 % (7.7 %)
Cu	0.10 – 17 (6.7 – 1100)	5.0 – 65 (100 – 1300)	6.0 % (8.4 %)

To quantify intra- and inter-device variability, assays were conducted for all three metals with large sample sizes (i.e. n > 100). A minimum of three independent reagent solutions were made, and at least three separate sheets of devices were fabricated. Reagent printing was performed over the course of one week. Weighted confidence and prediction intervals ($\alpha = 0.05$) are provided in Figure A2-2 for Ni, Cu, and Fe. Capturing the variability present in solution preparation, reagent printing, and device fabrication enabled us to quantify the error around the measurement of a single unknown sample, which is relevant for actual use in the field. When measuring Ni, for example, if the nominal mass being measured were 15 μg (lower end of dynamic range), we would expect the multi-channel device to measure distances ranging from 9–13 mm, corresponding to a measured Ni mass between 12-18 μg , which is $\pm 20\%$ (n = 140). If the nominal mass measured were 45 μg (higher end of the dynamic range), we would expect distances between 23-30.5 mm (37-53 μg Ni, which is $\pm 18\%$).

Table 4-2 | Common metal alloys used for welding and their chemical composition (% m/m).

Alloy	% Nickel	% Chromium	% Copper	% Iron	% Manganese	% Zinc
SS301	6-8	16-18	Trace	> 70	0-2	Trace
SS304	8-10.5	18-20	0-1	> 60	0-2	Trace
SS308	10-12	19-21	Trace	> 65	0-2	Trace
SS309-EL	12-15	22-24	Trace	> 55	0-2	Trace
SS17-4 PH	3-5	15-17.5	3-5	> 60	0-1	Trace
SS20	32-38	19-21	3-4	> 30	0-2	Trace
Brass	0.2-1	Trace	55-95	0-2	0-1.8	4-43.5
INCONEL® (Ni alloy)	72	15.5	0.5	8	1	Trace

Interferences

Welding fumes contain numerous metal and gaseous compounds. Respirable fume composition varies based on the welding technique performed and on the composition of the welding rod, flux, shielding gas, and metal substrate being welded.⁵⁰ Stainless steel, perhaps the most common commercially welded metal, contains large quantities of Ni (6-15% wt%), Cr (16-24% wt%), and Fe (\geq 50% wt%). A short list of common metal alloys and their chemical composition is provided in Table 4-2. The complexity of the welding-fume matrix suggests that other metal species may interfere with our analysis, so a tolerance study was performed. The tolerance ratio is defined as the mass of metals that generates no more than a 10% change in the distance measured versus the control, for Fe, Ni, and Cu.⁵¹ Analytes, Fe, Ni, and Cu, were held at 10 μ g while the mass of each interfering metal species was varied according to the ratio (μ g interference / μ g analyte) presented in Table 4-3. Interfering metals were not evaluated above 10 \times the analyte mass. From the results, it was determined that Ni(II), Fe(II), Zn(II), Co(III), Cd(II), Pb(II), Mn(II), V(III), Mg(II), Al(III), or Ba(II) did not interfere with distance-based detection of Fe, Ni, or Cu based on the average

Table 4-3 | Matrix interferences evaluated by tolerance ratios. Analytes, Fe, Ni, and Cu, were held at 10 µg and the mass of each interfering metal species was varied according to the ratio (µg interference / µg analyte).

Interfering Ion	10% Tolerance Ratio		
	Ni	Cu	Fe
Ni(II)	--	≥ 10	0.5
Fe(II)	≥ 10	≥ 10	--
Fe(III)	5	≥ 10	≥ 10
Cu(II)	1	--	≥ 10
Zn(II)	≥ 10	≥ 10	1
Co(III)	1	≥ 10	1
Cd(II)	≥ 10	≥ 10	≥ 10
Pb(II)	≥ 10	≥ 10	≥ 10
Mn(II)	≥ 10	≥ 10	≥ 10
V(III)	1	≥ 10	1
Cr(VI)	10	5	0.5
Mg(II)	≥ 10	≥ 10	≥ 10
Al(III)	1	≥ 10	5
Ba(II)	≥ 10	≥ 10	≥ 10

chemical composition of stainless or mild steel. The relative percent composition of Ni in most metal alloys is not expected to reach 0.5× of Fe. Similarly for Co(II), the percent composition should rarely meet or exceed that of Ni. When Fe(III) was present at more than 5× the mass of Ni, competition occurs for ligand coordination with DMG.⁵² For example, if 50 µg Fe(III) were added in the presence of 10 µg Ni, the resulting color band for Ni would travel ~20 ± 2 mm (vs. ~7 mm for 10 µg Ni alone). This was likely a consequence of the higher solubility of the Fe(DMG)₂(OH)₂

Table 4-4 | Ni, Cu, and Fe detection from certified welding fumes. Reference fume was certified for Fe, Mn, and Zn. n = 3

WF Sample	Actual Level (μg)			Measured Level (μg)			Percent Recovery (%)		
	Fe	Ni	Cu	Fe	Ni	Cu	Fe	Ni	Cu
119_11	59.6	7.4	Trace	57 \pm 4.5	6.9 \pm 1.6	--	96 \pm 7.6	93 \pm 21	--
119_21	59.6	7.4	5.0	65 \pm 4.7	7.5 \pm 0.9	4.5 \pm 2.0	109 \pm 7.9	102 \pm 12	90 \pm 40
119_31	15.0	6.9	5.0	15 \pm 2.1	9.0 \pm 4.5	5.1 \pm 1.5	99 \pm 14	131 \pm 66	102 \pm 30

complex, based on infrared absorbance spectra data, than the Ni(DMG)H₂ complex.⁵² Of interest however, was that the distance traveled by the color band was predictable, suggesting that a correction factor could be implemented to account for the presence of Fe(III). It should be noted, however, that in practice, a 10% change in sensor response is not large from an exposure stance. For example, if the permissible exposure limit (PEL) for soluble Fe compounds is 10,000 $\mu\text{g m}^{-3}$ (OSHA), it is unlikely to matter whether the response of the paper sensor has an error of even 20%. If the nominal concentration of Fe being measured were 20 $\mu\text{g m}^{-3}$, for example, it is insignificant if the sensor reported a concentration that ranged from 16-24 $\mu\text{g m}^{-3}$ (\pm 20%).

Welding Fume Reference Material

A certified stainless steel reference fume was digested and assayed for Fe, Ni, and Cu with the multi-channel device. Results are presented in Table 4-4. Three different fume samples were tested, each in triplicate. In the first sample, trace levels of Cu were below the detection limit of the device. Standard addition of 5 μg Cu was used for two other samples. Percent recovery was close to 100%. The percent error for detection of low (< 10 μg) metal mass was due to high relative percent error. This represents a limitation of our system when measuring analyte mass near the detection limit. Reference samples used for testing were in powder form, but typically, welding fumes would be collected through collection of the fume onto air sampling filters. Metals would

be subject to acid digestion procedures, as described previously.¹¹ Although additional sample preparation would be necessary in this event, digestion would be carried out with small filters (1-10 mm diameter), which would require small (μL) reagent volumes and some power (e.g. low-wattage microwave), both which represent improvements over traditional preparation methods.

Conclusions

Paper microfluidics presents many advantages over traditional analytical instruments for exposure monitoring, such as portability, cost, ease-of-use, and complexity of operation. Colorimetric detection is one of the most commonly utilized detection motifs in paper microfluidics; however, the need for external detection tools makes the technique less ideal for on-site application. Distance-based detection captures the simplicity of colorimetric measurement but is more cost effective for widespread deployment. In this work, we utilized the precision and gradient-printing capabilities of commercial inkjet printing to extend the dynamic range of distance-based detection for Ni and Cu, and improve the linearity for Fe. As was demonstrated, the multi-channel device can measure Ni, Cu, and Fe simultaneously from many sources of metal particulates (e.g. welding fumes) with minimal matrix effects on the analytical signal.

REFERENCES FOR CHAPTER 4

1. D. M. Cate, W. Dungchai, J. C. Cunningham, J. Volckens and C. S. Henry, *Lab on a Chip*, 2013, **13**, 2397-2404.
2. C. A. Pope III, M. J. Thun, M. M. Namboodiri, D. W. Dockery, J. S. Evans, F. E. Speizer and C. W. Heath Jr, *American journal of respiratory and critical care medicine*, 1995, **151**, 669-674.
3. United States Environmental Protection Agency, Nickel Compounds, <http://www.epa.gov/ttnatw01/hlthef/nickel.html>, (accessed March 2015).
4. W. M. Draper, K. Ashley, C. R. Glowacki and P. R. Michael, *Analytical chemistry*, 1999, **71**, 33-60.
5. M. R. Gomez, S. Cerutti, L. L. Sombra, M. F. Silva and L. D. Martínez, *Food and Chemical Toxicology*, 2007, **45**, 1060-1064.
6. J.-P. Gouillé, L. Mahieu, J. Castermant, N. Neveu, L. Bonneau, G. Lainé, D. Bouige and C. Lacroix, *Forensic Science International*, 2005, **153**, 39-44.
7. C. C. Conrad and K. G. Hilchey, *Environmental monitoring and assessment*, 2011, **176**, 273-291.
8. M. M. Mentele, J. Cunningham, K. Koehler, J. Volckens and C. S. Henry, *Analytical chemistry*, 2012, **84**, 4474-4480.
9. S. Z. Hossain and J. D. Brennan, *Analytical chemistry*, 2011, **83**, 8772-8778.
10. A. Apilux, W. Dungchai, W. Siangproh, N. Praphairaksit, C. S. Henry and O. Chailapakul, *Analytical chemistry*, 2010, **82**, 1727-1732.
11. D. M. Cate, P. Nanthalasurasak, P. Riwkulkajorn, C. L'Orange, C. S. Henry and J. Volckens, *Annals of occupational hygiene*, 2014, met078.
12. G. G. Lewis, J. S. Robbins and S. T. Phillips, *Chemical Communications*, 2014, **50**, 5352-5354.
13. S. Z. Hossain, R. E. Luckham, M. J. McFadden and J. D. Brennan, *Analytical chemistry*, 2009, **81**, 9055-9064.
14. B. M. Jayawardane, S. Wei, I. D. McKelvie and S. D. Kolev, *Analytical chemistry*, 2014, **86**, 7274-7279.
15. R. V. Taudte, A. Beavis, L. Wilson-Wilde, C. Roux, P. Doble and L. Blanes, *Lab on a Chip*, 2013, **13**, 4164-4172.
16. W. Dungchai, Y. Sameenoi, O. Chailapakul, J. Volckens and C. S. Henry, *Analyst*, 2013, **138**, 6766-6773.
17. Y. Sameenoi, P. Panymeesamer, N. Supalakorn, K. Koehler, O. Chailapakul, C. S. Henry and J. Volckens, *Environmental science & technology*, 2012, **47**, 932-940.
18. D. M. Cate, J. A. Adkins, J. Mettakoonpitak and C. S. Henry, *Analytical chemistry*, 2014, **87**, 19-41.
19. A. K. Yetisen, M. S. Akram and C. R. Lowe, *Lab on a Chip*, 2013, **13**, 2210-2251.
20. A. K. Ellerbee, S. T. Phillips, A. C. Siegel, K. A. Mirica, A. W. Martinez, P. Striehl, N. Jain, M. Prentiss and G. M. Whitesides, *Analytical chemistry*, 2009, **81**, 8447-8452.
21. S. C. Lou, C. Patel, S. Ching and J. Gordon, *Clinical chemistry*, 1993, **39**, 619-624.
22. G. G. Lewis, M. J. DiTucci and S. T. Phillips, *Angewandte Chemie*, 2012, **124**, 12879-12882.

23. Y. Zhang, C. Zhou, J. Nie, S. Le, Q. Qin, F. Liu, Y. Li and J. Li, *Analytical chemistry*, 2014, **86**, 2005-2012.
24. G. G. Lewis, J. S. Robbins and S. T. Phillips, *Analytical chemistry*, 2013, **85**, 10432-10439.
25. R. Zuk, V. Ginsberg, T. Houts, J. Rabbie, H. Merrick, E. Ullman, M. Fischer, C. Sizto, S. Stiso and D. Litman, *Clinical chemistry*, 1985, **31**, 1144-1150.
26. R. Masoodi, M.S. Thesis, The University of Wisconsin-Milwaukee, 2010.
27. R. Masoodi and K. M. Pillai, *AICHE journal*, 2010, **56**, 2257-2267.
28. D. J. Cohen, R. C. Morfino and M. M. Maharbiz, *PloS one*, 2009, **4**, e7086.
29. B. Derby, *Journal of Materials Chemistry*, 2008, **18**, 5717-5721.
30. N. Komuro, S. Takaki, K. Suzuki and D. Citterio, *Analytical and bioanalytical chemistry*, 2013, **405**, 5785-5805.
31. K. Abe, K. Suzuki and D. Citterio, *Analytical chemistry*, 2008, **80**, 6928-6934.
32. X. Li, J. Tian, G. Garnier and W. Shen, *Colloids and Surfaces B: Biointerfaces*, 2010, **76**, 564-570.
33. K. Abe, K. Kotera, K. Suzuki and D. Citterio, *Analytical and bioanalytical chemistry*, 2010, **398**, 885-893.
34. K. Maejima, S. Tomikawa, K. Suzuki and D. Citterio, *RSC advances*, 2013, **3**, 9258-9263.
35. S. Z. Hossain, R. E. Luckham, A. M. Smith, J. M. Lebert, L. M. Davies, R. H. Pelton, C. D. Filipe and J. D. Brennan, *Analytical chemistry*, 2009, **81**, 5474-5483.
36. W. W. Yu and I. M. White, *Analytical chemistry*, 2010, **82**, 9626-9630.
37. W. Y. Wei and I. M. White, *Analyst*, 2013, **138**, 1020-1025.
38. University of Washington, MicroFluidics 2.0, <http://www.mf20.org/>, (accessed March 2015).
39. E. Tekin, P. J. Smith and U. S. Schubert, *Soft Matter*, 2008, **4**, 703-713.
40. W. D. Jacobs and J. H. Yoe, *Analytica Chimica Acta*, 1959, **20**, 332-339.
41. M. Soylak and N. D. Erdogan, *Journal of Hazardous Materials*, 2006, **137**, 1035-1041.
42. K. D. Charleton, A. E. Smith and D. M. Goltz, *Analytical Letters*, 2009, **42**, 2533-2546.
43. V. Rouchon, M. Duranton, O. Belhadj, M. Bastier-Deroches, V. Duplat, C. Walbert and B. V. Hansen, *Polymer Degradation and Stability*, 2013, **98**, 1339-1347.
44. F. E. Grubbs, *The Annals of Mathematical Statistics*, 1950, 27-58.
45. A. Paul, *Analytical Chemistry*, 1963, **35**, 2119-2121.
46. E. Schlemper and R. K. Murmann, *Inorganic Chemistry*, 1983, **22**, 1077-1081.
47. G. F. Smith, W. H. McCurdy and H. Diehl, *Analyst*, 1952, **77**, 418-422.
48. E. W. Washburn, *Physical review*, 1921, **17**, 273.
49. United States Department of Labor, Occupational exposure to hazardous chemicals in laboratories.,
https://www.osha.gov/pls/oshaweb/owadisp.show_document?p_id=10106&p_table=STANDARDS, (accessed March 2015).
50. J. T. Karlsen, G. Farrants, T. Torgrimsen and A. Reith, *The American Industrial Hygiene Association Journal*, 1992, **53**, 290-297.
51. S. Chaiyo, O. Chailapakul, T. Sakai, N. Teshima and W. Siangproh, *Talanta*, 2013, **108**, 1-6.
52. K. Burger, I. Ruff and F. Ruff, *Journal of Inorganic and Nuclear Chemistry*, 1965, **27**, 179-190.

CHAPTER 5: EMPIRICAL OBSERVATIONS ON FLOW RATE AND ANALYTE DEPOSITION FOR DISTANCE-BASED DETECTION

Chapter Overview

This chapter covers important variables that influence bulk flow and analyte deposition during μ PAD analysis of Ni, Cu, and Fe. Flow through porous networks is considered first, and theoretical flow models are compared with empirical flow data. The influence of hydrophobic barriers, lamination, and reaction kinetics are also covered. This chapter is intended to lay the foundation of future efforts to approximate wicking distance as a function of metal-ligand complex chemistry.

Capillary-Driven Flow in Porous Media

Filter paper has been used for centuries to extract, separate, trap, and inhibit chemical species of interest due to paper's unique physical and chemical composition. High surface-to-volume ratios of cellulosic fibers are particularly adept at trapping chemical agents while spontaneously wicking hydrophilic (or hydrophobic depending on fiber chemistry) media through a complicated fibrous network. Modeling the flow of a liquid in a porous membrane is complex, as such flows depend on average pore size of the fibrous network, pore size distribution, thickness, and porosity as well as the properties of the fluid. The pore size distribution refers to the range of pore sizes in the membrane. Filter papers with identical average pore size can have significantly different pore size distributions; consequently, capillary flow rate is determined more by pore size distribution than on average pore size.¹ As the aggregate pore size increases, however, capillary flow rate increases as well. Porosity is the volume occupied by air in a membrane and is typically given as a percentage of the membrane's total volume. For example, a strip of paper measuring $1 \times 1 \times 180 \mu\text{m}$ (i.e. a

square sheet of Whatman 1 paper) has a volume of $180 \mu\text{m}^3$ ($\sim 1 \text{nL}$). The porosity (or void fraction) of Whatman 1 paper, as published by the manufacturer, is $\sim 68\%$, hence the volume occupied by air in the membrane is $\sim 0.68 \text{nL}$ ($0.68 \times 1 \text{nL}$). Alternatively, porosity (ϕ) can be estimated based on the basis weight of paper (m_0), density of cellulose (ρ_c), and paper thickness (b) as

$$\phi = 1 - \frac{m_0}{\rho_c b}.$$
² The density of cellulose is $\sim 1540 \text{ kg m}^{-3}$. The void fraction can also be used to calculate the volume of liquid required to completely “wet” the membrane.

The most well-known models for understanding imbibition, or the spontaneous movement of a liquid into a porous medium, were postulated by Lucas, Washburn, Darcy, and Poiseuille.³⁻⁶ The relation between wicking rate and the square root of time was found to be linear, i.e. $L = at^m$ where L is wicked mass or height, a is a proportionality constant, and m is approximately 0.5.⁷

Assumptions made for simple, one-dimensional modeling include treating the porous structure as a bundle of aligned (parallel) capillary tubes and neglecting effects from inertia and gravity. Groups have since derived relationships to take effects from these forces into account; however, in some cases, the resulting equations were nonlinear, second order, and could not be solved analytically.⁸ In certain cases, such as when fluid displacement occurs over much larger distances ($\sim \text{cm}$) than the pore size ($\sim \mu\text{m}$), local flow through small pore spaces can be overlooked.⁹ The flow rate in the devices described in this dissertation can be modeled by Darcy’s law in 1D:

$$v(x) = -\frac{k}{\mu} \frac{dp}{dx} \quad \text{where } v \text{ is fluid velocity in the direction of flow } x, k \text{ is the permeability of the}$$

substrate (and is treated as a constant), μ is fluid viscosity, and $\frac{dp}{dx}$ is the change in pressure along

the direction of flow. Substrate permeability can be estimated empirically.^{10, 11} Additional conditions of the system include:

1. Macroscopic flow is stationary and free of inertia
2. System is isothermal
3. Low Reynolds numbers
4. Force due to gravity is negligible
5. Fluid is incompressible
6. Evaporation and condensation effects are negligible
7. Substrate is isotropic, macroscopically homogeneous, and rigid
8. Fiber swelling effects are negligible
9. Hydrodynamic resistance is negligible
10. γ , r_{eff} , and θ are constant

In the model system, capillary action drives flow in one direction with an average velocity $v(x)$, where the capillary pressure (p_c) at the location of the fluid front is expressed by Laplace's

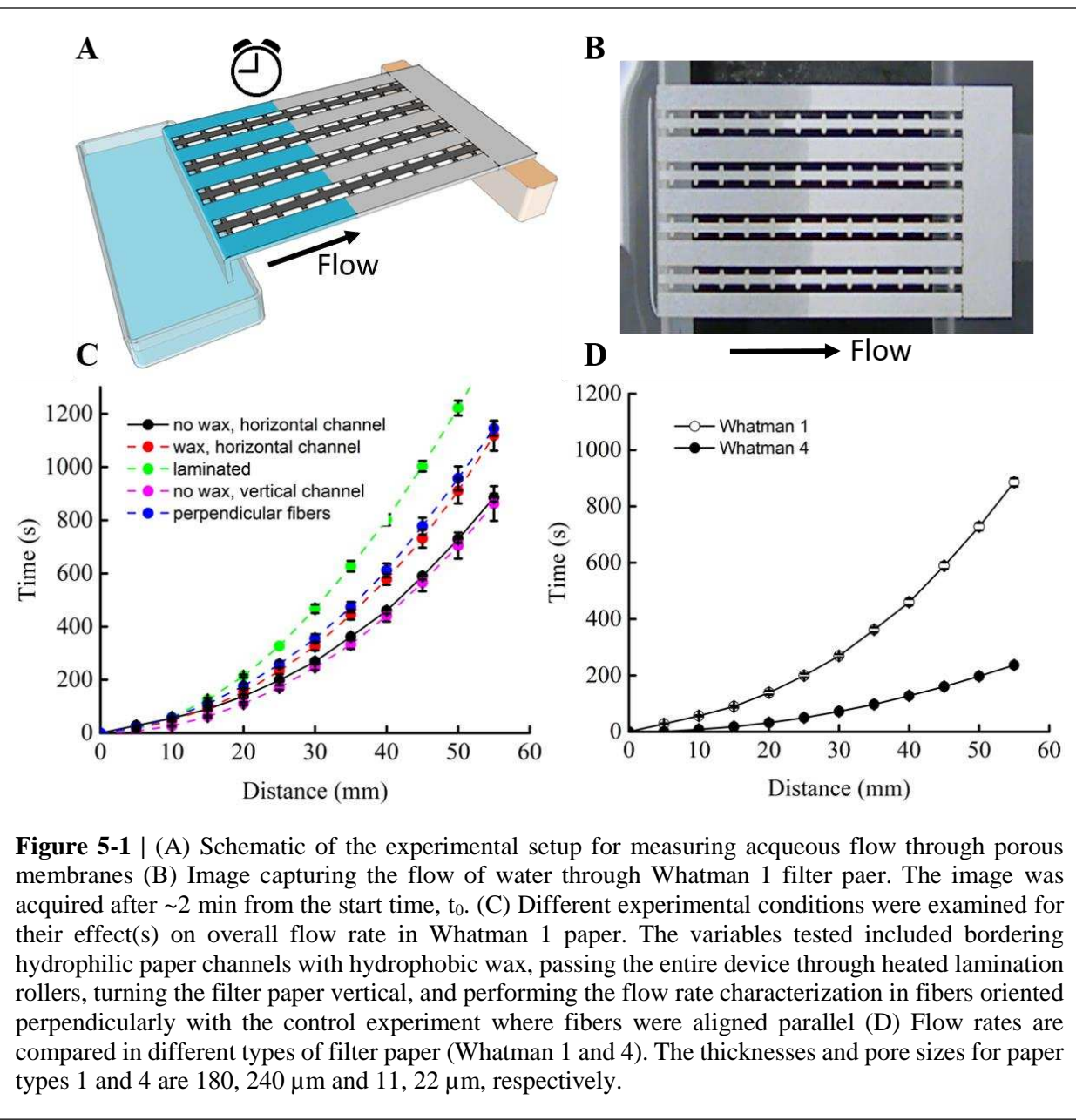
equation: $p_c = p_{\text{atm}} - \frac{2\gamma \cos \theta}{r_{\text{eff}}}$ where γ is the liquid-air surface tension, θ is liquid-solid contact

angle, and r_{eff} is the effective pore radius (essentially the average pore radius) in the substrate.

Elizalde et al.,⁹ used Darcy's law as described above to estimate the position of the liquid front, l ,

versus time, t , according to: $\frac{k}{\mu} \int_0^l A(l') dl' + \int_0^l \left[A(l') \int_0^{l'} \frac{dx}{A(x)} \right] dl' = \frac{k \Delta p}{\mu} t$, where $A(l)$ is the cross

sectional area of the porous channel and because channels in my experiments have constant width, $A(x)$ is constant (5 mm in Figure 5-1c). A fit of experimental parameters for both Darcy and Washburn models is shown in Figure 5-2. Although the fit is fairly predictive of flow behavior,



some incongruities (especially for low values of t) could stem from systematic errors in the experiment such as incorrectly estimating the time elapsed for the fluid front to reach the first 5 mm mark in each channel.

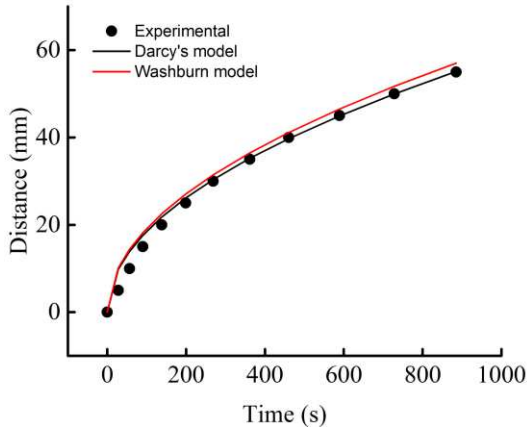


Figure 5-2 | Two models of flow in porous networks is compared with experimental data obtained using Whatman 1 filter paper.

Influence of Variables

Gravity

For flow through a single capillary tube, the influence of gravity versus capillary forces scales with the Bond number, $Bo = \rho g l d / \sigma$, which is a function of fluid density (ρ), gravitational acceleration (g), capillary diameter (d), penetration distance (l), and surface tension (σ).¹² For a wicking distance of 50 mm (typical for experiments described in chapters 3 and 4), $Bo \sim 10^{-2}$ for Whatman paper 1 and 4, hence gravitational effects are negligible. Demonstrated in Figure 5-1c is the difference in penetration distance for colored water in vertical and horizontal strips of Whatman 1 paper. Flow in vertical strips is against the force of gravity, which is approximately two orders of magnitude weaker than the capillary force. Other constants such as capillary diameter (d) and porosity (ϕ) play an important role in determining flow velocity (Figure 5-1d). Typical values for d and ϕ in Whatman 1 and 4 paper are $d = 11, 22 \mu\text{m}$ and $\phi = 0.686, 0.691$, respectively.

Wax Boundaries

Water imbibition is commonly described in the literature by Washburn's equation describing the dynamics of one-dimensional fluid flow through a cellulose matrix, provided that gravitational and inertial effects are negligible.^{3, 13-15} Washburn's equation deduced that imbibition distance l is given by $l = k \sqrt{\frac{\sigma}{\mu} t}$, where k is a proportionality constant, σ is surface tension, μ is dynamic viscosity, and t is time. Although wicking phenomena through a cellulose network has been described with this model, recently, several groups have observed imbibition dynamics that are inconsistent with Washburn's model, especially for flow in narrow channels bordered by hydrophobic walls.¹⁶⁻¹⁸ The inconsistency is likely due to the fact that Washburn's model anticipates that wicking speed is independent of channel width; however, observations suggest that wicking speed in narrow channels (bordered by a hydrophobic barrier) was lower than as predicted by Washburn's model. This effect was also observed in my experiments for 1.5 mm wide channels in Whatman 1 paper, bordered by a wax barrier (Figure 5-1c). My hypothesis for this observed flow rate reduction is that the contact angle between an imbibing fluid (e.g. water) and a hydrophobic barrier (e.g. wax) is greater than 90°, whereas the contact angle between water and capillaries in bulk is less than 90°. Strong ionic interactions between polar water molecules and the hydroxide groups of linked glucose units in cellulose produce better capillary action than when channels are bordered by wax, where repulsive forces between water and wax impede flow velocity. Hong et al.¹⁹ introduced an empirically-determined constant in their model, β , to consider the length of an advancing fluid front in contact with wax boundaries. The form they derived for

predicting imbibition length, l_m , was $l_m = k \sqrt{(1 + \beta \frac{d}{w\phi^{1/3}} \frac{\cos\theta_b}{\cos\theta}) \frac{\sigma}{\mu} t}$, which is a function of surface tension σ , viscosity μ , capillary diameter d , contact angle of the fluid-capillary θ , contact

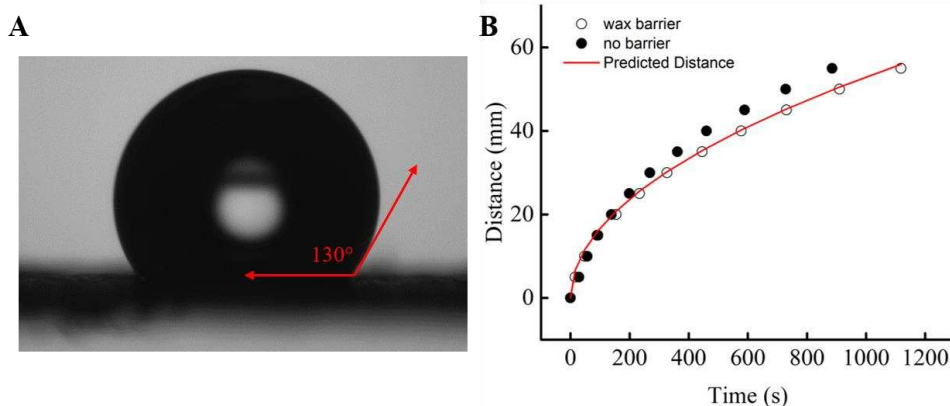


Figure 5-3 | (A) Static contact angle measured for a $2 \mu\text{L}$ water droplet on wax that was printed and melted into Whatman 1 filter paper. The mean static angle (degrees) for the drops on wax was $130 \pm 1.2^\circ$ ($N = 5$). (B) Predicted wicking distance (red line) as a function of time for channels bordered by wax (open circles) compared with a control (filled circles).

angle of the fluid-boundary θ_b , channel width w , and paper porosity ϕ . The ratio $\frac{\theta_b}{\theta}$ is greater than 1.0 in my devices because the contact angle at the fluid-wax boundary is greater than 90° , as shown in Figure 5-3a, suggesting that narrow channels bordered by wax will tend to have reduced flow velocity compared with a channel without hydrophobic barriers. The above equation was fitted to experimental data from Figure 5-1c where flow velocity in a narrow (~1.5 mm wide) channel was observed over time. The proportionality constant, k was decreased by ~25% (from 0.264 to 0.200) to ensure the fit was accurate. Because the proportionality constant was determined empirically (for Whatman 1 paper) by Hong et al., it's feasible that k should also be determined for my system, where differences in experimental protocol could account for a 25% change in k .

Lamination

Lamination has been used to fabricate microfluidic devices since the 1990's,^{20, 21} but it was not until 2008 when lamination for μPADs was first reported.^{22, 23} Patterning with hydrophobic chemicals (e.g. wax, fluoropolymers, AKD)^{13, 24, 25} or forming physical boundaries (e.g. laser or

craft cutting)^{26, 27} provides limited mechanical stability to paper, especially when wet (it is considerably worse if the wetted surface area is large relative to the overall sheet size). To address this concern, groups have turned to clamps,²⁸ tape,²⁹ additional layers of paper,³⁰ and printing toner³¹ not only to provide additional support for the paper substrate (except for the toner), but also to prevent solvent evaporation and reagent contamination from the environment. Although these methods have merit, certain adhesives dissolve in organic solvents, and clamps are not practical for large-volume manufacturing. In this work, devices were laminated to strengthen the paper substrate during chemical analysis, to prevent solvent evaporation, and to protect the user from contacting reagents printed on the devices. The effect of lamination on flow velocity was studied using Whatman 1 filter paper with the same geometry as described above. Briefly, paper devices cut via laser cutter were passed through a laminator at 340 °F once. Thermal lamination sheets are coated with an adhesive designed to melt at temperatures below 100 °F; with filter paper, the adhesive penetrates into cellulose fibers, which further holds the laminate and paper together. The results of the flow rate study are shown in Figure 5-1c (N = 5). After 15 and 55 mm, the average flow velocity for unbonded channels was 0.17 and 0.06 mm s⁻¹, respectively (a 2.7× reduction), whereas after the same distance, the average flow velocity for bonded (laminated) channels was 0.12 and 0.04 mm s⁻¹, respectively (a 3.2× reduction). The average time delay for the wicking front to reach 15 and 55 mm between unbonded and bonded channels was 36 and 576 s, respectively.

Reduced flow velocity in bonded channels was initially thought to be due to increased resistance from the hydrophobic lamination sheet in contact with the carrier fluid. However, water contact angles determined for lamination sheets both before and after lamination, as shown in Figure 5-4, demonstrated that the surface energy of the sheet was fairly low (contact angle ~65°). Another

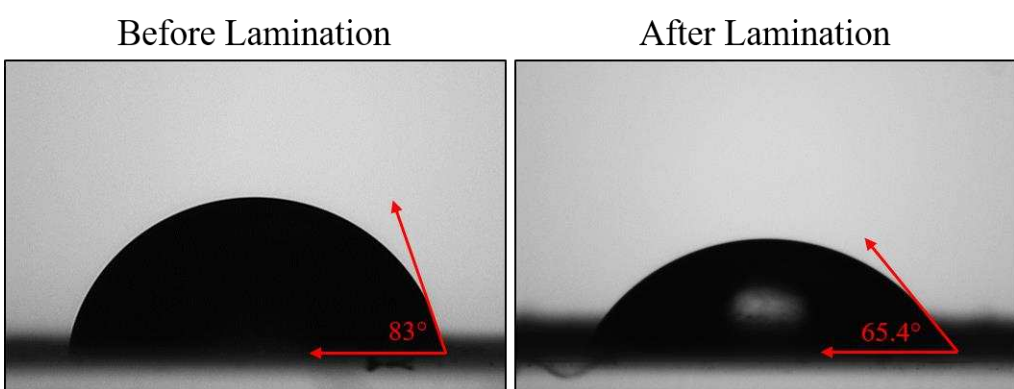


Figure 5-4 | Static contact angles measured for 2 μL water drops before and after thermal lamination. The mean static angle (degrees) for the drops on the left and right images was $83 \pm 2.5^\circ$ ($N = 4$) and $65.4 \pm 8.9^\circ$ ($N = 3$), respectively.

hypothesis is that paper fibers are compressed by the rollers during lamination. If paper is not allowed to re-expand – as is the case here because the thermal lamination sheet prevents it – then the effective capillary radius of the fibers decreases, resulting in a decrease in flow rate.³ Cassano et al. demonstrated that flow rate could be controlled by changing the distance between rollers during device lamination; they found that smaller spacing (38.1 vs. 1 mm) between rollers produced the largest compression force on paper and the greatest reduction in flow rate.³² Roller temperature was also investigated for its influence on flow rate; however, it was determined to be negligible as long as the temperature was sufficient to melt adhesive on the laminate sheets. Any small gaps formed at the edges of the paper by the lamination process are also inconsequential because the wax barrier completely contains the analyte solution in the hydrophilic channel (i.e. no leaking). Encapsulating the device may also increase back pressure by not allowing air to escape from the paper matrix, which could decrease flow rate. During the melting process, adhesive may also be partially blocking pores in the paper.

Determining capillary flow rate is important for laminated devices because the effective concentration (C) of analyte in any given sample is inversely proportional to the square of the change in flow rate.¹ In other words, $C \propto \left(\frac{v_{unbonded}}{v_{bonded}}\right)^{-2}$, where $v_{unbonded}$ and v_{bonded} are linear flow rates for non-laminated and laminated paper channels. Using the flow rates obtained from Figure 5-1c, the effective analyte concentration at 15 mm, for example, would be $\sim 2\times$ higher in a bonded device compared with one that is unbonded. This implies that the location of reagent deposition is important to consider regarding assay sensitivity because flow velocity is always decreasing with penetration distance (and time) in paper. If reagents are deposited further from the location of analyte introduction, the volume of sample that physically passes through the reagent zone decreases, lowering detection sensitivity of the entire assay.

Reaction Rate Constants

Determining the rate constants for reactions between analyte and metal is important for effectively modeling the rate at which an analyte precipitates on the substrate for distance-based detection. Slow (or fast) reaction kinetics could change how frequently collisions between product and reaction occur, which could dictate the location of complex precipitation in the detection channel. The amount of complex (C), formed is generally defined as $C = k[A][B]$ where k is a rate constant and A, B are the concentrations of the metal ion and the colorimetric reagent, respectively. In this example, the rate of the reaction is 1st order. An assumption here is that reagent B becomes immobilized on the paper surface because its solubility in water (the eluent) is very low.

Perhaps the most well-characterized chemistry of Ni is in the +2 oxidation state.³³ The reagent used in this work for the detection of soluble Ni is dimethylglyoxime (dmgH₂), the dioxime derivative of diketone butane-2,3-dione. The conjugate base (dmgH⁻) is responsible for forming metal-ligand charge-transfer complexes with divalent Ni to form a bright pink-red complex Ni(dmgH)₂.³⁴ Poor solubility in aqueous media facilitates rapid precipitation of the complex, which was why it was an attractive analyte for distance-based detection (Chapters 3, 4). Nitrogen atoms in dmgH₂ are sp² hybridized and gives rise to a five-member, square-planar geometric complex with Ni. The specificity of dimethylglyoxime for Ni is pH dependent; a UV-Vis analysis of the complex has concluded that the maximum absorption peak occurs between pH 9.3-9.5. The overall reaction for Ni with DMG is $Ni^{2+} + 2DMG \xrightarrow{k} Ni(DMG)_2$ is considered pseudo-first order with respect to Ni concentration with the overall reaction rate being expressed as

$$\frac{d[Ni(DMG)_2]}{dt} = k[Ni][DMG] \text{ where } [DMG] \gg [Ni] \text{ in solution.}^{35}$$

Integrating both sides with respect to t produces an expression for $[Ni(DMG)_2] = [DMG]_0 e^{kt}$ where the overall rate constant measured using adsorptive differential pulse cathodic stripping voltammetry is $\sim 3 \times 10^5 \text{ s}^{-1}$.³⁶

Less characterized are colored ligand-metal exchange processes concerning Cu and Fe with the colorimetric reagents dithiooxamide and bathophenanthroline used in chapters 3 and 4. Dithiooxamide (rubeanic acid) is tetradentate and forms a linear coordination complex with weakly acidic Cu(III) salt solutions in water.³⁷ One hypothesis for the formation complex between Cu and dithiooxamide is that the metal atom is heavily shielded inside a coordinated polymer structure, potentially forming a linear polymer.³⁸ The 1:1 reaction is very selective for Cu at low pH; sub ppm detection sensitivities have been reported for spectroscometric determination of Cu

at 650 nm, even in the presence of other metals.³⁹ Dithiooxamide is known to exist in a tautomerization equilibrium depending on solution pH, but the acid form must be deprotonated to form metal-ligand complexes.^{40, 41} The solubility product constant of the metal-ligand precipitate is $\sim 7.7 \times 10^{-15}$.⁴² A common reagent for spectrophotometrically determining Fe(II) in solution is bathophenanthroline (4,7-diphenyl-1,10-phenanthroline, Bphen), forming a red complex that is highly insoluble in water. The Fe(II)-Bphen complex has a high molar extinction coefficient of $\sim 22,400 \text{ M}^{-1} \text{ cm}^{-1}$ at 533 nm, which contributes to its high detection sensitivity for Fe species in solution. Solution pH plays an important role for detection specificity; groups have found that a solution pH of 4-5.5 produces the most sensitive results.⁴³ It has been postulated that the nitro-group in nitroferroin diminishes the basicity of the nitrogen atom to increase the stability of the Fe-Bphen complex, enabling detection in strongly acidic media.⁴⁴ The equilibrium constant for the first order reaction between Fe and Bphen is $\sim 2.5 \times 10^6 \text{ s}^{-1}$.⁴⁴

Closing Comments

To develop an analytical model that describes analyte complexation, precipitation, and detection requires knowledge of capillary wicking, reaction kinetics, and molecular transport. This chapter was intended to be a foundation for future modeling efforts using distance-based detection. In this chapter, certain environmental and substrate-specific variables were not considered, some of which may contribute significantly to the response of the device, depending on the application. For instance, evaporation of the analyte droplet was not considered. In certain cases where long flow residence times or if the analyte drop volume is small (~ single microliters), solvent evaporation could lead to significant variability in the device. Evaporation was not considered in this work, however, because experiments performed in chapter 3 demonstrated that even with an analyte drop

volume of 15 μL , ambient temperature was insignificant from 20-50° C. Above 50°C, evaporation became an issue to the point that analyte was not being carried into the detection channel. There are two solutions to this problem: 1) develop calibration curves which account for ambient temperature/relative humidity effects (evaporation of known a volume and analyte concentration is quantitative), or 2) enclose the device to control solvent evaporation and condensation.⁴⁵ Neither the Darcy or Washburn theoretical models of flow accounted for fiber swelling due to fluid wetting or a non-constant effective pore radius. Although not absolutely necessary to approximate flow in the channels in my experiments, being able to account for these effects would still improve the accuracy of the model. Both variables have been investigated by other groups and models have been developed that account for both effects.^{46, 47}

REFERENCES FOR CHAPTER 5

1. EMD Millipore, Rapid Lateral Flow Test Strips, <http://www.emdmillipore.com/>, (accessed 2015).
2. J. Wang, M. R. N. Monton, X. Zhang, C. D. Filipe, R. Pelton and J. D. Brennan, *Lab on a Chip*, 2014, **14**, 691-695.
3. E. W. Washburn, *Physical review*, 1921, **17**, 273.
4. R. Lucas, *Kolloid Z*, 1918, **23**, 15-22.
5. H. Darcy, *Les fontaines publiques de la ville de Dijon*, Victor Dalmont, 1856.
6. S. P. Sutera and R. Skalak, *Annual Review of Fluid Mechanics*, 1993, **25**, 1-20.
7. P. K. Chatterjee, *Absorbency*, Elsevier Scientific Pub.; Distributors for the United States and Canada Elsevier Science Pub. Co., 1985.
8. J. Szekely, A. Neumann and Y. Chuang, *Journal of Colloid and Interface Science*, 1971, **35**, 273-278.
9. E. Elizalde, R. Urteaga and C. L. Berli, *Lab on a Chip*, 2015, **15**, 2173-2180.
10. R. Masoodi and K. M. Pillai, *AICHE journal*, 2010, **56**, 2257-2267.
11. A. Koponen, D. Kandhai, E. Hellen, M. Alava, A. Hoekstra, M. Kataja, K. Niskanen, P. Sloot and J. Timonen, *Physical Review Letters*, 1998, **80**, 716.
12. R. Clift, J. R. Grace and M. E. Weber, *Bubbles, drops, and particles*, Courier Corporation, 2005.
13. Y. Lu, W. Shi, L. Jiang, J. Qin and B. Lin, *Electrophoresis*, 2009, **30**, 1497-1500.
14. D. A. Bruzewicz, M. Reches and G. M. Whitesides, *Analytical chemistry*, 2008, **80**, 3387-3392.
15. W. Dungchai, O. Chailapakul and C. S. Henry, *Analyst*, 2011, **136**, 77-82.
16. A. Böhm, F. Carstens, C. Trieb, S. Schabel and M. Biesalski, *Microfluidics and Nanofluidics*, 2014, **16**, 789-799.
17. E. Evans, E. F. M. Gabriel, W. K. T. Coltro and C. D. Garcia, *Analyst*, 2014, **139**, 2127-2132.
18. X. Li, P. Zwanenburg and X. Liu, *Lab on a chip*, 2013, **13**, 2609-2614.
19. S. Hong and W. Kim, *Microfluidics and Nanofluidics*, 2015, 1-9.
20. R. M. McCormick, R. J. Nelson, M. G. Alonso-Amigo, D. J. Benvegnu and H. H. Hooper, *Analytical Chemistry*, 1997, **69**, 2626-2630.
21. S. A. Soper, S. M. Ford, S. Qi, R. L. McCarley, K. Kelly and M. C. Murphy, *Analytical chemistry*, 2000, **72**, 642 A-651 A.
22. H. Liu and R. M. Crooks, *Analytical chemistry*, 2012, **84**, 2528-2532.
23. A. W. Martinez, S. T. Phillips and G. M. Whitesides, *Proceedings of the National Academy of Sciences*, 2008, **105**, 19606-19611.
24. Y. Lu, W. Shi, J. Qin and B. Lin, *Analytical chemistry*, 2009, **82**, 329-335.
25. X. Li, J. Tian and W. Shen, *Cellulose*, 2010, **17**, 649-659.
26. E. Fu, B. Lutz, P. Kauffman and P. Yager, *Lab on a Chip*, 2010, **10**, 918-920.
27. M. A. Nash, J. M. Hoffman, D. Y. Stevens, A. S. Hoffman, P. S. Stayton and P. Yager, *Lab on a chip*, 2010, **10**, 2279-2282.
28. P. Kauffman, E. Fu, B. Lutz and P. Yager, *Sensors and Actuators B: Chemical*, 2010, **149**, 325-328.

29. E. Canellas, M. Aznar, C. Nerín and P. Mercea, *Journal of Materials Chemistry*, 2010, **20**, 5100-5109.
30. E. M. Fenton, M. R. Mascarenas, G. P. López and S. S. Sibbett, *ACS applied materials & interfaces*, 2008, **1**, 124-129.
31. K. M. Schilling, A. L. Lepore, J. A. Kurian and A. W. Martinez, *Analytical chemistry*, 2012, **84**, 1579-1585.
32. C. L. Cassano and Z. H. Fan, *Microfluidics and nanofluidics*, 2013, **15**, 173-181.
33. K. Nag and A. Chakravorty, *Coordination Chemistry Reviews*, 1980, **33**, 87-147.
34. L. Tschugaeff, *Berichte der deutschen chemischen Gesellschaft*, 1905, **38**, 2520-2522.
35. V. Celo, J. Murimboh, M. S. A. Salam and C. L. Chakrabarti, *Environmental Science & Technology*, 2001, **35**, 1084-1089.
36. H. B. Xue, S. Jansen, A. Prasch and L. Sigg, *Environmental science & technology*, 2001, **35**, 539-546.
37. G. Peyronel, G. C. Pellacani and A. Pignedoli, *Inorganica Chimica Acta*, 1971, **5**, 627-633.
38. F. Feigl and V. Anger, *Spot tests in inorganic analysis*, Elsevier, 2012.
39. S. Son, S. Ueda, F. Kanamaru and M. Koizumi, *The Journal of Physical Chemistry*, 1976, **80**, 1780-1782.
40. Y.-T. Gong, M.-S. Won, Y.-B. Shim and S.-M. Park, *Electroanalysis*, 1996, **8**, 356-361.
41. R. N. Hurd, G. DeLaMater, G. C. McElheny and L. V. Peiffer, *Journal of the American Chemical Society*, 1960, **82**, 4454-4458.
42. S. Kanda, K. Yamashita and K. Ohkawa, *Bulletin of the Chemical Society of Japan*, 1979, **52**, 3296-3301.
43. E. M. Penner and W. R. Inman, *Talanta*, 1962, **9**, 1027-1036.
44. A. T. Pilipenko and E. R. Falendysh, *Russian Chemical Reviews*, 1972, **41**, 991.
45. K. Birdi, D. Vu and A. Winter, *The Journal of physical chemistry*, 1989, **93**, 3702-3703.
46. D. R. Schuchardt and J. C. Berg, *Wood and fiber science*, 1991, **23**, 342-357.
47. I. Jang and S. Song, *Lab on a Chip*, 2015, **15**, 3405-3412.

CHAPTER 6: CONCLUSIONS AND CONSIDERATIONS FOR THE FUTURE OF MICROFLUIDIC PAPER-BASED ANALYTICAL DEVICE TECHNOLOGY

Chapter Overview

This section presents alternative applications for μPAD technology and suggestions for improving the technology presented in Chapters 2–4 of this dissertation. Work in this chapter was not published at the time of writing, but may be included in future publications. Improvements in surface modification, reagent immobilization, substrate/support materials, inkjet-printing chemistry, and new modeling theory have opened many doors for future efforts in the field. The work in this dissertation describes measurement techniques that can be applied for rapid, on-site detection of targeted analytes, which is critical for understanding sources, transformations, and fates of environmental contaminants. This technology represents a step towards empowerment of the ‘citizen scientist’ - the idea that people will not only be able to monitor their exposure to harmful pollutants on a personal level but can also rapidly identify sources of pollution for scientific evaluation and remediation.

Improving μPAD Detection of Metals

Chemical Modification of the Substrate

The paper-based methods described in preceding chapters for determining metal concentrations in air pollution have detection limits as low as $0.71 \mu\text{g m}^{-3}$ (based on 37 mm sample filter, 4 L min^{-1} , 8 hr work-day) without additional substrate modification or sample pre-concentration. Although the reported detection limits are adequate in environments like in the occupational sector where acute exposure levels to toxic metals can exceed 2 mg m^{-3} ,¹ ambient exposure levels are typically

10–1000x lower.^{2,3} In drinking water for example, average Ni concentrations range from 5.5×10^{-4} – 0.025 mg m⁻³.⁴ Therefore, methods for improving detection sensitivity and selectivity could extend the μ PAD technology presented in this dissertation to applications where metals are expected to be present at low (near background) levels (*e.g.* home kitchens, drinking water, roadside emissions).⁵ Separating metals of interest from complexes and complicated matrices is vital for improving method sensitivity. My approach (Chapters 2–4) utilized masking chemistry to reduce the binding constants of interfering metal cations for the colorimetric reagent via: 1) an oxidizing or reducing agent (*e.g.* hydroxylamine hydrochloride reduced Fe(III) to Fe(II), preventing interference for Ni detection), and 2) altering solution pH.^{6,7} Solution chemistry is powerful, but the signal-to-noise ratio can be further improved; other methods have been reported recently for chemically and physically altering the paper substrate itself. Fortunately, cellulose is a relatively forgiving substrate for modifying surface chemistry to entrap chemicals. There are many methods for activating cellulose, usually with a small molecule or polymer, to generate surface functional groups suitable for analyte immobilization or physical adsorption.⁸ Depending on the application, methods have been reported for covalently linking aldehyde, epoxy, amines, benzophenones, phosphates, and carboxylic acid groups on the surface of paper.^{8–12} “Bioactive paper”, a term recently coined to describe paper sensors with activated surfaces for bioanalytical applications, has been developed using immobilized β -Galactosidase and CPRG for multiplexing the detection of Hg(II), Ag(I), Cu(II), Cd(II), Pb(II), Cr(VI), and Ni(II).¹³ The advantage of modifying the substrate to immobilize the analyte is that it enables parallel detection; complexation chemistry that is not carried in the solution phase as analyte is transported through the device means multiple processes can occur sequentially. Instead of needing to separate chemical processes for each metal (as was the case in Chapter 4), multiplexed detection can occur within

the same channel or physical zone in a device. Chemical immobilization will not automatically lower detection limits for every device, though, because buffer chemistry (and ionic strength) play very important roles in detection sensitivity and selectivity. Physical separation of detection chemistry may still be required, even if reagents are immobilized.

Introducing electrostatic attractive/repulsive chemistry between an analyte and the surface has also become a common approach for pre-concentrating the sample and improving signal-to-noise. For example, a passive sampling method for waterborne Zn(II) was recently developed by Almeida et al.¹⁴ where a polymer inclusion membrane functionalized with di-2-(ethylhexyl) phosphoric acid facilitated transport of divalent Zn from aquatic systems, through a sorbent membrane, to a receiving solution for collection and analysis. A similar approach has been used by others for selective determination of Cu(II) from samples of urban water.¹⁵ The reported detection limit of the method was 1×10^{-4} mg m⁻³. Additionally, multiple charged species can be sequentially added to the surface of paper in a layer-by-layer assembly to build or trap/enclose polar analytes within the poly-layer.¹⁶ Other promising possibilities for improving detection sensitivity includes imparting chelation, adsorption, hydrophilic, or hydrophobic properties to paper.

Physical Modification of the Substrate

During paper wetting, analytes become homogenously distributed throughout the thickness of the porous medium. For μ PADs, where quantification is commonly based on integrating the intensity of a colored product, vertical analyte transport can inhibit accurate (colorimetric) quantitation because visible light readily scatters off most paper types, meaning that much of the colored “signal” is lost beyond the first ~50 μ m of the paper surface.¹⁷ To improve detection efficiency,

analyte can be confined to a smaller surface area (assuming paper thickness remains constant), increasing analyte density and generating a higher colorimetric signal.⁷ The benefits of this approach have been reported for detecting gold nanorods at $< 10^{-18}$ M using surface-enhanced Raman scattering.¹⁸ In this work, the authors designed an octagonal star-shaped sensor where analyte added to the device wicked radially from the center of the device to the tip of each point, resulting in an extreme increase in analyte concentration.

Moving Away from the Benchtop

The sensor presented in Chapter 2 has only been tested in the laboratory, but of course, the ultimate goal for any μPAD technology is field deployment at the point-of-need. Two primary limitations impeding its portability are analyte quantification by desktop scanning and the need to physically compact the sample filter punch and device during operation. The first problem is easily addressable now that acceptance of camera phones is nearly ubiquitous worldwide.¹⁹ Details of camera phone-based applications for μPADs are discussed in Chapter 1. To quantify metal particulate sampled from air pollution, a pretreatment process (Chapter 2), must be performed which degrades the physical integrity of the sampling filter. The result of this process is an uneven (non-flat) filter. We found that interdevice reproducibility was improved if the filter punch (containing the metals of interest) was in as much contact with the cellulose substrate as possible. For early attempts, a couple textbooks (~5 lbs total) provided sufficient weight to press the filter flat; however, alternative methods are necessary if a truly field-deployable sensor is to be realized.²⁰ Figure 6-1 is a schematic of a 3D-printed cassette holder which houses a μPAD sandwiched between two poly(methyl methacrylate) (PMMA) layers. The PMMA layers were cut

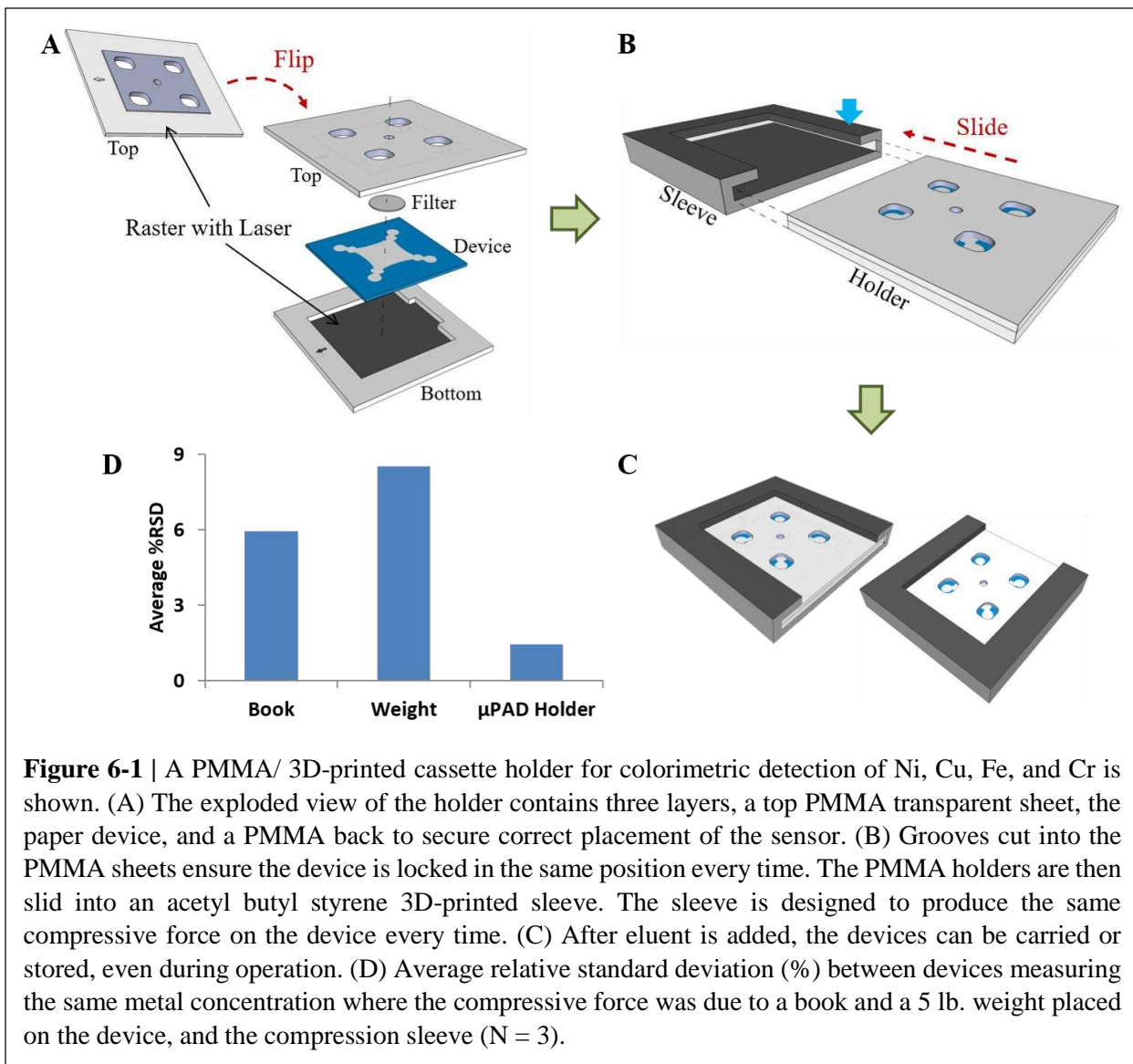


Figure 6-1 | A PMMA/ 3D-printed cassette holder for colorimetric detection of Ni, Cu, Fe, and Cr is shown. (A) The exploded view of the holder contains three layers, a top PMMA transparent sheet, the paper device, and a PMMA back to secure correct placement of the sensor. (B) Grooves cut into the PMMA sheets ensure the device is locked in the same position every time. The PMMA holders are then slid into an acetyl butyl styrene 3D-printed sleeve. The sleeve is designed to produce the same compressive force on the device every time. (C) After eluent is added, the devices can be carried or stored, even during operation. (D) Average relative standard deviation (%) between devices measuring the same metal concentration where the compressive force was due to a book and a 5 lb. weight placed on the device, and the compression sleeve ($N = 3$).

with a CO₂ laser in strategic areas such that eluent could be added while preventing the filter punch from losing contact with the paper surface.

Potential Pitfalls Inhibiting Widespread Use

Future improvements must be made to control liquid handling of strong bases and acids such that a minimally trained individual in the field can perform all sample preparation processes without undue risk to themselves. The vision for the future of μ PAD-based assessment of airborne metals

is that field analysis of metal analytes on filters could be performed by industrial hygienists having little technical training in chemistry or microfluidic fields.

A major reason μ PADs may have trouble translating from the benchtop to the field is lack of a true market need. In order for individuals to adopt any new technology, there must be a considerably motivating factor driving change. The low cost of paper sensors and convenience, as was the case for the at-home pregnancy test strip, may ultimately bridge the gap for other μ PADs. For now, significant limitations exist in emerging μ PAD assays such as detection sensitivity, selectivity, and sample size. Detection methods are continuing to improve, but how long will it be before assays can measure clinically relevant bio-analytes (in the biomedical case), or epidemiologically relevant contamination in drinking water? Current μ PADs are typically not stable or robust enough to handle complicated sample matrices, which is why they are relegated to the benchtop, for now. At present, there have been a few case studies where groups have attempted to commercialize new μ PAD technology, such as Microchips Biotech, Inc., Diagnostics For All, Optofluidics, Inc., Access Sensor Technologies, RainDance Technologies, Inc., and Smart Holograms Ltd. The market presence of these companies varies thus far, but because this field is still in its infancy, it will take a few more decades before μ PADs find their niche.

Considerations for the Future

The intent of paper-based analytical device technology is to change the paradigm of exposure assessment and biomedical diagnosis, driving costs down while simultaneously increasing the throughput of testing. In the end, the success or failure of μ PADs will likely be determined by their use outside of academic research laboratories, much like traditional microfluidic devices. While

significant attention has rightfully been placed on the potential for improved clinical diagnostics, there remain many other areas for future expansion. Particularly exciting is the potential for application of μ PADs for large epidemiology studies where analytical measurements have traditionally been a cost limiting factor. In a similar fashion, the low cost and ease of use may open the door to wide spread analytical measurements thereby enabling the growing field of citizen science. In fashion similar to precipitation monitoring in the United States by everyday citizens,²¹ μ PADs may open the door to wide spread environmental monitoring with spatial resolution that has never been achieved in previous studies.²² To achieve these endpoints, however, requires continued development of the basic chemistry of sensing with μ PADs.

REFERENCES FOR CHAPTER 6

1. J. Kim, J. Chen, P. Boyce and D. Christiani, *Occupational and environmental medicine*, 2005, **62**, 157-163.
2. K. Das, S. Das and S. Dhundasi, *Indian Journal of Medical Research*, 2008, **128**, 412.
3. G. J. Li, L.-L. Zhang, L. Lu, P. Wu and W. Zheng, *Journal of occupational and environmental medicine/American College of Occupational and Environmental Medicine*, 2004, **46**, 241.
4. Center for Disease Control, Toxicological profile for nickel, <http://www.atsdr.cdc.gov/HAC/pha/pha.asp?docid=257&pg=3>, (accessed 2015).
5. É. Nerriere, H. Guegan, B. Bordigoni, A. Hautemaniere, I. Momas, J. Ladner, A. Target, P. Lameloise, V. Delmas and M.-B. Personnaz, *Science of the Total Environment*, 2007, **373**, 49-56.
6. D. M. Cate, W. Dungchai, J. C. Cunningham, J. Volckens and C. S. Henry, *Lab on a chip*, 2013, **13**, 2397-2404.
7. D. M. Cate, P. Nanthalasurasak, P. Riwkulkajorn, C. L'Orange, C. S. Henry and J. Volckens, *Annals of occupational hygiene*, 2014, met078.
8. R. Pelton, *TrAC Trends in Analytical Chemistry*, 2009, **28**, 925-942.
9. D. Kong, W. Schuett, J. Dai, S. Kunkel, M. Holtz, R. Yamada, Y. Yu and H. Klinkmann, *Artificial organs*, 2002, **26**, 200-208.
10. A. Reinhartz, S. Alajem, A. Samson and M. Herzberg, *Gene*, 1993, **136**, 221-226.
11. S. Zadegan, M. Hosainalipour, H. Rezaie, H. Ghassai and M. Shokrgozar, *Materials Science and Engineering: C*, 2011, **31**, 954-961.
12. A. Böhm, M. Gattermayer, C. Trieb, S. Schabel, D. Fiedler, F. Miletzky and M. Biesalski, *Cellulose*, 2013, **20**, 467-483.
13. S. M. Z. Hossain and J. D. Brennan, *Analytical Chemistry*, 2011, **83**, 8772-8778.
14. M. I. G. S. Almeida, C. Chan, V. J. Pettigrove, R. W. Cattrall and S. D. Kolev, *Environmental Pollution*, 2014, **193**, 233-239.
15. B. M. Jayawardane, R. W. Cattrall and S. D. Kolev, *Analytica chimica acta*, 2013, **803**, 106-112.
16. R. S. Alkasir, M. Ornatska and S. Andreeescu, *Analytical chemistry*, 2012, **84**, 9729-9737.
17. A. K. Ellerbee, S. T. Phillips, A. C. Siegel, K. A. Mirica, A. W. Martinez, P. Striehl, N. Jain, M. Prentiss and G. M. Whitesides, *Analytical chemistry*, 2009, **81**, 8447-8452.
18. A. Abbas, A. Brimer, J. M. Slocik, L. Tian, R. R. Naik and S. Singamaneni, *Analytical Chemistry*, 2013, **85**, 3977-3983.
19. P. B. Lillehoj, M.-C. Huang, N. Truong and C.-M. Ho, *Lab on a chip*, 2013, **13**, 2950-2955.
20. M. M. Mentele, J. Cunningham, K. Koehler, J. Volckens and C. S. Henry, *Analytical chemistry*, 2012, **84**, 4474-4480.
21. Colorado Climate Center, Community Collaborative Rain, Hail & Snow Network, (accessed 2015).
22. C. C. Conrad and K. G. Hilchev, *Environmental monitoring and assessment*, 2011, **176**, 273-291.

APPENDIX 1: RECORDING COLORIMETRIC INTENSITY FOR QUANTIFYING METALS WITH μ PADS

Colorimetric intensity from reaction complexes in paper devices was quantified with a desktop scanner (XEROX DocuMate 3220) in TIFF format at 600 dpi to preserve image quality. Average pixel intensity was measured with public domain software (Image J, National Institutes of Health) in which the average pixel intensity contributed by red, green, and blue pixels was recorded at each detection zone. The process for analyzing paper devices by colorimetry is detailed here and is shown graphically in Figure A1-1.

1. Access the “Color Threshold” context menu in Image J through “Image/Adjust/Color Threshold”.
2. Select HSB detection mode which enables adjustment of image saturation, brightness, and hue.
3. Hue was adjusted empirically and the values for each metal are provided in Table A1-1.
4. Before integrating color intensity, images were inverted such that a pixel intensity value of 255 (range 0-255) corresponded to high metal concentration. If the images are not inverted, a brighter (or darker) color spot (i.e. high analyte concentration) would appear darker. Although technically correct, this method of analysis is less intuitive.
5. The mean intensity was measured by selecting “limit to threshold” in the “set measurements window”. The areas to be measured were selected via the wand tool which finds a grouping of similar pixels based on average pixel intensity.

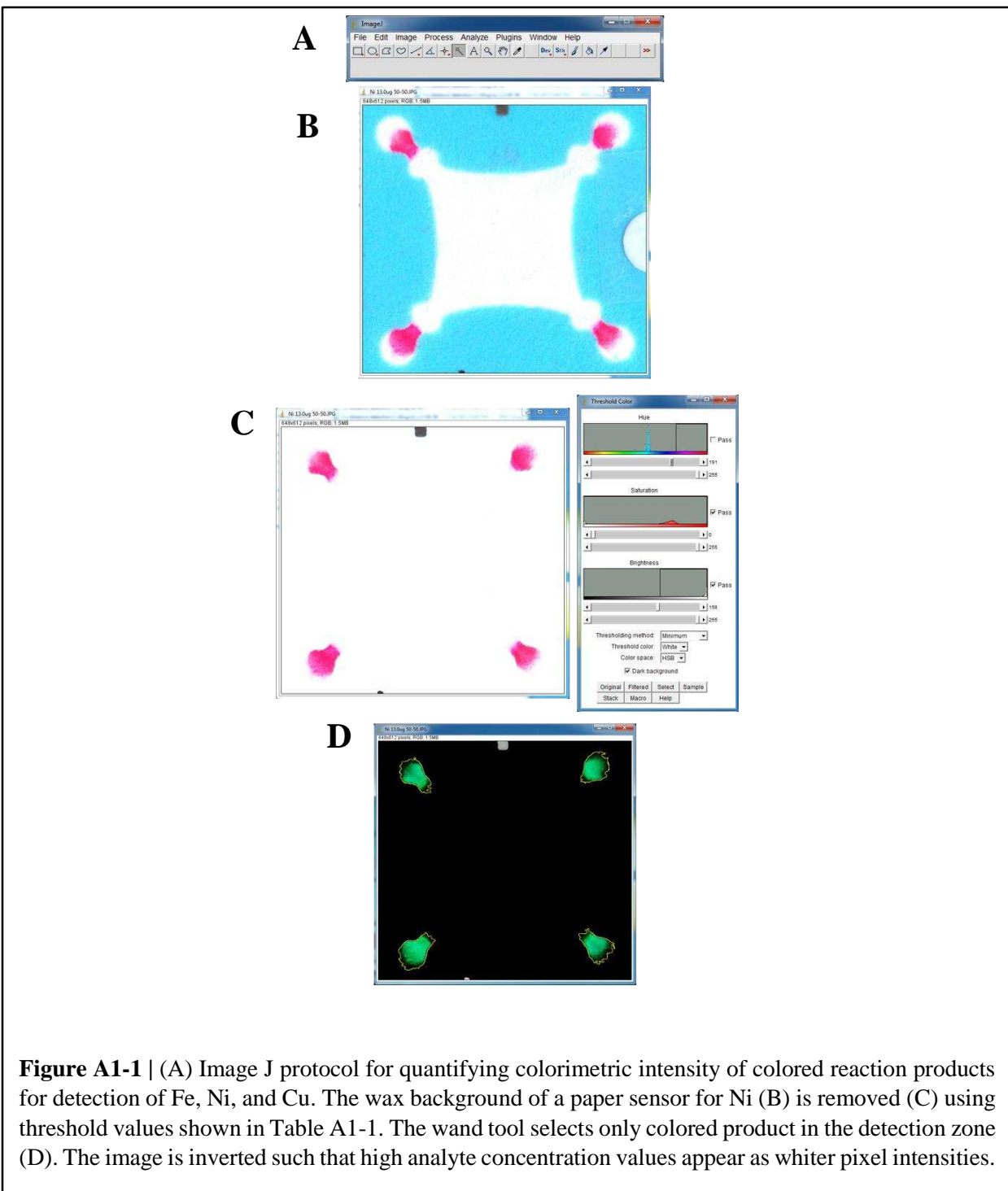


Table A1-1 | Threshold values for four metals using Image J software. The range of pixel intensity units is given for each metal, as well as the time-weighted average concentration for each. The TWA is the average concentration for which a person can be exposed for 8 hr per day over a career without measurable ill effects.

Analyte	μ PAD Signal Intensity Range (PIU ^a \pm SD)	Color Hue Thresholding Window Applied	TWA ^b Detection Range (μ g m ⁻³ \pm SD)
Fe	18.7-121 \pm 6.5	18 - 230	7.80-107 \pm 6.9
Cu	27.0-79.3 \pm 5.6	35 - 225	10.7-121 \pm 8.9
Ni	19.1-48.0 \pm 5.6	10 - 210	7.80-64.2 \pm 5.8
Cr	17.7-87.9 \pm 3.7	0 - 180	2.66-42.8 \pm 3.9

^a Pixel Intensity Unit

^b Time Weighted Average

Interdevice variability was measured for four paper sensors for Fe using desktop scanning and Image J for analysis. New solutions were made for each set of experiments over the course of seven days. The same protocol was followed for each analysis; results of the scan are given in Figure A1-2.

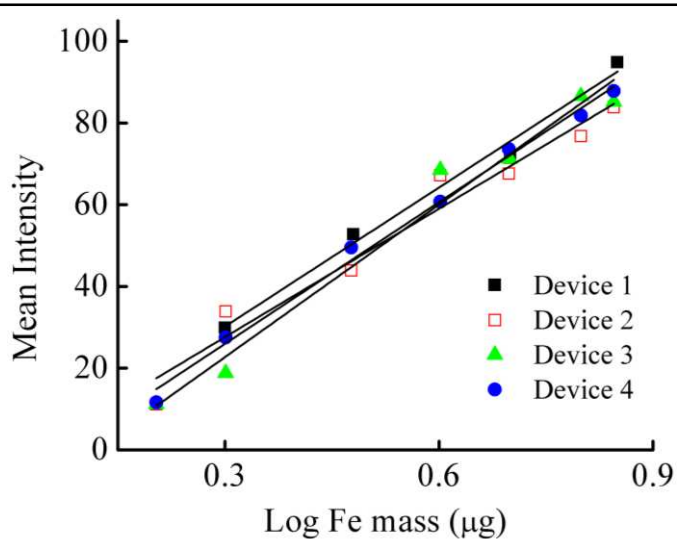


Figure A1-2 | Interdevice variability for Fe detection across four paper devices. The average difference in measured intensity per Fe mass (slope) was 4.8 ± 4.4 % across all curves.

APPENDIX 2: PRINTING COLORIMETRIC REAGENTS FOR DISTANCE-BASED DETECTION OF MULTIPLE METALS

A list of common solvents and a few of their properties is given in table A2-1. The surface tension, viscosity, and density are important parameters which determine how well a solution can be printed with common desktop thermal and piezoelectric printers. Another important factor to consider is solution vapor pressure because printing resolution is directly related to how quickly a droplet evaporates after deposition. For instance, under isothermal conditions, drops composed entirely of water (17.5 torr) will not evaporate as readily as isopropyl alcohol (32.4 torr) and will wick for a longer time in porous media. Ink formulations that were deemed “printable” were developed according to the reciprocal of the Ohnesorge number $Z = Oh^{-1}$ where $Oh = \frac{(d\rho\gamma)^{1/2}}{\eta}$ and is a function of print head diameter d , surface tension γ , density ρ , and dynamic viscosity η .

Creating Reagent Gradients

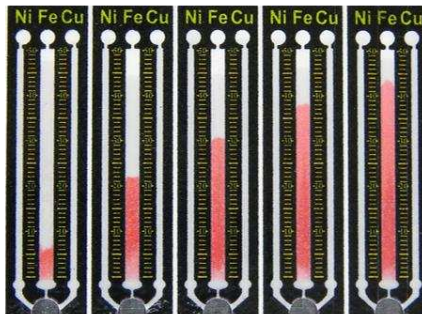
A reagent gradient was printed onto paper to change the distance-based output of metal detection. The method used to determine which gradient function was appropriate for printing is outlined in Figure A2-1. Briefly, the flow rate of several devices over a range of concentrations for a given metal were measured. A counter function was created such that it mirrored the best fit curve of the before-measured flow rates. A reagent gradient was printed according to the mirrored function, where the concentration of reagents were determined empirically.

Table A2-1 | Z values for common solvents. Values were quantified using Oh^{-1} based on a print head nozzle diameter of 90 μm .

Solvent Name	Vapor Pressure (Torr)	Viscosity (N s/m^2)	Density (kg/m^3)	Surface Tension (N/m)	Z value
<i>n</i> -Butyl Alcohol	4.4	0.00298	809.7	0.02457	14.1994
Isobutyl Alcohol	8.8	0.00285	801.6	0.02298	14.2866
Isopropyl Alcohol	32.4	0.0024	785.4	0.02179	16.3525
<i>n</i> -Propyl Alcohol	15	0.0023	803.7	0.0237	18.0017
Dimethyl Acetamide	1.3 (25°C)	0.00214	941.5	0.03243	24.4958
2-Methoxyethanol	6.2	0.00172	964.6	0.0318	30.5478
Dimethylsulfoxide	0.42	0.00199	1100	0.04354	32.992
Ethanol	40	0.001144	789	0.0221	34.6282
Ethyl Alcohol	43.9	0.0011	789.2	0.02232	36.1967
1,4-Dioxane	29	0.00137	1033.6	0.03445	41.3211
Cyclohexane	77.5	0.001	778.5	0.02498	41.8357
<i>o</i> -Dichlorobenzene	1.2	0.00132	1305.8	0.02684	42.5478
<i>o</i> -Xylene	6.6	0.000812	880	0.0301	60.1298
Pyridine	18	0.00095	983.2	0.03688	60.1332
<i>o</i> -Xylene	6	0.00081	880.2	0.03003	60.215
<i>n</i> -Butyl Acetate	7.8	0.00074	879.6	0.02509	60.2258
<i>N,N</i> -Dimethylformamide	2.7	0.00092	948.7	0.03676	60.8956
Methanol	97	0.00059	791.3	0.02255	67.9224
Iso-Octane	41	0.0005	691.9	0.01877	68.3762
Methyl Isobutyl Ketone	16	0.00058	800.8	0.02364	71.1671
Chlorobenzene	8.8	0.0008	1105.8	0.03328	71.9385
m-xylene	8.3	0.00062	860	0.0289	76.283
Ethylene Dichloride	83.35	0.00079	1253	0.03223	76.3132
Toluene	28.5	0.00059	866.9	0.02853	79.9659
Water	17.54	0.001	998.2	0.0728	80.8715

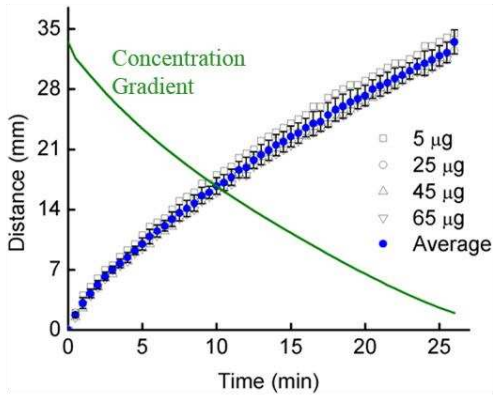
Measure Velocity of Fluid Front

Step 1



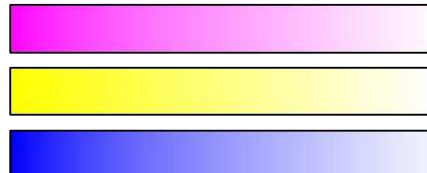
Create Counter Function, $G(D)$

Step 2



Convert $G(D)$ into Colored Image

Step 3



Print Concentration Gradient on Substrate

Step 4

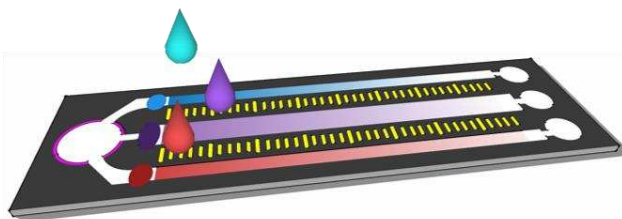


Figure A2-1 | Steps to create a printable reagent gradient.

Empirically derived equations given below were used to print colorimetric gradients for measuring Ni, Cu, and Fe. For each equation, eluent flow rates were first measured in the multi-channel device for several analyte concentrations. The equations below were normalized to 255, the maximum intensity in RGB space for a given color. For the following equations, the units on the vertical and horizontal axes were RGB intensity and distance in pixels, respectively.

$$\text{Equation for Ni: } y = -7.6 \times 10^{-8}x^4 + 4.4 \times 10^{-5}x^3 - 1.0 \times 10^{-2}x^2 + 2.1x + 5.7$$

$$\text{Equation for Cu: } y = -7.0 \times 10^{-8}x^4 + 4.0 \times 10^{-5}x^3 - 1.1 \times 10^{-2}x^2 + 2.2x + 6.3$$

$$\text{Equation for Fe: } y = -6.0 \times 10^{-8}x^4 + 4.0 \times 10^{-5}x^3 - 9.6 \times 10^{-3}x^2 + 2.1x + 4.1$$

Statistical Analysis of Distance-Based Detection

For analysis in this work, weighting was given to distance (y) to the -1 power, according to:

$$w_i = \frac{ny_i^{-1}}{\sum_{i=1}^n y_i^{-1}}$$

Confidence and prediction intervals were calculated from the following equations with respect to the best-fit regression line.

$$CI = \pm t_{\alpha/2,DOF} \hat{s} \sqrt{\frac{1}{n} + \frac{(x - \bar{x})^2}{S_{xx}}}$$

$$PI = \pm t_{\alpha/2,DOF} \hat{s} \sqrt{\frac{1}{w_i} + \frac{1}{n} + \frac{(x - \bar{x})^2}{S_{xx}}}$$

Here, $t_{\alpha/2,DOF}$ corresponds to a two-tail distribution of the t distribution and DOF are the degrees of freedom equal to n-2 for linear fits. S-hat is a function of the sum of squared error (SS_E), given by:

$$\hat{s} = \sqrt{\frac{SS_E}{DOF}}$$

X-bar corresponds to the weighted x-centroid given by:

$$\bar{x} = \frac{\sum_{i=1}^n w_i x_i}{\sum_{i=1}^n w_i}$$

S_{xx} corresponds to the weighted sum of squares between x_i and x -bar, given by:

$$S_{xx} = \sum_{i=1}^n w_i (x_i - \bar{x})^2$$

Ink chemistry was investigated as a means of precisely controlling reagent deposition; however, not all reagents are compatible with inkjet printing. In previous efforts, bathocuproine was utilized as a complexing agent for Cu detection, but it was discovered that the rapid-prototyped plastic housing comprising the ink reservoirs in the printer were incompatible with bathocuproine. An alternative solution was found with dithiooxamide, a ligand for Cu that was compatible with the Epson R280 model used here. A comparison between ligands and their effect on distance-based detection of Cu is shown in Figure A2-3.

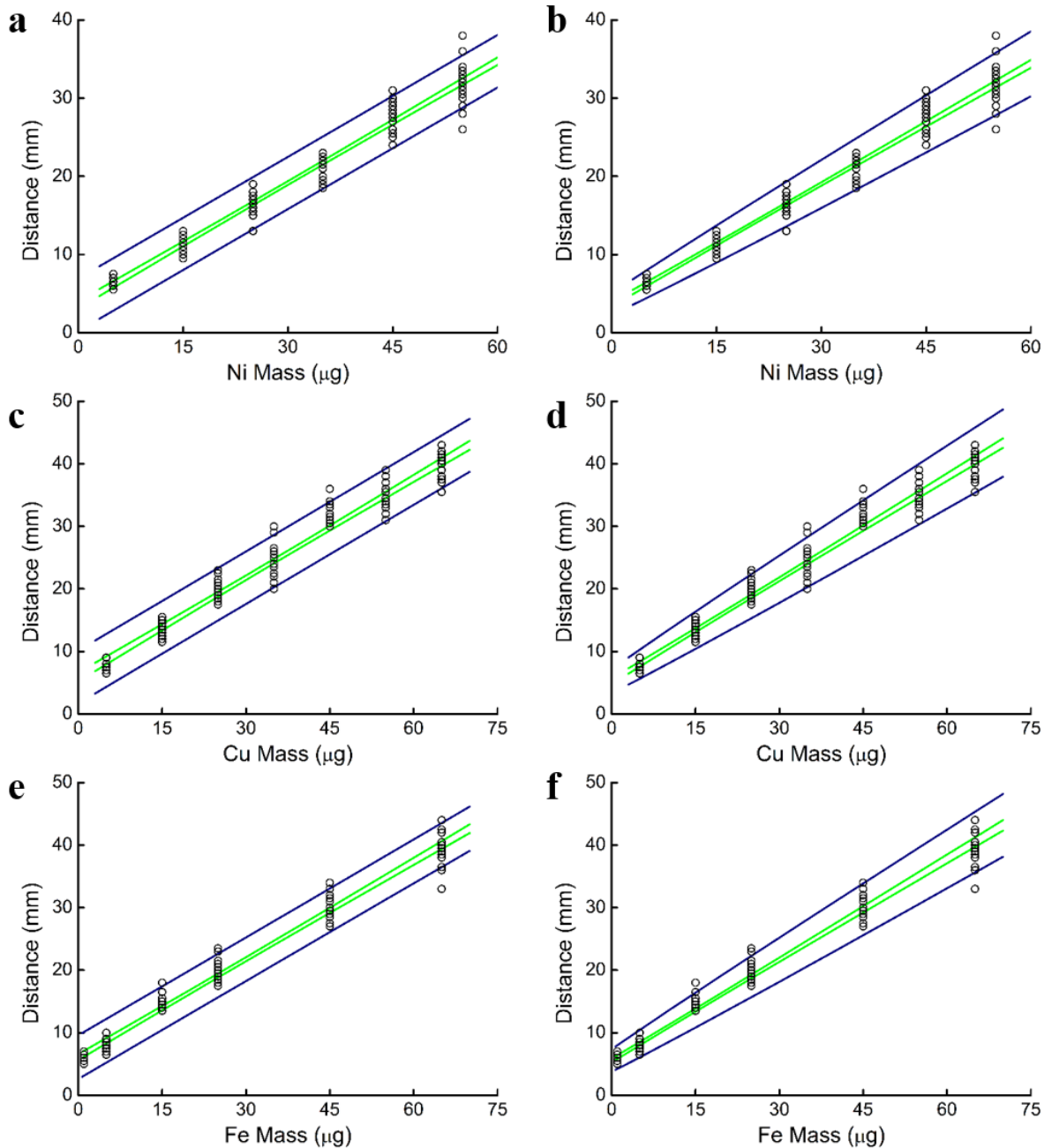


Figure A2-2 | Unweighted (A, C, E) and weighted (B, D, F) linear regression fits for Ni, Cu, and Fe showing 95% prediction (blue) and confidence (green) intervals.

